# A new perspective on atmospheric blocking from observations – detection, analysis, and impacts

Lukas Brunner

June 2018

The **Wegener Center for Climate and Global Change** combines as an interdisciplinary, internationally oriented research institute the competences of the University of Graz in the research area "Climate, Environmental and Global Change". It brings together, in a dedicated building close to the University central campus, research teams and scientists from fields such as geo- and climate physics, meteorology, economics, geography, and regional sciences. At the same time close links exist and are further developed with many cooperation partners, both nationally and internationally. The research interests extend from monitoring, analysis, modeling and prediction of climate and environmental change via climate impact research to the analysis of the human dimensions of these changes, i.e., the role of humans in causing and being effected by climate and environmental change as well as in adaptation and mitigation. (more information at www.wegcenter.at)
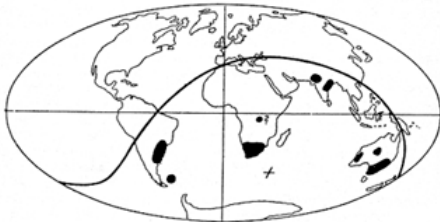
**Alfred Wegener** (1880–1930), after whom the Wegener Center is named, was founding holder of the University of Graz Geophysics Chair (1924–1930). In his work in the fields of geophysics, meteorology, and climatology he was a brilliant scientist and scholar, thinking and acting in an interdisciplinary way, far ahead of his time with this style. The way of his ground-breaking research on continental drift is a shining role model–his sketch on the relations of continents based on traces of an ice age about 300 million years ago (left) as basis for the Wegener Center Logo is thus a continuous encouragement to explore equally innovative ways:
*paths emerge in that we walk them* (Motto of the Wegener Center).

## Wegener Center Verlag • Graz, Austria

June 2018

*Contact: Dr. Lukas Brunner*
*lukas.brunner@live.at*

BRUNNER Lukas

# A new perspective on atmospheric blocking from observations – detection, analysis, and impacts

## PhD thesis

to obtain the academic degree
Doctor of Natural Sciences

submitted to the

Faculty of Environmental and Regional Sciences and Education
University of Graz

First referee: Assoc. Prof. Dr. STEINER Andrea K.
Wegener Center for Climate and Global Change, University of Graz

Second referee: Univ. Prof. Dr. HEGERL Gabriele C.
School of Geosciences, University of Edinburgh

Third referee: Dr. FISCHER Erich M.
Institute for Atmospheric and Climate Science, ETH Zurich

**2018**

Supervisor

**Assoc. Prof. Dr. Andrea K. Steiner**
University of Graz, Austria

Co-supervisor

**Univ. Prof. Dr. Steffen Birk**
University of Graz, Austria

External supervisors

**Univ. Prof. Dr. Gabriele C. Hegerl**
University of Edinburgh, United Kingdom

**Dr. Jana Sillmann**
Center for International Climate Research, Norway

# Abstract

Stationary high-pressure systems at mid-latitudes, termed atmospheric blocking, are frequently connected to extreme weather events such as cold spells and heat waves. Their evolution and impacts in our changing climate have, hence, been extensively investigated in recent decades but several aspects still remain uncertain.

This work introduces observations from GPS radio occultation (RO) as a new data set for blocking research. RO is a satellite-based, remote-sensing technique, observing key atmospheric variables such as geopotential height (GPH), temperature, and specific humidity with high accuracy. RO measurements processed at the Wegener Center are used from 2006 to 2016. The feasibility of blocking detection with RO is demonstrated for two blocking events in the Northern Hemisphere. The evolution of both events in summer 2010 and winter 2013 is correctly captured by RO and strong anomalies in atmospheric GPH and temperature are revealed.

Observations over the entire RO period are used to systematically detect blocking in both hemispheres. All main blocking regions and the seasonal variability are well represented in the RO data set. The vertical atmospheric structure is particularly well resolved, revealing strong impacts on temperature and specific humidity throughout the entire troposphere and up into the lower stratosphere during blocking. RO is found to be a promising new method, enabling blocking detection and analysis from a single, comprehensive data set available globally at the same high quality.

Impacts of blocking on surface extremes in Europe are investigated for a longer period from 1979 to 2014 in the observation-based ERA-Interim and E-OBS records. Statistically significant links between blocking and European temperature extremes are found that change during spring. Blocking impacts in spring are of particular relevance for vegetation and, therefore, need further research, especially in light of continued climate change.

# Zusammenfassung

Blockierende Hochdrucklagen in mittleren Breiten (en. *Blocking*) sind ein atmosphärisches Phänomen, das häufig zu Extremereignissen wie Kälte- und Hitzewellen führt. Im Licht des Klimawandels wurde Blocking daher in den letzten Jahrzehnten intensiv erforscht, doch wesentliche Aspekte bleiben weiter unsicher.

Diese Arbeit stellt die satellitenbasierte GPS Radiookkultationsmethode (RO) für die Blocking-Forschung vor. RO liefert vertikal hochaufgelöste Messungen wichtiger atmosphärischer Parameter wie Geopotentielle Höhe (GPH), Temperatur und Spezifische Feuchte. Es werden RO Daten von 2006 bis 2016 verwendet, die am Wegener Center prozessiert wurden. In einer Fallstudie, die jeweils ein Blocking in Sommer und Winter untersucht, wird gezeigt, dass RO gut zur Detektion und Untersuchung von Blocking geeignet ist. Die Entwicklung wird korrekt dargestellt und starke Anomalien von atmosphärischer Temperatur und GPH während Blocking werden aufgezeigt.

In einer systematischen Untersuchung wird Blocking im gesamten RO Datensatz und global analysiert. Die Blocking-Regionen und saisonale Änderungen werden korrekt abgebildet und es werden Anomalien von Temperatur und Spezifischer Feuchte während Blocking in der gesamten Troposphäre und bis in die untere Stratosphäre nachgewiesen. RO stellt daher einen vielversprechenden, neuen Datensatz für die Blocking-Forschung dar, der die globale Detektion und Analyse von Blocking aus einer einzelnen Quelle mit hoher Qualität erlaubt.

Die Auswirkung von Blocking auf Kälte- und Hitzewellen im europäischen Frühling wird für eine längere Zeitspanne von 1979 bis 2014, basierend auf ERA-Interim und E-OBS Daten, untersucht. Die Ergebnisse zeigen statistisch signifikante Verbindungen zwischen Blocking und Temperaturextremen in Europa. Die Auswirkungen von Blocking-Lagen im Frühling sind von besonderer Wichtigkeit für die Landwirtschaft und gerade im Licht des Klimawandels ist weitere Forschung in diesem Bereich essenziell.

# Acknowledgments

*It's the job that's never started*
*as takes longest to finish*
*— J. R. R. Tolkien*

While this thesis formally constitutes the final part of my PhD it represents much more beyond that for me. It marks the completion of a chapter of life that started almost a decade ago. A chapter in which I was fortunate to meet a lot of people and learn much from them. I am deeply grateful to everybody who went part of this way with me, although it is not possible to thank all of you individually here – I hope you understand.

My sincerest thanks go to my supervisor Andrea Steiner, who always supported me and who has taught me a lot throughout my master and PhD. Thank you for providing guidance whenever I needed it and freedom whenever I wanted it. I also thank my co-supervisor Steffen Birk, my mentor Astrid Veronig, and the whole team of the Wegener Center for their help whenever I asked for it. I particularly thank Barbara, Betti, Florian, Gottfried, Marc, and Sabine – you made working at the Wegener Center productive *and* fun.

Sincere thanks to Gabi Hegerl for inviting me to Edinburgh and for supporting me in various ways. Thanks also to the entire group at the University of Edinburgh for welcoming me so nicely! Thanks to Sabine for many good coffee chats and the hospitality, and to Chris for many Munros. And thanks to Hayley for showing me how cool being a nerd can be.

Many thanks you to Jana Sillmann for hosting me at the CICERO in Oslo. Your outgoing personality and openness are an inspiration for me! Thanks to George, Maja, Nathalie, Sarin, and many others for a great time in Oslo!

I am most grateful to all my friends in Vorarlberg for still being there whenever I come back home. Dagmar, Danio, Dominik, Isi, Kerby, Michi, Mo, Silvia, and Steffi – you are the best! Many thanks to the physics-clique for the long hours of equations, discussions, and drinks over the years. Andi, Bernhard, Georg, Markus, Pamina, Pascal, and Robert – I could not have done this without you!

Thanks also to the students, administrative staff, and faculty of the Doctoral Programme Climate Change for the great working-atmosphere and many interesting

# Contents

*Contents*

# Preface

This thesis is based on the following peer-reviewed publications:

**Brunner, L.**, A. K. Steiner, B. Scherllin-Pirscher, and M. W. Jury (2016). "Exploring atmospheric blocking with GPS radio occultation observations". *Atmos. Chem. Phys.* 16.7, pp. 4593–4604. DOI: 10.5194/acp-16-4593-2016 (2016 IF 5.318)

*Contributions:* I collected the data, performed the analysis, created the figures, and wrote the manuscript. A. K. Steiner and B. Scherllin-Pirscher provided guidance on all aspects of the study, contributed to the text, and advised the work. M. W. Jury provided expertise and help on the methodological aspects of the work and contributed to the text.

**Brunner, L.** and A. K. Steiner (2017). "A global perspective on atmospheric blocking using GPS radio occultation – one decade of observations". *Atmos. Meas. Tech.* 10, pp. 4727–4745. DOI: 10.5194/amt-10-4727-2017 (2016 IF 3.089)

*Contributions:* I collected the data, performed the analysis, created the figures, and wrote the manuscript. A. K. Steiner provided guidance on all aspects of the study, contributed to the text, and advised the work.

**Brunner, L.**, G. C. Hegerl, and A. K. Steiner (2017). "Connecting atmospheric blocking to European temperature extremes in spring". *J. Climate* 30.2, pp. 585–594. DOI: 10.1175/JCLI-D-16-0518.1 (2016 IF 4.161)

*Contributions:* I collected the data, performed the analysis, created the figures, and wrote the manuscript. G. C. Hegerl and A. K. Steiner provided guidance on all aspects of the study, contributed to the text, and advised the work.

In addition I contributed to the following published and submitted papers in the course of my PhD work, which are not part of this thesis:

**Brunner, L.**, N. Schaller, J. Anstey, J. Sillmann, and A. K. Steiner (in press). "Dependence of present and future European temperature extremes on the location of atmospheric blocking". *Geophys. Res. Lett.* DOI: 10.1029/2018GL077837

*Contents*

Unterberger, C., **L. Brunner**, S. Nabernegg, K. Steininger, A. K. Steiner, E. Stabentheiner, S. Monschein, and H. Truhetz (accepted). "Spring frost risk for regional fruit production under a warmer climate". *PLOS ONE*

Mohankumar, S. E. P., K. Mintz-Woo, M. Damert, **L. Brunner**, and J. Eise (accepted). "Blogging Climate Change: A Case Study". *2nd World Symposium on Climate Change Communication* (conference paper)

The thesis starts with a synopsis in part I in which the research questions are introduced and motivated. The scientific context and background is given and an overview on used methods and data sets is provided. Part II presents the main scientific results in the form of three published papers. A complete list of acronyms, figures, and tables as well as a bibliography can be found at the end of this thesis.

# Part I.

# Synopsis

# 1. Introduction

Weather and climate at mid-latitudes are strongly linked to large-scale atmospheric circulation and phenomena, such as the jet stream, storm tracks, and blocking. Some of these processes and their interlinkages are not yet fully understood, introducing a high level of uncertainty to their predictability and the modeling of their future evolution (Woollings 2010). This is particularly relevant when one considers weather and climate extremes and their impacts. The World Climate Research Programme (WCRP) regards "advances in the understanding of the physical mechanisms leading to extremes" as a crucial development for the Grand Challenge on Weather and Climate Extremes (Zhang et al. 2013). In the 2015 Paris Agreement, the parties to the United Nations Framework Convention on Climate Change (UNFCCC) recognized the "importance of averting, minimizing and addressing loss and damage associated with the adverse effects of climate change, including extreme weather events and slow onset events, and the role of sustainable development in reducing the risk of loss and damage" (United Nations 2015). This underlines the need to understand and predict the atmospheric processes involved in the development of such extremes to provide a reliable scientific foundation for policy makers.

In this context, atmospheric blocking, which describes stationary high-pressure systems blocking the westerly (i.e., eastward) flow at mid-latitudes, is a particularly important phenomenon. Blocking-related extremes repeatedly affect densely-populated and heavily-cultivated areas, causing severe damage to society and economy. At the same time, key mechanisms involved in blocking evolution are still unclear, and its occurrence is still underestimated in current weather and climate models (e.g., Pfahl et al. 2015, and references therein). Recent examples of such extreme events are the heat wave that occurred in eastern Europe and Russia during the summer of 2010 and the cold spell that occurred in central Europe during the spring of 2016 (Matsueda 2011; AGRI4CAST 2016).

Especially in a changing climate reliable information on the future development of extremes is essential for policy makers to be able to minimize or avoid negative impacts on human health and economy. In this context, atmospheric blocking is also highlighted in the Intergovernmental Panel on Climate Change (IPCC)

Fifth Assessment Report (AR5) as an important source of climate anomalies and extreme events in regions such as Europe, North America, and Australia. The future evolution of atmospheric blocking with regard to its locations and frequency is seen as "crucially important for understanding regional climate change in particular with respect to extreme conditions" (Christensen et al. 2013). But at the same time, it is stated that there is only "medium confidence that the frequency of [...] blocking will not increase, while trends in blocking intensity and persistence remain uncertain" (Christensen et al. 2013). Barnes et al. (2014), for example, investigated historical blocking occurrence and did not find any robust trends across different reanalyses and using different detection methods. Many studies were carried out on the evaluation of blocking frequencies in climate models. Findings show a general tendency toward decreasing blocking occurrence in the future from models (e.g., Matsueda and Endo 2017), but also a considerable under-representation of blocking compared to reanalyses (e.g., Davini and D'Andrea 2016) due to, e.g., too sparse resolution and too strong climatological westerly flow (e.g., Scaife et al. 2010).

In this context, the work presented in this thesis gives a new perspective on atmospheric blocking from observations. Satellite-based observations from Global Positioning System (GPS) radio occultation (RO) are introduced for blocking detection in order to better quantify and eventually reduce uncertainties in blocking representation across different data sets (Brunner et al. 2016, presented page 45ff.). In a next step a detailed global analysis of blocking occurrences based on a decade of RO observations is presented and blocking impacts in the free atmosphere, from the troposphere to the lower stratosphere, are investigated (Brunner and Steiner 2017, presented page 57ff.).

Highlighting the importance of blocking in the spring season, which has rarely been considered in the scientific literature, this work looks into blocking impacts on surface temperature extremes in spring. The link between blocking and the occurrence of cold spells and warm spells in Europe is investigated (Brunner et al. 2017, presented page 77ff.).

In summary, this work is driven by two main aims:

1. To introduce the novel GPS RO record for blocking research, testing the feasibility of RO observations for blocking detection and using the data to analyze the atmospheric structure during blocking on a global scale.

2. To investigate the link between blocking and large-scale surface temperature extremes, such as heat waves and cold spells during the spring season, based on established observational data sets.

The following synopsis is structured as follows: In chapter 2, the current state of knowledge on changes in the atmospheric circulation and their connection to changes in extremes is addressed, with a focus on the role of atmospheric blocking. In chapter 3, a historical overview is given on the development of blocking definitions from 1950 to the present. A global blocking detection index is presented, which was developed in the course of this work and which is used in all three publications. In chapter 4, climate models and reanalyses and their use in blocking research are summarized. GPS RO observations are introduced as a new data set for blocking research. Chapter 5 provides a summary of this work and concluding remarks.

# 2. Weather and climate

"Human influence on the climate system is clear. This is evident from
the increasing greenhouse gas concentrations in the atmosphere, positive
radiative forcing, observed warming, and understanding of the climate
system" (IPCC 2013).

## 2.1. Extremes in a changing climate

The increase in global mean surface temperature is the most frequently-used proxy
in the public discourse about climate change (e.g., United Nations 2015; Knutti
et al. 2016; Medhaug et al. 2017; Millar et al. 2017; Fig. 2.1). However, changes in
extreme temperature can exceed the mere change in the mean by far (e.g., Schär
et al. 2004; Clark et al. 2006; Perkins 2015) and can have significantly greater effects
than changes in the mean on society as adaptation to extremes is considerably
more difficult (Seneviratne et al. 2006). For this reason the occurrence of extreme
events often triggers public interest in topics related to climate change (Center for
Research on Environmental Decisions 2009).

Whether a certain weather event was caused by climate change, a then frequently-
posed question, does not have an easy answer (Hegerl and Zwiers 2011; Hulme 2014;
National Academies of Sciences, Engineering, and Medicine 2016). The fraction of
attributable risk (FAR) (e.g., Stone and Allen 2005; Pall et al. 2011) is one way
to express the contribution of human-caused climate change to a certain event.
Stott et al. (2004) calculated that the risk that mean temperatures, such as those
observed during the record summer of 2003 in Europe, would be exceeded was very
likely doubled due to human interference. The IPCC AR5 found an increasing
amount of evidence for human contributions to the increase in the frequency and
intensity of daily temperature extremes (IPCC 2013). Fischer and Knutti (2015)
calculated that in our current climate up to 75 % of hot extremes are attributable to
increased temperatures, and many other studies have shown a significant increase
in the frequency and intensity of hot extremes in recent decades (Della-Marta et al.
2007a; Della-Marta et al. 2007b; Hansen et al. 2012; IPCC 2012; Hartmann et al.
2013; Christidis et al. 2015).
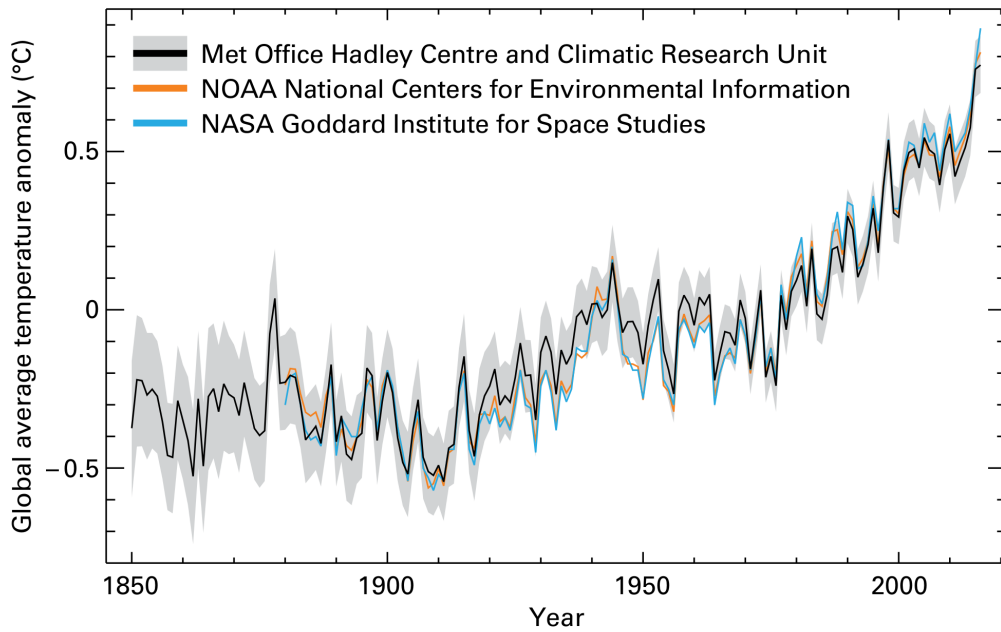
**Figure 2.1.:** Global average temperature anomalies relative to the 1961 to 1990 climatology from three data sets as given in the figure. The gray shading indicates the 95 % confidence range from the Met Office data set. Reprinted from WMO (2017).

Figure 2.1 shows global average temperature anomalies from 1850 to 2016 relative to the 1961 to 1990 reference climatology for three different data sets. 2016 was on average $0.83\,°C \pm 0.10\,°C$ warmer than the climatology and was found to be the warmest year on record so far (WMO 2017). Figure 2.2 shows the fraction of land area that has been affected by anomalously cold and warm temperatures from 1950 to 2010. The anomalies are classified based on multiples of the standard deviation $\sigma$, assuming a Gaussian temperature distribution over the base period 1951 to 1980. Hot or cold temperatures are defined if the anomalies exceed $\pm 0.43\sigma$, respectively. With that definition there is a one-third chance for each of the three cases hot, cold, and "normal" during the base period (Hansen et al. 2012). A general increase in the fraction of land affected by hot temperatures as well as a general decrease in the fraction of land affected by cold temperatures is clearly visible. Based on these results, Hansen et al. (2012) stressed the fact that an "emergence of a new category of 'extremely hot' summers, more than $3\sigma$ warmer than the base period mean" was observed.

Concerning future changes, the importance of stabilizing global temperatures as soon as possible is often stressed, since the probability of hot extremes increases nonlinearly with mean temperature (Fischer and Knutti 2015; Schleussner et al.
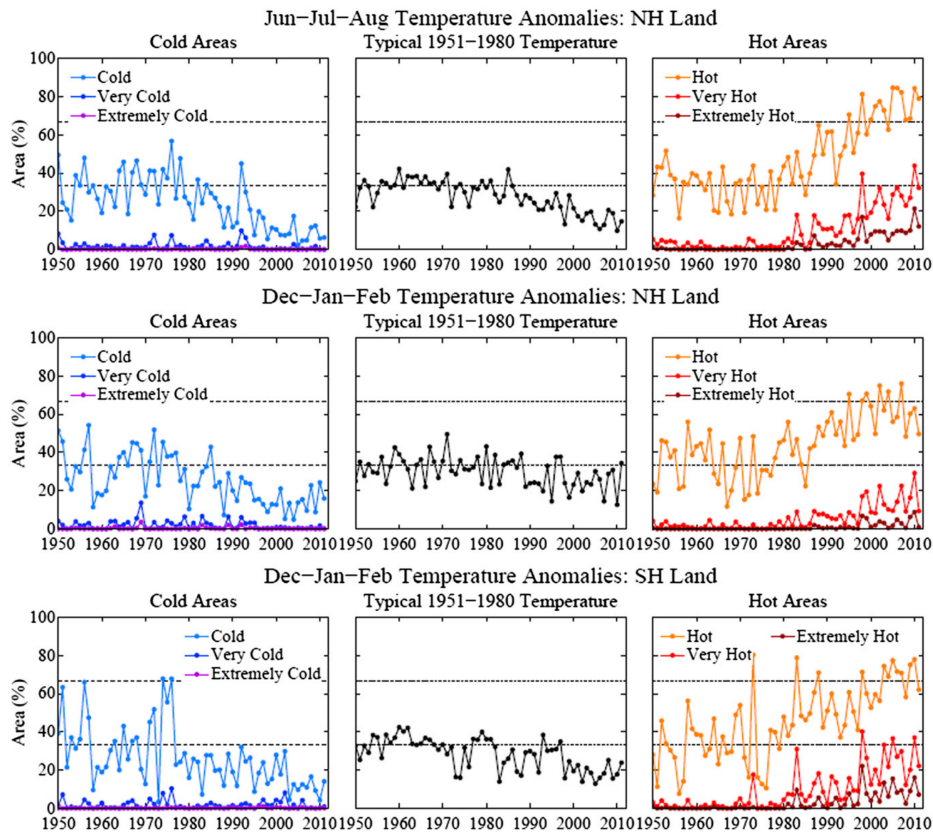
**Figure 2.2.:** Area covered by temperature anomalies in the categories defined as hot ($> 0.43\sigma$), very hot ($> 2\sigma$), and extremely hot ($> 3\sigma$), with analogous divisions for cold anomalies. Anomalies are relative to 1951–1980 base period, with $\sigma$ also from 1951–1980 data. Lowest row is Southern Hemisphere summer. Reprinted from Hansen et al. (2012).

2016; Mitchell et al. 2017; Schleussner et al. 2017). Figure 2.3 depicts three possible mechanisms that can lead to a change in the occurrence of extremes: a shift in the mean temperature, increased temperature variability, or a changed symmetry of the temperature Probability Density Function (PDF) (IPCC 2012). Indeed, studies found that the European climate has become more extreme, and the observed increase in the frequency of temperature extremes can only be explained by a combination of a change in the mean accompanied by a change in the variance (Schär et al. 2004; Della-Marta et al. 2007a).

Hot temperature extremes like heat waves are almost always connected to an atmospheric high-pressure system (Perkins 2015). If such a high-pressure system is located in the zone of prevailing westerlies at mid-latitudes and if the system is stationary for several days, it is usually referred to as a blocking high-pressure
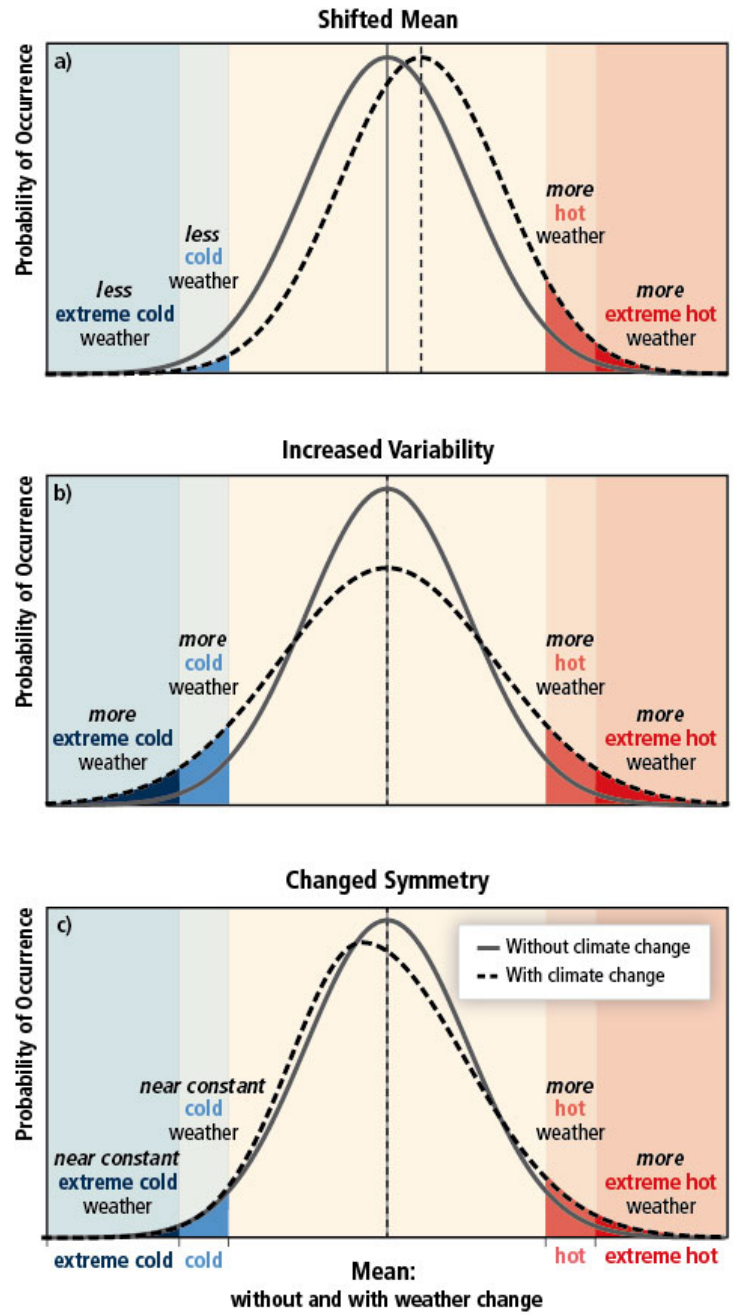
**Figure 2.3.:** The effect of changes in temperature distribution on extremes. Different changes in temperature distributions between present and future climate and their effects on extreme values of the distributions: (a) effects of a simple shift of the entire distribution toward a warmer climate; (b) effects of an increase in temperature variability with no shift in the mean; (c) effects of an altered shape of the distribution, in this example a change in asymmetry toward the hotter part of the distribution. Reprinted from IPCC (2012).

system (Rex 1950a). Particularly persistent blocking events, lasting for up to several weeks, can lead to severe heat waves, as they allow for an increasing amount of heat to build up in the atmospheric boundary layer (Kyselý 2007; Miralles et al. 2014).

Beside blocking, other mechanisms also contribute to the development of heat waves, most notably soil moisture (Fischer et al. 2007a; Stefanon et al. 2012; Perkins 2015; Sillmann et al. 2017). In the example of the European heat wave of 2003, Fischer et al. (2007b) showed that without the negative soil moisture anomalies, due to the precipitation deficit in early 2003, temperature anomalies would have been about 40 % lower. In addition, land-atmosphere interactions are found to increase the diurnal temperature variability (Fischer et al. 2007a) and may play even more important roles in a warming climate (Seneviratne et al. 2006).

On the other side of the temperature distribution, extreme cold events like cold spells continue to have severe impacts even in a warming climate (Cattiaux et al. 2010; Wang et al. 2010), and temperature-related excess mortality is still mostly attributable to extreme cold (Gasparrini et al. 2015). A range of studies has shown that atmospheric blocking –beside its impacts on heat waves– also significantly contributes to cold extremes such as the severe winter 2010 (Trigo et al. 2004; Barriopedro et al. 2008; Cattiaux et al. 2010; Buehler et al. 2011; Sillmann et al. 2011; Whan et al. 2016). For the future, Sillmann et al. (2011) found that model projections show a persistent link between extreme low temperatures and blocking. These findings have been confirmed by Brunner et al. (in press) in a study using a 50-member ensemble of the second Canadian Earth System Model (CanESM2).

Finally, changes also occur during the transition seasons of spring and fall. Using a metric based on circulation patterns, Cassou and Cattiaux (2016) showed that the onset of summer has shifted by about 10 days from mid-April towards early April in the period between 1960 and 2010. These changes are of particular relevance as they also influence the growing periods of plants. Menzel et al. (2006), for example, investigated several hundred plant species in Europe over the period from 1971 to 2000 and found that most of them showed an advance towards earlier leafing and flowering in spring by about 2.5 days per decade. This advance can have potentially devastating effects, as an earlier onset of the vegetation period may increase the risk of susceptibility to severe frost damages (Hufkens et al. 2012; Menzel et al. 2015; Brunner et al. 2017; Unterberger et al. accepted). In this regard, blocking can, on the one hand, contribute to early warm spells, which may favor a premature greening onset. On the other hand, blocking can lead to late cold spells in spring, which can be devastating for vegetation and lead to high economic damages (Brunner et al. 2017; Unterberger et al. accepted).

## 2.2. Changes in atmospheric circulation

In parallel to the ongoing changes in extreme temperature occurrence, there is also evidence that atmospheric circulation patterns are shifting due to climate change. The stronger warming in the Arctic region compared to the warming at lower latitudes (referred to as Arctic amplification) is often discussed as one of the drivers behind changes in the jet stream (Feldstein and Lee 2014; Barnes and Screen 2015; Francis and Vavrus 2015; Hall et al. 2015), planetary waves (Barnes 2013; Screen and Simmonds 2013), and blocking (Woollings et al. 2014; Barnes and Polvani 2015). Francis and Vavrus (2015) suggested that the Arctic amplification leads to a wavier jet stream, which favors more persistent weather. Observational studies have also noted a weakening (Archer and Caldeira 2008) and a northward shift (Fu and Lin 2011) of the Northern Hemisphere (NH) jet stream.

The North Atlantic storm tracks are another important driver of European weather variability and are also expected to change in a warming climate (Yin 2005; Bengtsson et al. 2005; Kyselý 2008; Dong et al. 2013; Catto et al. 2014; Lau and Nath 2014). Most studies agree that a poleward shift of the storm tracks is occurring, which is found to be "likely to support more persistent circulation patterns over Europe, and impacts of the climate change on the occurrence and severity of temperature extremes may be exacerbated" (Kyselý 2008).

Blocking of the mid-latitude climatological flow by stationary high-pressure systems is closely connected to all of the features described above and, therefore, is likely to change as well in a warming climate (e.g., Barnes et al. 2014; Vries et al. 2013; Dong et al. 2013; Kennedy et al. 2016). The results of model studies suggest that winter blocking in the Euro-Atlantic sector will decrease towards the end of the 21st century (Masato et al. 2013; Kennedy et al. 2016; Matsueda and Endo 2017; Brunner et al. in press). Masato et al. (2013) and Matsueda and Endo (2017) found a decrease of blocking frequency of up to 30 % in winter in Europe. However, in some regions, like eastern Europe, no such trend has been detected (Masato et al. 2013; Matsueda and Endo 2017). Authors of some studies have, therefore, noted that the detection of trends in blocking may be sensitive to the selected region and that some part of the blocking decline, particularly over Europe, may in fact be a shift to the east (Vries et al. 2013; Masato et al. 2014; Brunner et al. in press). Analyzing reanalyses, Croci-Maspoli et al. (2007) found negative trends in NH winter blocking, while Barnes et al. (2014) concluded that they did not find any trend over the period of 1980 to 2012. Such inconclusive results highlight the need for continued research to focus on the current and future evolution of blocking, particularly in light of the expected continuing climate change.

## 2.3. Atmospheric blocking and its impacts

Atmospheric blocking describes a synoptic situation in which a strong and stationary anti-cyclone weakens or reverses the climatological westerly flow at mid-latitudes for up to several weeks (Rex 1950a). Due to its persistence, it can lead to strong anomalies in key atmospheric variables such as temperature and humidity via direct and remote effects (Pfahl 2014; Bieli et al. 2015). It also frequently contributes to surface extremes, such as heat waves, cold spells, droughts, and flooding, with potentially disastrous effects for human society and economy (e.g., Cattiaux et al. 2010; Barriopedro et al. 2011; Galarneau Jr. et al. 2012) as mentioned in the previous sections.

One of the strongest and longest blocking cases in recent history occurred over eastern Europe and Russia during the summer of 2010. It was closely linked to a severe heat wave, which broke temperature records in many regions of Europe and Russia and is, therefore, often referred to as the 2010 Russian heat wave. Fig. 2.4 (top) shows the distribution of European summer temperatures for the period 1500 to 2010. The summer of 2010 clearly stands out as it was about 1.8 °C (3.5 standard deviations) warmer than the climatological mean of 1970 to 1999. The heat led to over 50 000 additional deaths and over 10 billion USD in economic losses in Russia alone (Barriopedro et al. 2011, and references therein). At the same time, the blocking also contributed to intensify the Monsoon rain fall, which led to one of the worst flooding events in Pakistan and northwestern India ever recorded. Over 20 million people were affected, and the economic damage was estimated to exceed 40 billion USD (Hong et al. 2011). The crucial role of the extraordinary synoptic condition during the summer of 2010 in the development of theses extremes has been noted by many authors in the aftermath of the event (Hong et al. 2011; Houze Jr. et al. 2011; Schneidereit et al. 2012; Galarneau Jr. et al. 2012; Lau and Kim 2012; Lupo et al. 2012; Martius et al. 2013; Miralles et al. 2014).

In general, blocking has been identified as a main contributor to summer hot extremes by a range of authors (e.g., Black et al. 2004; Meehl and Tebaldi 2004; Pfahl and Wernli 2012; Rodrigues and Woollings 2017). It affects co-located regions by leading to persistent clear-sky conditions, increasing the radiative heating, and diverting the succeeding cyclonic systems and their fronts (Pfahl 2014; Bieli et al. 2015). Pfahl and Wernli (2012) found that up to 80 % of NH hot extremes coincide with a co-located blocking. A similar result was found by Rodrigues and Woollings (2017) for the Southern Hemisphere (SH).
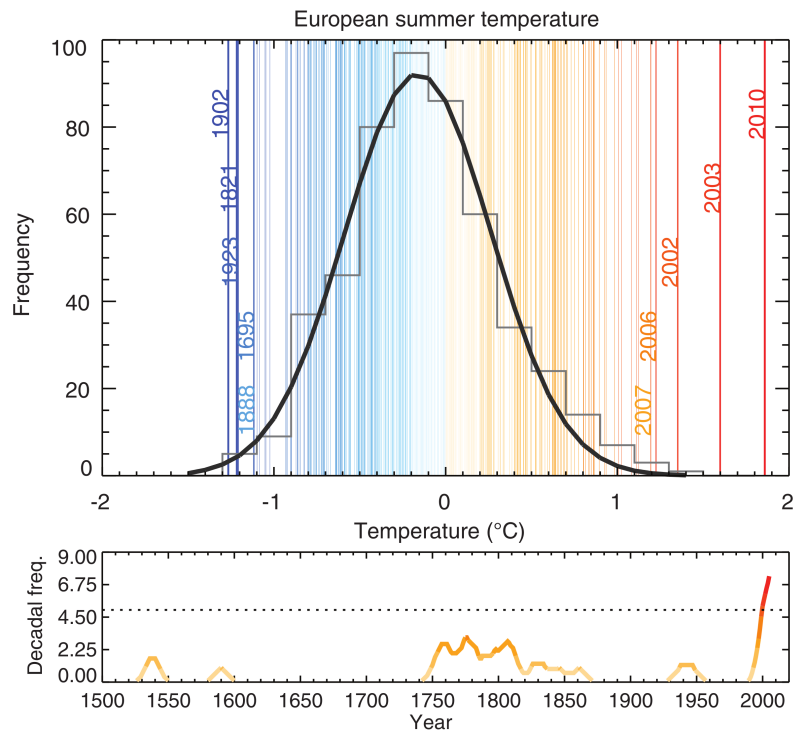
**Figure 2.4.:** (Top) Statistical frequency distribution of reconstructed and instrument-based European (35 °N to 70 °N and 25 °W to 40 °E) summer land temperature anomalies (relative to the 1970 to 1999 mean) shown from 1500 to 2010 (vertical lines). The five warmest and five coldest summers are labeled. Gray bars represent the distribution with a Gaussian fit in black. (Bottom) The running decadal frequency of extreme summers, defined as those with temperature above the 95th percentile of the 1500 to 2002 distribution. A 10-year smoothing is applied. The dotted line shows the 95th percentile of the distribution of maximum decadal values that would be expected by random chance. Reprinted from Barriopedro et al. (2011) with permission from AAAS.

In winter, the most frequently-noted temperature effect of blocking comes from the advection of cold air, which mainly affects the regions surrounding the block and can lead to severe cold spells (e.g., Trigo et al. 2004; Mendes et al. 2008; Sillmann et al. 2011; Pfahl 2014; Rimbu et al. 2014; Whan et al. 2016). Pfahl (2014), for example, found that "cold temperature extremes at most locations in Europe are found to be associated with blocking over northern Europe and the North Atlantic".

Brunner et al. (in press) showed that blocking is statistically significantly linked to European heat wave and cold spells during present (1981 to 2010) conditions and will remain so in a future (2070 to 2099) scenario, driven by the Representative
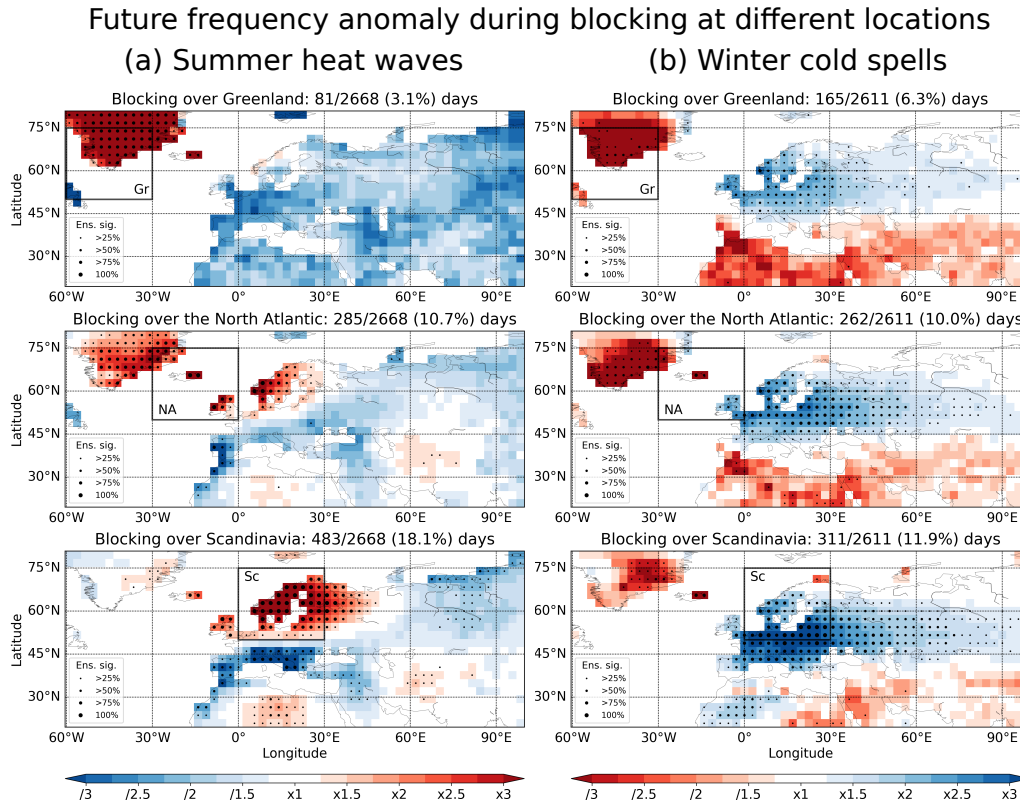
**Figure 2.5.:** Extreme temperature occurrence anomaly for blocking in different regions (gray boxes) for future (2070 to 2099) conditions based on the CanESM2 ensemble mean. Shown is the (a) summer heat wave anomaly and the (b) winter cold spell anomaly. The statistical significance at the 10 % (2-sided) level is indicated by dots and the dot size indicates the number of ensemble members which show significance. Adapted from Brunner et al. (in press).

Concentration Pathway 8.5 (RCP8.5). Fig. 2.5 shows the frequency anomaly for summer heat waves and winter cold spells during blocking in the future (2070 to 2099) period. The impact of blocking on triggering summer heat waves (Fig. 2.5a) is strongest at the location of the block. For blocking over Greenland no significant effects on temperatures in Europe is found (Fig. 2.5a, top). In contrast, for blocking over Scandinavia (Fig. 2.5a, bottom), a strong correlation to co-located heat waves is observed while "less than 10 % of [heat waves] in southern Europe co-occur with blocking" (Brunner et al. in press). Regarding the impacts of blocking in winter, strong remote effects are visible, and a strong and statistically significant increase in the occurrence of cold spells in Europe for blocking in all regions is found (Fig. 2.5b).
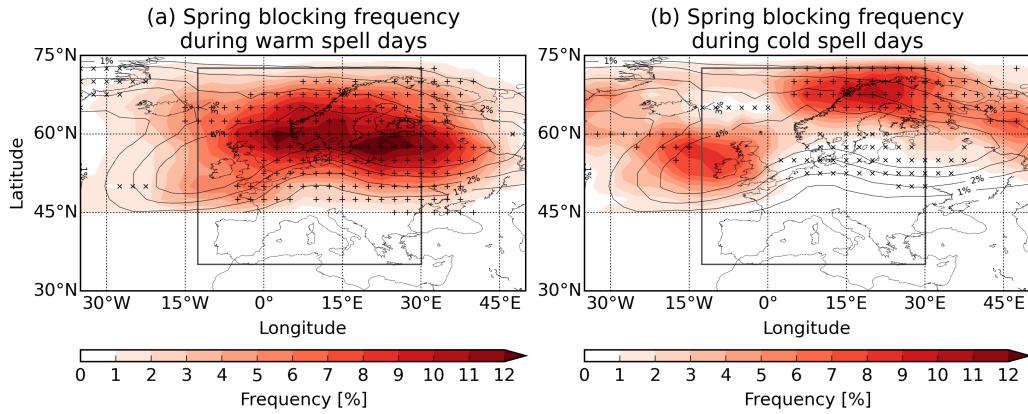
**Figure 2.6.:** Spring blocking frequency during days with (a) warm and (b) cold spells in Europe (black box) in the period 1979 to 2014. The 1979 to 2014 blocking climatology in spring is indicated by black contour lines, values that are statistically significantly larger than the number of blocks from random days (above 95th percentile) are marked with a plus sign, and values that are statistically significantly lower (below 5th percentile) are marked with a times sign. Adapted from Brunner et al. (2017).

Only a few studies have investigated blocking in the spring and fall seasons, mostly looking into the blocking climatology and possible trends (Wiedenmann et al. 2002; Croci-Maspoli et al. 2007; Tyrlis and Hoskins 2008a). The link to temperature anomalies during these transition seasons has, so far, not been a focus of the literature. However, especially in the phase in spring during which vegetation emerges and flowers blossom, plants are particularly vulnerable to (blocking-induced) cold spells (e.g., Eccel et al. 2009). In late spring 2016, for example, a persistent blocking situated over the British Isles led to the advection of cold air from the north into Europe. The resulting frost and snow caused severe damages in many regions in central Europe (AGRI4CAST 2016). The connection between blocking and temperature anomalies in Europe in historical springs from 1979 to 2014 is addressed in Brunner et al. (2017, presented page 77ff.), who found the "occurrence of atmospheric blocking in the European region [. . .] crucial for the development of both extended cold and warm spells in spring". Figure 2.6 shows the blocking frequency during warm spells (Fig. 2.6a) and cold spells (Fig. 2.6b) compared to the climatological frequency. For both cases a statistically significant link between blocking and temperature is found, highlighting the importance of blocking in the spring season. Therefore, it is essential that further research is conducted to address the effects of blocking also in spring and fall, particularly with regard to vegetation.

# 3. Blocking detection methods

In the following a historical overview of the development of blocking detection algorithms is given in chapter 3.1. The blocking detection algorithm developed as part of this work is presented in chapter 3.2.

## 3.1. History of blocking definitions

Blocking detection indices are used to objectively identify stationary high-pressure systems associated with a reversal of the climatological westerly flow at mid-latitudes. The first description of blocking was made by E. B. Garriott in 1904 (Garriott 1904, cited by Rex 1950a) although the classical definition was given in 1950 by Rex (1950a) via five criteria:

1. the basic westerly current must split into two branches

2. each branch current must transport an appreciable mass

3. the double-jet system must extend over at least 45° of in longitude

4. a sharp transition in the westerlies from a zonal type flow upstream to a meridional type downstream must be observed across the current split

5. the pattern must persist with recognizable continuity for at least 10 days

Following the work of Rex (1950a), authors of several studies have investigated blocking and its impacts on weather and climate (e.g., Rex 1950b; Rex 1951; Sumner 1954; White and Clark 1975; Dole and Gordon 1983). The main characteristics for defining blocking have, in principle, hardly changed over the years. At its core, blocking is an atmospheric pattern, which is located in the zone of prevailing westerlies at mid-latitudes. It is persistent and stationary, and hence, diverts the climatological flow. The two main blocking types are termed Rex block (also: dipole block, diffluent block) and Omega block. A schematic view of the involved high- and low-pressure systems is shown in Fig. 3.1. A Rex type block consists of a dipole pattern with a high-pressures system to the north and a low-pressure system to the south, which split the jet stream as indicated by the black arrows in
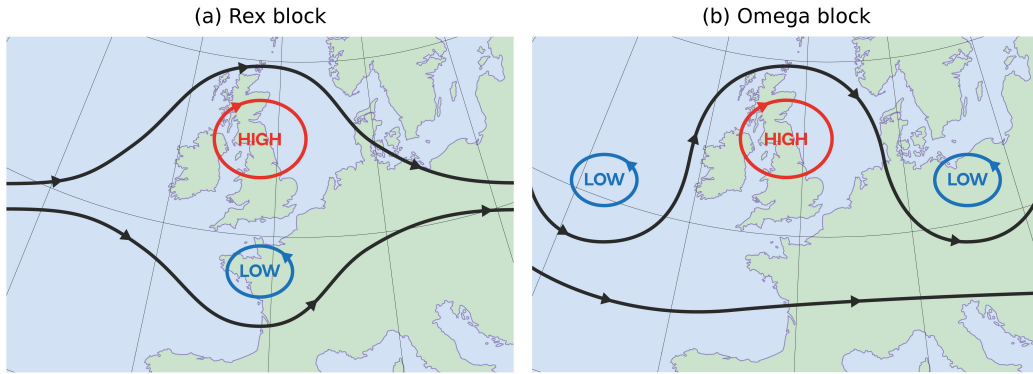
**Figure 3.1.:** Schematic pressure patterns during the two main blocking types: (a) Rex block and (b) Omega block. Lines of constant geopotential height on a given pressure level (isohypses) are shown in black, red, and blue, the embedded arrows indicate the direction of the flow. Adapted from Met Office. Contains public sector information licensed under the Open Government Licence v1.0.

Fig. 3.1a. Omega blocks consist of a central high-pressure system with low-pressure on the south-western and south-eastern flanks, creating a pattern shaped like the Greek letter $\Omega$.

About 30 years after Rex introduced his definition, Lejenäs and colleagues, in a two paper series, presented a blocking climatology for the NH (Lejenäs and Økland 1983) as well as for the SH (Lejenäs 1984). They introduced an objective daily blocking index, noting that the description by Rex "is difficult to translate [. . . ] into a computer program" (Lejenäs and Økland 1983). A typical blocking pattern was, at the time, considered to be composed of an anti-cyclone centered at about 60 °N in the NH and at about 50 °S in the SH and of a cyclone on the equatorward side. To detect these structures, geopotential height (GPH) gradients $\Delta Z$ at 500 hPa were defined in both hemispheres as:

$$\Delta Z(\lambda) = Z_{40\,°\mathrm{N}}(\lambda) - Z_{60\,°\mathrm{N}}(\lambda) \quad \text{in the NH} \tag{3.1}$$
$$\Delta Z(\lambda) = Z_{35\,°\mathrm{S}}(\lambda) - Z_{50\,°\mathrm{S}}(\lambda) \quad \text{in the SH,}$$

where $Z_\phi(\lambda)$ is the GPH at 500 hPa at longitude $\lambda$ and latitude $\phi$.

Figure 3.2 shows the mean GPH field at 500 hPa during NH meteorological summer (June, July, August – JJA) computed over the 10-year period from September 2006 to August 2016. Under climatological conditions, GPH increases from the poles towards the Equator at a rate of 10 m/(° lat.) to 20 m/(° lat.) and the gradients $\Delta Z(\lambda)$ are positive. The gradient is generally stronger in the SH and in the winter hemisphere, indicating stronger westerlies.
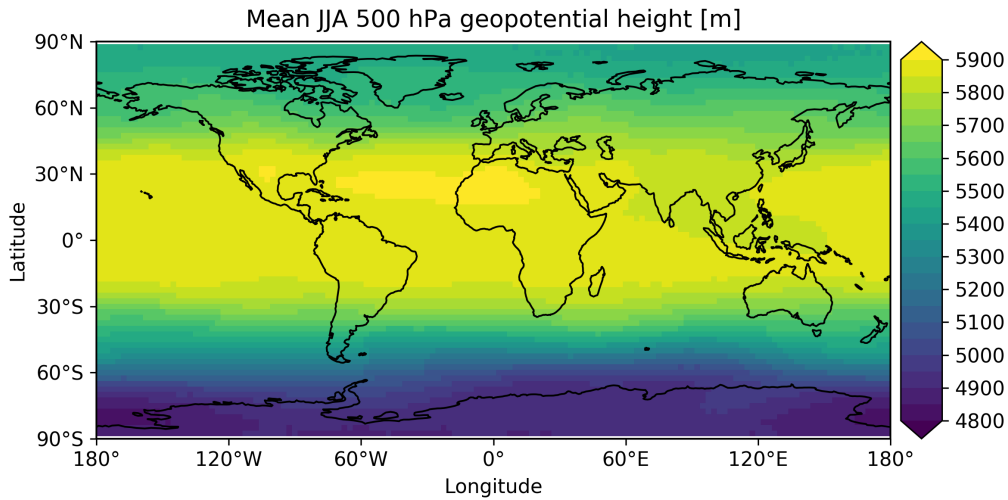
**Figure 3.2.:** Mean geopotential height at 500 hPa in Northern Hemisphere summer (JJA) based on radio occultation data from September 2006 to August 2016.

Lejenäs and Økland ([1983]) and Lejenäs ([1984]) defined a certain longitude $\lambda'$ in the NH or SH as blocked if the GPH gradient is reversed, that is, if $\Delta Z(\lambda')$ is negative:

$$\Delta Z(\lambda') < 0\,\text{m}/(^\circ\,\text{lat.}) \tag{3.2}$$

This blocking index did not include any criteria for the extent or persistence of the block or an actual split of the jet, but was solely based on the reversal of the GPH gradient. Figure 3.3 shows this reversal for an exemplary day during the Russian heatwave in summer 2010 when an Omega-block was located over eastern Europe and Russia. The local maximum in the GPH field was centered at about 50 °E and 60 °N and is clearly visible in this view.

Tibaldi and Molteni ([1990]) adapted Eq. (3.1) for the NH and laid the basis for most modern definitions of GPH-based blocking indices. They allowed for slight variations in the central blocking latitude $\phi$, that is, $Z_{60\,^\circ\text{N}}(\lambda) \to Z(\lambda, \phi)$, with $\phi$ being either 56 °N, 60 °N, or 64 °N. Moreover, to exclude a pure southward shift of the mid-latitude jet from the blocking definition, they used two GPH-gradients $\Delta Z_\text{N}$ and $\Delta Z_\text{S}$:

$$\Delta Z_\text{N}(\lambda, \phi) = \frac{Z(\lambda, \phi + \Delta\phi) - Z(\lambda, \phi)}{\Delta\phi}$$
$$\Delta Z_\text{S}(\lambda, \phi) = \frac{Z(\lambda, \phi) - Z(\lambda, \phi - \Delta\phi)}{\Delta\phi}, \tag{3.3}$$

## 3. Blocking detection methods
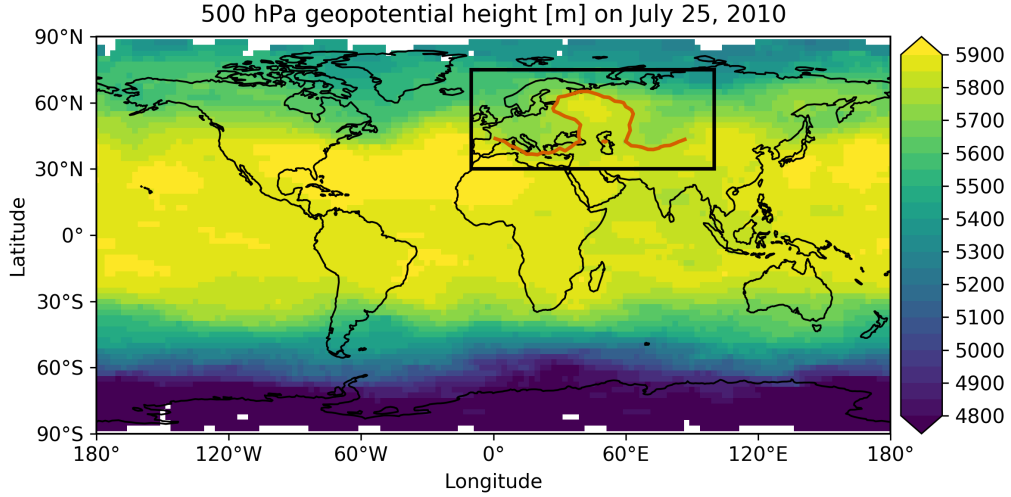


**Figure 3.3.:** Geopotential height at $500\,\mathrm{hPa}$ on July 25, 2010 showing a blocking that occurred over eastern Europe and Russia (black box) based on radio occultation data. The red line shows the $5800\,\mathrm{m}$ GPH contour in the blocking region.

where $\Delta\phi = 20°$. $\Delta Z_\mathrm{S}$ is termed *southern gradient* and is equivalent to $\Delta Z$ in Eq. (3.1) but with the opposite sign, and $\Delta Z_\mathrm{N}$ is the additional *northern gradient.* According to this definition, a certain longitude $\lambda'$ is blocked if the gradients simultaneously fulfill:

$$\Delta Z_\mathrm{N}(\lambda',\phi) < -10\,\mathrm{m}/(°\,\mathrm{lat.}) \tag{3.4}$$
$$\Delta Z_\mathrm{S}(\lambda',\phi) > 0\,\mathrm{m}/(°\,\mathrm{lat.}) \quad \text{with } \phi \text{ in } 56\,°\mathrm{N},\ 60\,°\mathrm{N},\ 64\,°\mathrm{N}$$

for at least one latitude $\phi$.

Scherrer et al. (2006) used the gradient definition from Eq. (3.3), but extend the blocking detection to two dimensions by applying the gradient criteria to all latitudes $\phi$ between $35\,°\mathrm{N}$ and $75\,°\mathrm{N}$. According to their definition, a certain grid point $(\lambda',\,\phi')$ is blocked if the gradients meet:

$$\Delta Z_\mathrm{N}(\lambda',\phi') < -10\,\mathrm{m}/(°\,\mathrm{lat.}) \tag{3.5}$$
$$\Delta Z_\mathrm{S}(\lambda',\phi') > 0\,\mathrm{m}/(°\,\mathrm{lat.})$$

This adaptation broadened the classical blocking definition to include a far greater range of latitudes by also considering events at low latitudes, which are often not considered as blocking in a classical sense (sometimes referred to as *low-latitude blocking*) (e.g., Davini et al. 2012). Also, in order to allow blocking detection as far north as $75\,°\mathrm{N}$, the latitude width over which the gradients are calculated was reduced by $5°$ to $\Delta\phi = 15°$ in the definition by Scherrer et al. (2006).

To filter out events that are too short-lived, Scherrer et al. (2006) added a stationarity criterion. Only grid points where Eq. (3.5) is fulfilled for at least five consecutive days were considered blocked. A weaker form of this persistence criterion has been used by other authors before (e.g., D'Andrea et al. 1998; Doblas-Reyes et al. 2002).

Blocking indices giving a blocking distribution only with regard to longitude are often referred to as *one-dimensional* blocking indices. Indices that resolve blocking in longitude and latitude are equivalently termed *two-dimensional* blocking indices. When looking at the values of blocking frequency, one-dimensional indices often yield significantly higher values since they basically integrate over several latitudes. To compare one- and two-dimensional indices, two-dimensional indices can be reduced to one dimension by defining a certain longitude as blocked if at least one latitude in a certain range (e.g., 50 °N to 75 °N) is blocked.

In recent years, a range of variations and adaptions of the original index of Tibaldi and Molteni have been used (e.g., Barriopedro et al. 2006; Davini et al. 2012; Barnes et al. 2014). Pelly and Hoskins (2003) introduced a different approach based on potential temperature on a potential vorticity (PV) surface, building upon the earlier work by Hoskins et al. (1985). Their index differs from the Tibaldi and Molteni index in several aspects. It uses PV=2 as reference surface for the reversal of potential temperature. This surface corresponds to the approximate height of the dynamical tropopause at about 250 hPa and is, hence, considerably higher up in the atmosphere than the 500 hPa pressure surface, which is normally used in the GPH-based indices. The Pelly and Hoskins index yields maximum blocking frequencies that are almost twice as high compared to the Tibaldi and Molteni index and also shows deviations in the blocking regions and the seasonal variability. Pelly and Hoskins (2003) argued that their index, in particular, is more appropriate for the detection of certain blocking types, such as Omega-blocks.

Schwierz et al. (2004) suggested a blocking indicator based on anomalies of vertically-integrated PV from 500 hPa to 150 hPa. They argued that the choice of the 500 hPa pressure level in the GPH-based indices might not be ideal, since the largest GPH anomalies during blocking episodes tend to appear higher up between 300 hPa to 200 hPa. This was also discussed by Brunner et al. (2016) using GPS RO data. Figure 3.4 shows GPH gradients $\Delta Z_\mathrm{N}(\lambda, \phi)$ and $\Delta Z_\mathrm{S}(\lambda, \phi)$ (defined following Eq. 3.3 but for a larger range of latitudes $\phi$) in a selected region for climatological conditions and for a blocking in winter 2013. During climatological conditions the gradients are between $-15\,\mathrm{m}/(°\,\mathrm{lat.})$ and $-10\,\mathrm{m}/(°\,\mathrm{lat.})$ at 500 hPa, while the strongest gradients between $-20\,\mathrm{m}/(°\,\mathrm{lat.})$ and $-15\,\mathrm{m}/(°\,\mathrm{lat.})$ appear at about 300 hPa (Fig. 3.4a). During a blocking centered in the region, the southern
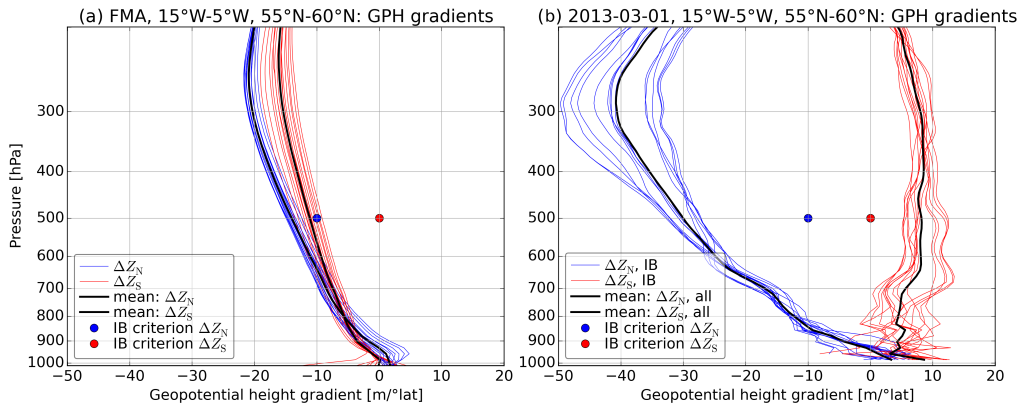
**Figure 3.4.:** Vertical profiles of geopotential height gradients $\Delta Z_S$ (red) and $\Delta Z_N$ (blue) during (a) climatological conditions in February, March, April (FMA) 2013 and (b) on March 1st 2013 during a blocking case. Adapted from Brunner et al. (2016).

gradients ($\Delta Z_S$) become positive in the entire troposphere, with highest values of about $10\,\mathrm{m}/(^\circ\mathrm{lat.})$ found from $500\,\mathrm{hPa}$ to $300\,\mathrm{hPa}$. The northern gradients ($\Delta Z_N$) become more negative, with the strongest decrease of about $-40\,\mathrm{m}/(^\circ\mathrm{lat.})$ found at approximately $300\,\mathrm{hPa}$. As evident from Fig. 3.4b, the largest gradient spread therefore appears considerably above the $500\,\mathrm{hPa}$ pressure level, as high up as $300\,\mathrm{hPa}$.

Several other studies have investigated atmospheric blocking using a PV index (e.g., Dong and Colucci 2005; Berrisford et al. 2007; Tyrlis and Hoskins 2008a; Tyrlis and Hoskins 2008b; Sillmann and Croci-Maspoli 2009; Small et al. 2014; Nakamura and Huang 2017) and a comparison of different blocking indices based on GPH and PV can be found in Barnes et al. (2012). In this work blocking indices are based on the classical $500\,\mathrm{hPa}$ GPH gradient-based approach, following a description given by Davini et al. (2012) and Davini et al. (2014b), which is an adaptation of the Scherrer et al. (2006) index. The main reason for the use of a GPH-based index in this work is that PV is not available as a variable in many data sets and, in particular, not in the GPS RO data set. The use of a gradient-based index also provides independence from a reference climatology, which is needed in anomaly-based approaches. This is particularly important when investigating longer time periods in a changing climate.

The index by Davini and colleagues uses a three-step approach (Davini et al. 2014b):

1. Instantaneous Blocking (IB): is defined at a grid point basis if the gradient criteria Eq. (3.5) are fulfilled on a given day.

2. Extended IB: only IBs with at least 15° continuous extent in longitude are considered to filter out events that are too small.

3. Blocking: is defined at a grid point if an extended IB is found within a region of 10°×5° in longitude and latitude for at least 5 days.

In this work, Brunner et al. (2016) and Brunner et al. (2017) use the same definition but a different implementation based on *Python* in order to allow for direct incorporation into the post-processing system of the Wegener Center for Climate and Global Change (WEGC). Brunner and Steiner (2017) introduce a further updated version as discussed in the next section.

## 3.2. Introducing a global blocking detection algorithm

A global blocking detection algorithm implemented in Python is presented that closely follows the one used by Brunner and Steiner (2017). The algorithm is based on Python's *xarray* package (Hoyer and Hamman 2017) and is available for download via a GitHub repository at https://github.com/lukasbrunner/blocking.git. It is published under the MIT License and, therefore, is open for use and further development.

Adding to the methods introduced above, this index allows the consistent and simultaneous detection of blocking in both hemispheres. It can be applied globally without needing to manually differentiate between NH and SH. In addition, all criteria presented below are optional and manually changeable, so that specific blocking definitions that are consistent, for example, with Lejenäs and Økland (1983), Tibaldi and Molteni (1990), Scherrer et al. (2006), and Davini et al. (2012) are also possible with this index. Furthermore, the index is not limited to the 500 hPa level, where GPH-based blocking detection if typically carried out, but can be applied at arbitrary pressure levels.

First, three GPH gradients at the 500 hPa pressure level over a latitude width of $\Delta\phi = 15°$ are calculated for each latitude between 75 °S and 75 °N:

$$\Delta Z_{\mathrm{N}}(\lambda, \phi) = \frac{Z(\lambda, \phi + \Delta\phi) - Z(\lambda, \phi)}{\Delta\phi} \tag{3.6}$$

$$\Delta Z_{\mathrm{S}}(\lambda, \phi) = \frac{Z(\lambda, \phi - \Delta\phi) - Z(\lambda, \phi)}{\Delta\phi}$$

$$\Delta Z_{\mathrm{Eq}}(\lambda, \phi) = \begin{cases} \Delta Z_{\mathrm{S}}(\lambda, \phi - \Delta\phi) & \text{if } \phi > 15 °\mathrm{N} \\ \Delta Z_{\mathrm{N}}(\lambda, \phi + \Delta\phi) & \text{if } \phi < 15 °\mathrm{S} \\ 0 & \text{else,} \end{cases}$$

where $\Delta Z_N$ and $\Delta Z_S$ are the northern and southern gradients, respectively. Note that, in contrast to some of the definitions given in the last section, both these gradients are defined positive if the GPH increases from the central latitude $\phi$ towards the south ($\phi - \Delta\phi$) or north ($\phi + \Delta\phi$). During climatological conditions, mid-latitude GPH increases from the poles towards the Equator with a rate of about $10\,\mathrm{m}/(°\,\mathrm{lat.})$ to $20\,\mathrm{m}/(°\,\mathrm{lat.})$ at $500\,\mathrm{hPa}$ (see Fig. 3.2), so that $\Delta Z_S$ is negative in the SH and positive in the NH and vice versa for $\Delta Z_N$.

In addition a third gradient is defined, $\Delta Z_{Eq}$, which is termed the *equatorward gradient*. In the SH, $\Delta Z_{Eq}$ is defined as positive at a latitude $\phi$ if at a distance $\Delta\phi$ northward (equatorward) of that latitude the northern gradient $\Delta Z_N(\phi + \Delta\phi)$ is positive. Equivalent considerations are valid for the NH. This third gradient is used to avoid the detection of low latitude blocking by ensuring a clear trough in the GPH field between the block and the Equator.

IB is defined at a certain grid point ($\lambda'$, $\phi'$) if the three gradients simultaneously fulfill:

$$
\begin{aligned}
\Delta Z_N(\lambda', \phi') &\begin{cases} < -10\,\mathrm{m}/(°\,\mathrm{lat.}) & \text{if } \phi' \geq 0° \\ < 0\,\mathrm{m}/(°\,\mathrm{lat.}) & \text{else} \end{cases} \\[2ex]
\Delta Z_S(\lambda', \phi') &\begin{cases} < 0\,\mathrm{m}/(°\,\mathrm{lat.}) & \text{if } \phi' \geq 0° \\ < -10\,\mathrm{m}/(°\,\mathrm{lat.}) & \text{else} \end{cases} \\[2ex]
\Delta Z_{Eq}(\lambda', \phi') &\ > 5\,\mathrm{m}/(°\,\mathrm{lat.})
\end{aligned}
\tag{3.7}
$$

Note that, although all GPH-gradients $\Delta Z$ are defined at the $500\,\mathrm{hPa}$ pressure level, they are not restricted to that level. The algorithm allows gradient calculation at arbitrary pressures levels $p$, hence, $\Delta Z(\lambda, \phi) \rightarrow \Delta Z(\lambda, \phi, p)$. The same considerations hold true for the definition of IB and all subsequent definitions.

Extended IB is defined as an IB that is continuously found over at least 15° in longitude, in order to filter out systems that are too small-scale. Finally, blocking is defined if extended IB is persistent and stationary, that is, if extended IB is also found on each of the neighboring ±2 days within a box of 10° in longitude ($\lambda' \pm 5°$) and 5° in latitude ($\phi' \pm 2.5°$) at a certain grid point at longitude $\lambda'$ and latitude $\phi'$. Figure 3.5 shows the steps of blocking detection in a Hovmöller diagram (time versus longitude) indicating IB, extended IB, and blocking over eastern Europe and Russia for the case of summer 2010. The effect of the extension and duration criteria can be seen from the fact that several light and dark gray features (IB and extended IB, respectively) are not identified as blocking as they are too small or do not last long enough.
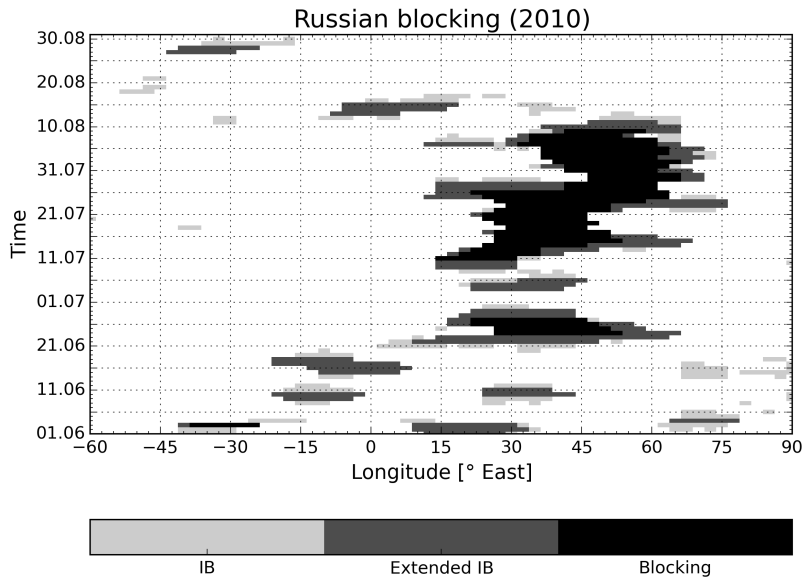
**Figure 3.5.:** Longitude-time (Hovmöller) diagram of blocking over eastern Europe and Russia during summer 2010. Blocking is considered from 50 °N to 65 °N. Shading indicates the three blocking detection steps: Instantaneous Blocking (light gray), extended Instantaneous Blocking (dark gray), and blocking (black). Adapted from Brunner et al. (2016).

Figure 3.6 shows two-dimensional, annual mean blocking frequencies based three variations of the global blocking detection index introduced above, using RO data for the period of September 2006 to August 2016. Figure 3.6a depicts the IB frequency, without applying the third gradient criterion $\Delta Z_{\mathrm{Eq}}$ defined in Eq. (3.7). The highest IB frequencies for this case are found equatorward of about 45° latitude. The black boxes highlight the 55° to 65° latitude range. Considering only IB in this area in the NH is approximately equivalent to the index used by Tibaldi and Molteni (1990). As can be seen from the IB frequency distribution, several main blocking areas are missed when restricting the detection latitudes to this rather narrow range for the NH. In the SH, the IB frequency maxima are, in fact, outside this range, since blocking there tends to be located at lower latitudes (Lejenäs 1984).

Figure 3.6b shows annual mean blocking frequencies again without the $\Delta Z_{\mathrm{Eq}}$ criterion. Using this definition yields a band of very high blocking frequencies at low latitudes in both hemispheres. When considering blocking in the classical sense, this figure clearly illustrates the need for a certain amount of restriction to avoid the detection of the slow moving atmospheric ridges at low latitudes. Different
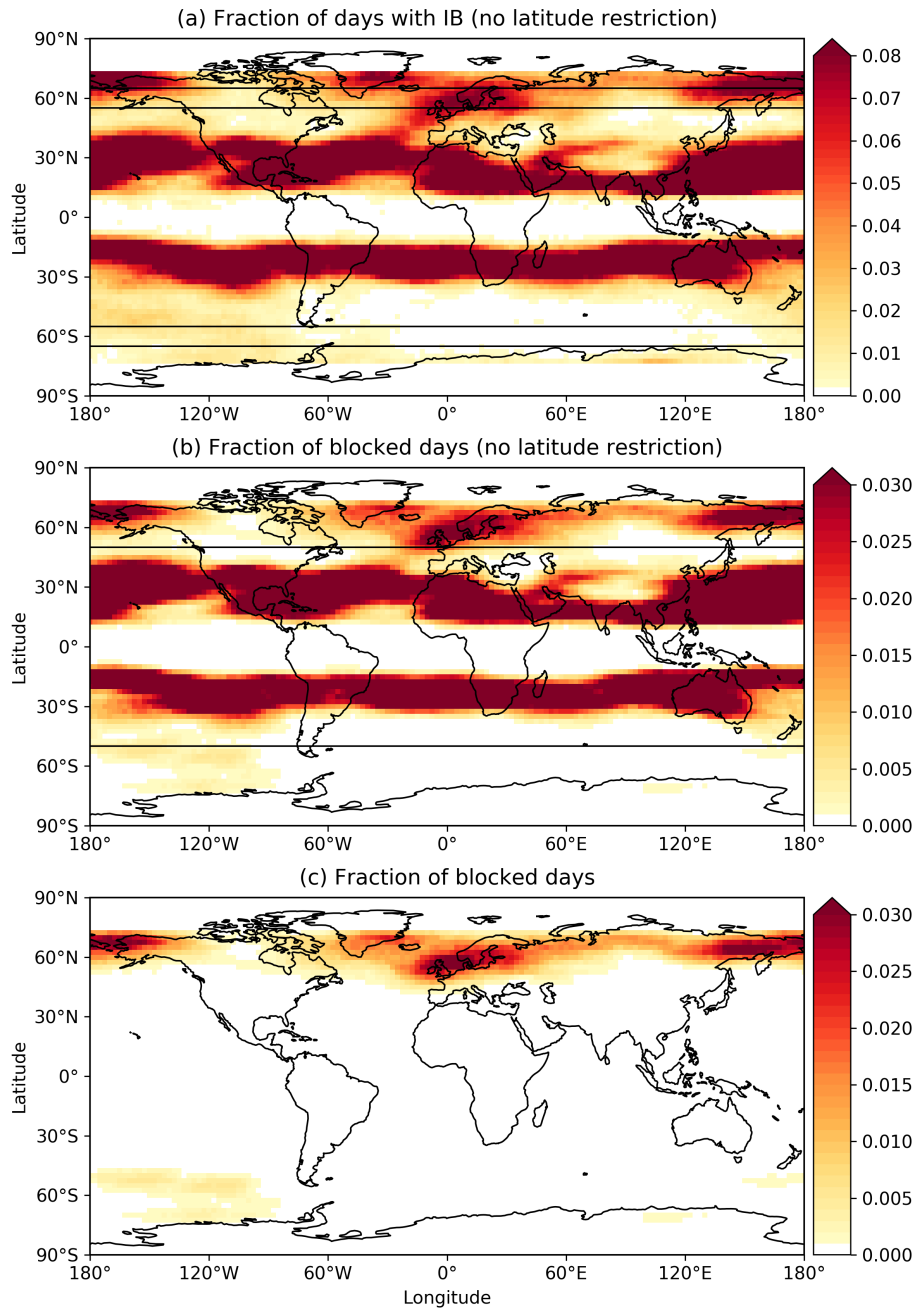
**Figure 3.6.:** Annual mean frequency of (a) instantaneous blocking without latitude restriction, (b) blocking without latitude restriction, and (c) blocking with latitude restriction. The black boxes in (a) indicate the 55° to 65° latitude range corresponding to the blocking index by Tibaldi and Molteni (1990) for the Northern Hemisphere. The black lines in (b) indicate 50° latitude as a possible cut-off for slow moving ridges at low-latitudes. Note the differing color bar range in (a).
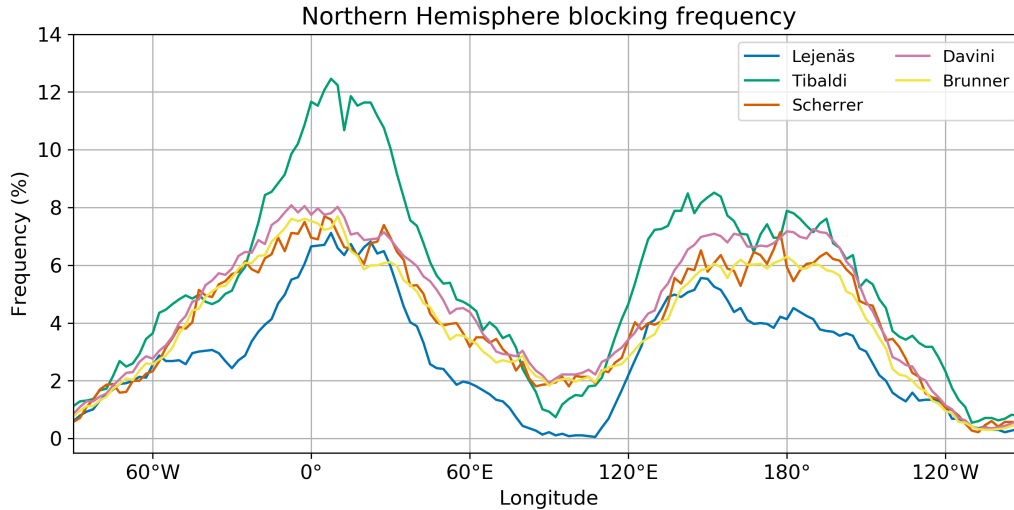
**Figure 3.7.:** Comparison of different blocking indices in the Northern Hemisphere based on radio occultation data from September 2006 to August 2016.

authors have used various latitude restrictions for blocking detection (Tibaldi and Molteni 1990; Barriopedro et al. 2006; Scherrer et al. 2006; Davini et al. 2012; Davini et al. 2014b), and the black lines in Fig. 3.6b indicate 50° latitude as one possible cut-off value. However, as can be seen from Fig. 3.6b, it does not seem feasible to separate blocking by a single cut-off latitude. Moreover, the zone of the low-latitude blocking maxima is not constant over the year but shifts poleward during the hemispheric summers, so that a seasonally moving cut-off latitude could be considered necessary. In the SH, a cut-off value near 40 °S would be more appropriate. So, in order to avoid the use of such multiple and somewhat arbitrary cut-off latitudes, a third gradient criterion is used in this work as defined in Eq. 3.7.

Figure 3.6c shows the annual mean blocking frequencies when restricting $\Delta Z_{\mathrm{Eq}} > 5 \, \mathrm{m}/(°\,\mathrm{lat.})$. While the mid-latitude blocking maxima in both hemispheres remain nearly constant, the low-latitude blocking disappears for this case. In this view, the three main blocking regions are clearly visible: the Euro-Atlantic region and the North Pacific region in the NH as well as the southeastern Pacific region in the SH.

Figure 3.7 presents a comparison of one-dimensional blocking frequencies based on several different indices in the NH using RO data in the period of September 2006 to August 2010. The indices by Scherrer et al. (2006) (labeled Scherrer in Fig. 3.7) and Davini et al. (2014b) (labeled Davini) have been reduced to one dimension by defining a certain longitude as blocked if at least one latitude between 50 °N and 75 °N is blocked. The index used in this work (labeled Brunner)

is reduced to one dimension by defining a certain longitude as blocked if at least one latitude in the NH is blocked. The definition of Tibaldi and Molteni (1990) (labeled Tibaldi) has been slightly adapted here in order to be able to use data on the same grid. Instead of the three defined latitudes (56 °N, 60 °N, 64 °N), five latitudes (55 °N, 67.5 °N, 60 °N, 62.5 °N, 65 °N) are used.

Comparing the index by Lejenäs and Økland (1983) (labeled Lejenäs) to the Tibaldi index, the dominating feature is an increase in frequency in the Tibaldi index due to the expansion of the blocking latitude from only 60 °N to five latitudes between 55 °N and 65°, superimposing the additional gradient criterion which is used in the Tibaldi index.

A notable difference is also visible between the indices without a persistence-criterion (Lejenäs, Tibaldi) and the indices which demand at least five consecutive blocked days (Scherrer, Davini, Brunner), particularly in the Euro-Atlantic blocking region. The maximum blocking frequency in the latter is clearly located further to the west, indicating that anti-cyclones westward of the British Isles are more persistent (compare frequency maxima over Greenland in Fig 3.6a and b with and without stationarity-criterion, respectively).

Only minor differences appear between the Scherrer, Davini, and Brunner indices, indicating that blocking frequency is not very sensitive to the exact definitions of the extension and stationarity-criterion.

# 4. Data sets for blocking research

The systematic and consistent detection of blocking on a global scale requires several demanding properties of potential data sets. Blocking indices are often applied at the 500 hPa pressure level, which excludes the direct use of any in situ measurements on the surface. For the calculation of the GPH gradients, data on a regular grid with a sufficiently fine temporal and horizontal resolution are needed. In situ measurements of the free atmosphere mostly rely on radiosondes or airplanes, which sample far too sparsely to allow for the creation of blocking-resolving GPH or PV fields. In recent decades, new, satellite-based, observational data records have become available which promise to overcome these constraints. The GPS RO method provides such a data set, which allows blocking detection and analysis based on a single, integrated measurement system.

So far, however, blocking research has mostly been based on reanalyses or climate models, which are discussed in chapter 4.1 and chapter 4.2, respectively. GPS RO observations, the data characteristics, and use for blocking research are introduced in chapter 4.3.

## 4.1. Reanalyses

Reanalyses are a frequently used data foundation in many fields of climate research. Observations from a range of different measurement systems are combined with a model to produce a global picture of the atmospheric state that is as accurate as possible (Dee et al. 2014; Parker 2016). Several large processing centers provide reanalysis products that are free to download for scientific use. Some of the most frequently-used reanalyses are produced by the European Centre for Medium-Range Weather Forecasts (ECMWF), the National Center for Atmospheric Research (NCAR)/National Centers for Environmental Prediction (NCEP), the National Aeronautics and Space Administration (NASA), and the Japanese Meteorological Agency (JMA). Table 4.1 summarizes some reanalyses products, available time periods, and reference publications. An overview of different reanalysis products can also be found in Fujiwara et al. (2017, Table 1) and in a regularly-updated, online summary by Dee et al. (2016).

**Table 4.1.:** Summary of frequently used reanalysis products, processing centers, coverage periods, and reference publications.

| Center | Product name | Coverage | Reference |
|---|---|---|---|
| ECMWF | ECMWF 40-year reanalysis (ERA-40) | 1957 - 2002 | Uppala et al. (2005) |
| | ECMWF Reanalysis Interim (ERA-Interim) | 1979 - present | Dee et al. (2011) |
| NCAR/ NCEP | NCAR reanalysis (R-1) | 1948 - present | Kalnay et al. (1996) |
| | NCEP–Department of Energy reanalysis (R-2) | 1979 - present | Kanamitsu et al. (2002) |
| NASA | Modern-Era Retrospective analysis for Research and Applications (MERRA) | 1979 - 2016 | Rienecker et al. (2011) |
| | MERRA-2 | 1980 - present | Gelaro et al. (2017) |
| JMA | Japanese 25-year reanalysis (JRA-25) | 1979 - 2004 | Onogi et al. (2007) |
| | JRA-55 | 1958 - present | Kobayashi et al. (2015) |

The representation of NH blocking frequencies in reanalyses has been investigated by Barnes et al. (2014) using different detection indices for four different reanalyses (ERA-Interim, MERRA, R-1, R-2). They particularly highlighted the fact that blocking trends can differ depending on the reanalysis in use, noting that "studies using different reanalysis products could disagree on 'observed' trends in blocking, even if the same blocking identification method is employed" (Barnes et al. 2014). More generally, it has been noted that the data assimilation process employed in the creation of reanalysis products, leads to a less well understood accuracy of variables (Parker et al. 2014) and can result in deficiencies in the representation of the free atmospheric state (Fujiwara et al. 2017). In this context, Simmons et al. (2017) concluded that the "use of reanalysis to monitor recent and future change requires a careful, comparative and selective approach. [...] Some reanalyses are more fit for purpose than others for a particular application such as surface temperature trends, whereas others may be competitive for other applications".

In blocking research, reanalyses have, so far, been the only observation-based data set in use. The reanalyses by NCAR/NCEP (e.g., Renwick and Revell 1999; Trigo et al. 2004; Davini et al. 2014b) and ECMWF (e.g., Sinclair 1996; Woollings et al. 2010; Sillmann et al. 2011; Schneidereit et al. 2012; Schiemann et al. 2017) are particularly frequently used.

In this thesis, ERA-Interim (Brunner et al. 2016; Brunner et al. 2017; Brunner and Steiner 2017) as well as JRA-55 and MERRA-2 (Brunner and Steiner 2017) are used for blocking detection and comparison to observations. ERA-Interim, JRA-55, and MERRA-2 have been chosen, since they constitute three of the most recent reanalyses and have been found to deliver consistent temperature fields (Brunner and Steiner 2017; Long et al. 2017). The GPS RO record introduced in chapter 4.3 has the potential to complement reanalyses as an observational data set of known accuracy and with clearly-defined uncertainties (e.g., Leroy et al. 2006; Foelsche et al. 2011; Schreiner et al. 2007). Brunner et al. (2016, presented page 45ff.) show the potential of RO for the first time for exemplary blocking events. Brunner and Steiner (2017, presented page 57ff.) analyze the complete RO record and compare it to reanalyses.

## 4.2. Climate models

For the prediction of blocking in numerical weather prediction (NWP) and for the investigation of future blocking evolution various models have been used over the years. Many researchers have also investigated the representation of historical blocking in models of different types and/or resolutions, especially in the NH.

D'Andrea et al. (1998) compared 15 models from the first Atmospheric Model Intercomparison Project (AMIP) (Gates 1992). They found a wide range of behaviors, with most models considerably underestimating the blocking frequency, with respect to reanalyses. Other studies have since found similar results in different model generations, especially for the Euro-Atlantic blocking region (Barnes et al. 2012; Vial and Osborn 2012; Anstey et al. 2013; Christensen et al. 2013; Dunn-Sigouin and Son 2013; Masato et al. 2013; Davini and D'Andrea 2016). Regarding the SH, researchers have found that the model performance in the representation of blocking in terms of both frequency and persistence also needs considerable improvement (Anderson 1993; Matsueda et al. 2010; Grose et al. 2012; Marshall et al. 2014).

Davini and D'Andrea (2016) investigated the development of blocking representation in models over the last 20 years. They used models included in the coordinated modeling approaches AMIP as well as the Coupled Model Intercom-
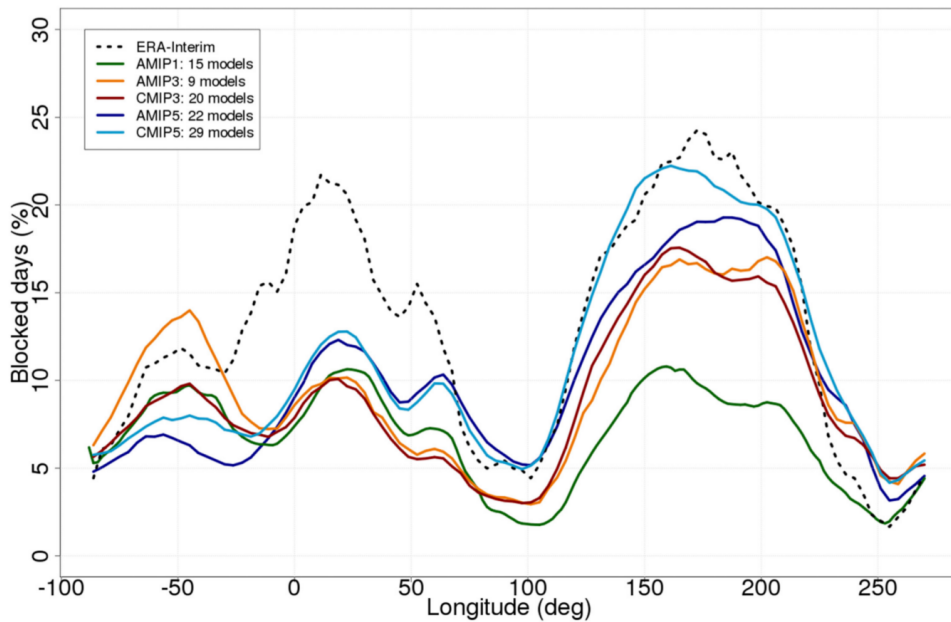
**Figure 4.1.:** Instantaneous blocking frequencies based on different multi-model ensemble means (colored lines) and ERA-Interim (black dotted line) in winter (DJF) over the period of 1979 to 1988. Reprinted from Davini and D'Andrea (2016) with permission from the authors.

parison Project phase three (CMIP3) (Meehl et al. 2007) and five CMIP5 (Taylor et al. 2012). The multi-model mean of the latest CMIP5 models still underestimates the maximum frequency in the Euro-Atlantic blocking sector by almost 50 % compared to ERA-Interim (Fig. 4.1). However, several individual models have developed significantly over the years, and the authors acknowledge the "slow but constant improvements" due to increased resolution, better dynamics, and new parameterization schemes (Davini and D'Andrea 2016).

Recently, Schiemann et al. (2017) analyzed the resolution sensitivity of NH blocking in atmospheric General Circulation Models (GCMs) with a very fine, 25 km grid spacing. They found increasingly realistic blocking representation with finer grid spacing, however, also highlighted that "considerable biases remain also at that resolution" (Schiemann et al. 2017).

It has also been shown that stratospheric processes and feedbacks play an important role in tropospheric dynamics. Karpechko and Manzini (2012) compared "low top" models, with the highest level at 10 hPa (about 30 km), with stratosphere-resolving "high top" models, which extend up to 0.01 hPa (about 80 km). They conclude that "stratosphere-resolving models can lead to a significant improvement

of tropospheric climate predictions" (Karpechko and Manzini 2012). Specifically for blocking, several researchers have investigated the connection to stratospheric processes and have found links to the stratospheric polar vortex, sudden stratospheric warming events, and stratospheric ozone (O'Neill et al. 1994; Taguchi 2008; Barriopedro et al. 2010a; Castanheira and Barriopedro 2010; Woollings et al. 2010; Cullen and Ngan 2013; Ayarzagüena et al. 2015).

Pfahl et al. (2015) discussed the importance of latent heat in the formation and maintenance of blocking. Their results indicate that "systematic problems in blocking forecasts [. . . ] may be due to an erroneous representation of latent heating in weather prediction models", and that "in addition to changes in horizontal temperature gradients, Rossby wave dynamics and sea ice cover, the enhanced atmospheric moisture content and its effect on latent heating must be considered when pondering about future changes of atmospheric blocking" (Pfahl et al. 2015).

In summary, there is increasing trust in the assessment of blocking occurrence and blocking impacts based on the latest, high-resolution climate models. Improved process understanding of the formation and evolution of blocks will contribute to an increasingly realistic blocking representation. Also, efforts are ongoing to further enhance model resolution, for example, within the frame of the High Resolution Model Intercomparison Project (HighResMIP) (Haarsma et al. 2016) as part of CMIP6 (Eyring et al. 2016).

To evaluate the model performance in blocking-representation reliable reference data sets, with high accuracy and known uncertainty are needed. Reanalyses are currently frequently used for this purpose. However accuracy and uncertainty in reanalyses are less well understood compared to observations (Parker 2016). In this context, the next section introduces the GPS RO record, which is the first observational data set to allow blocking detection and, therefore, has the potential to complement reanalyses as a reference data set.

## 4.3. Observations from radio occultation

Global Navigation Satellite System (GNSS) RO is a relatively new remote sensing technique for exploring the Earth's atmosphere (Kursinski et al. 1997; Hajj et al. 2002). It delivers key properties of the free atmosphere, such as pressure, GPH, temperature, and specific humidity. RO measurements are based on radio signals emitted by GNSS satellites, which operationally have, so far, only been GPS satellites (Anthes 2011; Steiner et al. 2011). The rays are refracted by the Earth's atmosphere and are received by a Low Earth Orbit (LEO) satellite in a limb-sounding geometry.
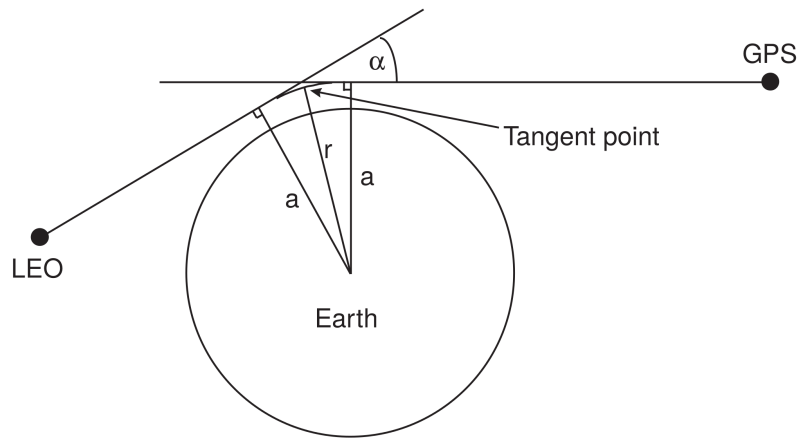
**Figure 4.2.:** Schematic GPS-LEO satellite occultation geometry. The ray path from the transmitter to the receiver is indicated, with the atmospheric bending angle $\alpha$, the impact parameter $a$, and the radius to the tangent point $r$. Reprinted from Steiner et al. (1999).

Figure 4.2 shows the schematic occultation geometry for an RO event. Due to the different orbits and resulting different relative velocities of the GPS and LEO satellites, the signal traveling from the GPS to the LEO satellite scans vertically through the atmosphere during such an *occultation event*. Each occultation event, therefore, yields a vertically-resolved measurement of the atmosphere (termed RO *profile* in the following). The profiles have a very high vertical resolution of about 100 m in the troposphere and 1.5 km in the stratosphere (Gorbunov et al. 2004). The horizontal resolution lies between about 60 km in the troposphere and about 300 km in the stratosphere along the ray and about 1.5 km across-ray at all altitudes (Kursinski et al. 1997). RO measurements are long-term stable and do not need satellite-to-satellite inter-calibration, since the phase measurements are based on time measurements with highly precise clocks aboard the GPS and LEO satellites (e.g., Foelsche et al. 2011; Ho et al. 2012; Steiner et al. 2013). The GPS radio waves (of about 20 cm wavelength) are not disturbed by clouds, allowing RO measurements to be taken under all weather conditions. The measurements provide data with high accuracy, of about 10 m for GPH in the upper troposphere/lower stratosphere region (Scherllin-Pirscher et al. 2011b; Scherllin-Pirscher et al. 2017).

The first RO measurements of the Earth's atmosphere were carried out during the GPS/Meteorology proof-of-concept mission conducted from 1995 to 1997 (Melbourne et al. 1994; Kursinski et al. 1996; Ware et al. 1996; Steiner et al. 1999). Since 2001 the Challenging Minisatellite Payload (CHAMP) satellite continuously provided about 200 RO profiles per day and since the launch of the first dedicated
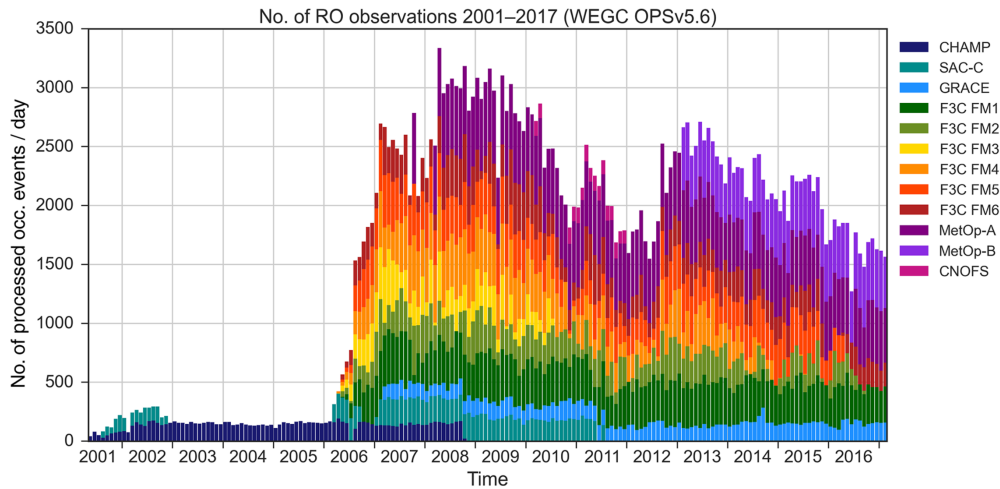
**Figure 4.3.:** Daily number of high-quality radio occultation profiles for different satellites (different colors) as a function of time from 2001 to 2017. Reprinted from Angerer et al. (2017).

RO mission, the Formosa Satellite mission #3/Constellation Observing System for Meteorology, Ionosphere, and Climate (FORMOSAT-3/COSMIC) in April 2006, about 1500 to 2500 RO profiles are available per day on average. Figure 4.3 shows the monthly mean of high-quality RO profiles per day in the WEGC occultation processing system version 5.6 (OPSv5.6) record from 2001 to 2017. With FORMOSAT-3/COSMIC global coverage is possible on a scale which allows the resolution of synoptic-scale atmospheric pattern such as blocking as depicted by Brunner et al. (2016, Fig. 1, page 48). In the future, further dedicated RO missions, like the planned FORMOSAT-7/COSMIC-2 mission (Yue et al. 2014) and the planned European MetOp follow-on series, will multiply the number of events and allow for an even finer resolution and better representation of blocking. Moreover, the launch of other GNSS systems beside GPS, like the European Galileo, the Russian GLONASS, and the Chinese BeiDou will significantly increase the number of potential transmitters and the number of total profiles (Anthes 2011).

RO observations have already been used for a range of weather (e.g., Healy and Thépaut 2006; Cardinali 2009) and climate applications (e.g., Anthes 2011; Steiner et al. 2011; Gleisner et al. 2015; Randel and Wu 2015) and are assimilated into several reanalyses (e.g., Poli et al. 2010; Kobayashi et al. 2015; McCarty et al. 2016), where they serve as anchor measurements. RO data were also used to investigate dynamical features of the Earth's atmosphere, such as the planetary boundary layer (Engeln et al. 2005), the tropopause (Schmidt et al. 2008; Rieckh et al. 2014; Peevey
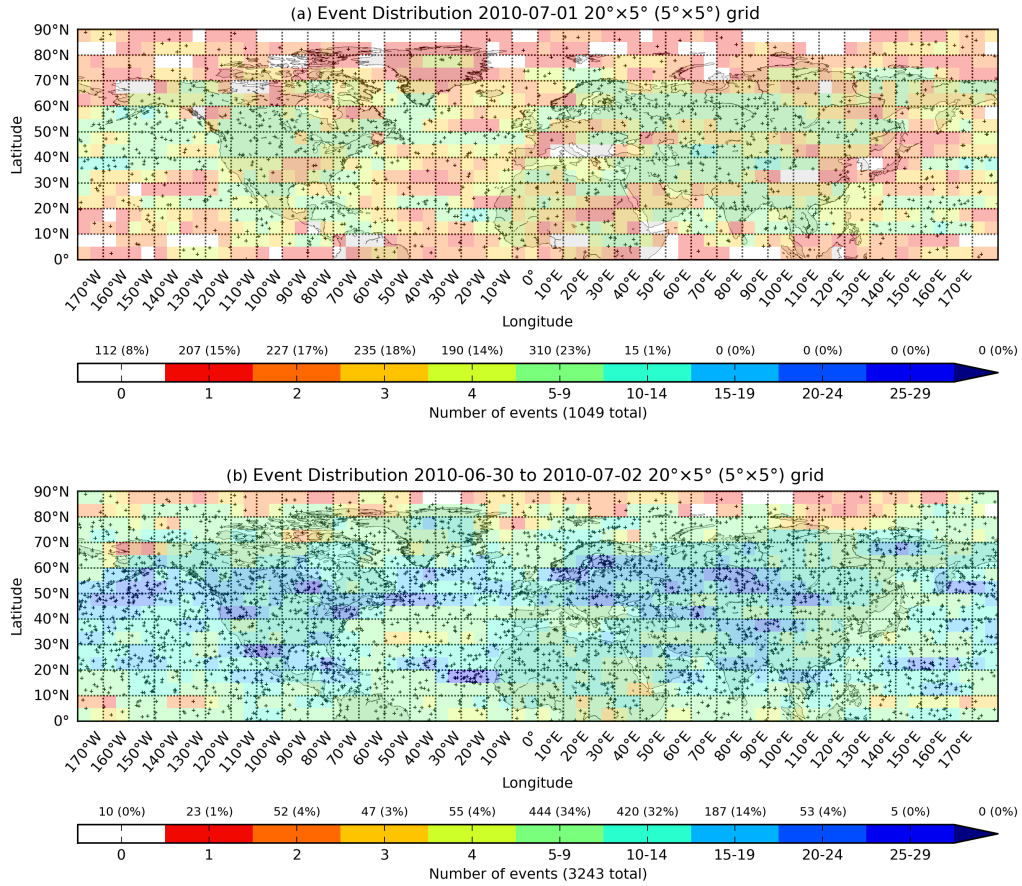
**Figure 4.4.:** Distribution of radio occultation profiles in the Northern Hemisphere for (top) one day on July 1, 2010 and (bottom) three days from June 30 to July 2, 2010 with an effective resolution of 20°×5° in longitude and latitude. The location of individual profiles is indicated by plus signs and the number of profiles per grid cell as shading.

et al. 2014), the El Niño-Southern Oscillation (ENSO) (Scherllin-Pirscher et al. 2012; Sun et al. 2014), wind fields (Scherllin-Pirscher et al. 2014), atmospheric tides and waves (Randel et al. 2003; Torre and Alexander 2005; Randel and Wu 2005; Schmidt et al. 2005; Pirscher et al. 2010; Tsuda 2014), the thermodynamic structure of cyclones (Biondi et al. 2015), and now –as part of this thesis– atmospheric blocking (Brunner et al. 2016; Brunner and Steiner 2017).

In this work, quality-controlled (Angerer et al. 2017) RO profiles that were processed with the WEGC OPSv5.6 (Schwärz et al. 2016) from September 2006 to August 2016 are used. Before the blocking detection, the profiles were brought to a consistent grid. In the vertical domain, each profile was interpolated to pressure

levels $p$ corresponding to an altitude grid $z$ with equidistant $200\,\mathrm{m}$ steps and calculated as

$$p(z) = p_0 \exp\left(-\frac{z}{H}\right), \tag{4.1}$$

with the standard surface pressure $p_0 = 1013.25\,\mathrm{hPa}$ and the scale height $H = 7000\,\mathrm{m}$. Horizontally, the profiles $x_i$ were averaged to a regular $2.5°\times2.5°$ longitude-latitude grid $x_\mathrm{grid}$ by applying a weighted mean given as:

$$x_\mathrm{grid}(\lambda, \phi, d) = \frac{\sum_i w_i x_i(\lambda_i, \phi_i, d_i)}{\sum_i w_i} \quad \text{with} \tag{4.2}$$

$$w_i = \begin{cases} \exp\left(-\left[\left(\frac{\Delta\lambda_i}{L}\right)^2 + \left(\frac{\Delta d_i}{D}\right)^2\right]\right) & \text{if } (\lambda_i, \phi_i, d_i) \text{ in } (\lambda \pm 7.5°, \phi \pm 2.5, d \pm 2) \\ 0 & \text{else,} \end{cases}$$

where $\Delta\lambda_i = \lambda - \lambda_i$ is the (continuous) longitudinal distance of a certain profile at a longitude $\lambda_i$ with reference to the grid center $\lambda$, $\Delta d_i = d - d_i$ is the (discrete) temporal distance of a certain profile on a day $d_i$ to the reference day $d$, $L = 7.5°$, and $D = 1$ day (see also Randel and Wu 2005). The grid resolution of $2.5°\times2.5°$ has been chosen to be consistent with many reanalyses and climate models and because it is a frequently-used resolution for blocking detection (Barriopedro et al. 2006; Scherrer et al. 2006; Davini et al. 2014b). The effective resolution to average the profiles of five days and $15°\times5°$ in longitude and latitude has been selected to minimize the number of empty grid cells, while still being able to resolve the maximum amount of atmospheric variability (Brunner et al. 2016).

During the course of this work, several other resolutions have been tested in order to find the optimal possible resolution. Figure 4.4 shows examples of the NH RO event distribution for two slightly different effective resolutions: $20°\times5°$ and for one day (Fig. 4.4a) as well as for three days (Fig. 4.4b). For the first case about $10\,\%$ of the grid cells are empty and empty cells can appear at all latitudes. Since the detection algorithm employed in this work requires blocking to extend *continuously* over $15°$ longitude and to persist for at least five *consecutive* days, empty grid cells can significantly lower the blocking frequency if they appear during a blocking, and hence, artificially interrupt it (Brunner and Steiner 2017). Also, more than $30\,\%$ of the grid cells in Fig. 4.4a have fewer than three contributing RO profiles, prohibiting the calculation of the standard deviation of individual profiles as a measure of uncertainty for many grid cells at this resolution. If also events from the neighboring days are used for computing the grid cell mean, over $90\,\%$ of grid cells have more than three contributing RO profiles and hardly any empty grid cells appear (Fig. 4.4b). Based on a comparison of different settings, averaging

over additional days was found to perform better in order to be able to increase the longitudinal resolution. Therefore the final effective resolution of five days and 15°×5° in longitude and latitude was chosen (Brunner et al. 2016, Fig. 1, page 48). The gridded RO data set, covering one decade from September 2006 to August 2016, is available online via the Climate Change Centre Austria (CCCA) under a CC BY license. The variables GPH (https://hdl.handle.net/20.500.11756/e4f48220), temperature (https://hdl.handle.net/20.500.11756/8245c63e), and specific humidity (https://hdl.handle.net/20.500.11756/122eeb7a) are provided.

The gridded daily RO fields have then been used to detect blocking and to analyze blocking impacts on free atmospheric variables (Brunner et al. 2016; Brunner and Steiner 2017). Data from RO measurements are found to be "very well suited for blocking detection and for providing information on the atmospheric structure during blocking episodes" (Brunner et al. 2016) and they provide a "mostly independent, comprehensive observation-based record of known accuracy [. . . ] complementing reanalyses and models" (Brunner and Steiner 2017). In this sense, RO data are a promising new data set for blocking research.

# 5. Summary and conclusions

Atmospheric blocking describes stationary high-pressure systems at mid-latitudes, which persist for up to several weeks. They interrupt the climatological westerly flow and can lead to the development of extreme events, such as heat waves and cold spells. Atmospheric blocking has been investigated intensively in recent decades based on data from reanalyses and models, and with a focus on impacts on the surface in summer and winter. However, blocking is still significantly underestimated in current climate models and its future evolution in a changing climate remains uncertain.

This thesis, including the synopsis in part I and foremost the published papers in part II, provided a new perspective on atmospheric blocking from observations. It addressed the detection of blocking on a global scale, analyzed the free atmospheric structure during blocking events, and looked into impacts of blocking on surface extremes. Measurements from GPS RO have, for the first time, been introduced for blocking research. Is has been shown that this highly accurate data set is fully capable of blocking detection and analysis on a global scale. Blocking development during the spring season has been investigated and statistically highly significant links to European temperature extremes have been proven.

Quality controlled RO measurements processed with the WEGC OPSv5.6 for the time period from September 2006 to August 2016 have been used in this work. We demonstrated the feasibility of blocking detection with RO for two well-known blocking events in summer 2010 and late winter 2013. Results of this work, presented in paper I, show that observations from RO capture the atmospheric structure during these two blocking cases well, compared to established reanalyses and the scientific literature (Brunner et al. 2016). The vertically resolved atmospheric GPH and temperature from RO reveals strong positive anomalies in the entire troposphere during both blocking events exceeding 300 m and 10 K (Brunner et al. 2016).

Building on the excellent performance of RO in the feasibility study, the RO record from 2006 to 2016 was used to systematically detect and analyze blocking in the entire period as well as on a global scale in paper II. Results show that RO data fully capture the main blocking regions in both hemispheres as well as the

seasonal variability. RO observations slightly underestimate blocking occurrences compared to reanalyses, which is expected to improve in the future as a denser RO measurement coverage becomes available from planned GNSS and RO missions (Brunner and Steiner 2017).

RO measurements are particularly well-suited for investigating the vertically resolved atmospheric structure during blocking events. Strong positive anomalies in tropospheric temperature and specific humidity composites occur at the location of the blocking. In the lower stratosphere, negative temperature anomalies are present while specific humidity anomalies decreased rapidly above the tropopause. A distinct band of tropospheric cold and dry anomalies surrounding the blocking center indicates for the anti-cyclonic motion of air around blocking high-pressure systems (Brunner and Steiner 2017).

RO measurements are available globally in the same high quality and, therefore, provide a consistent data basis for both hemispheres covering the troposphere and lower stratosphere. They are mostly independent and have clearly defined accuracy. Future planned development in the reprocessing will further improve the accuracy and make it traceable back to the standard of the International System of Units (SI) second (e.g., Schwarz et al. 2017, and references therein), making RO an ideal reference data set. The data used in this work will be made freely available for the community in the near future. In conclusion, RO measurements provide a promising new data set for blocking research, which can be used to detect and analyze blocking high-pressure systems and study their impacts on the free atmosphere.

In paper III we investigated the connection of blocking to warm and cold spells in Europe over a longer time span 1979 to 2014, using the observation-based ERA-Interim for blocking detection and the European daily high-resolution gridded dataset (E-OBS) for the detection of extremes. Results show for summer a statistically significant correlation of blocking to warm spells as well as a statistically significant anti-correlation with cold spells and vice versa for winter. In the transition season of spring blocking is linked to extremes on both ends of the temperature distribution. The link changes through the spring season with a decreasing impact of blocking on cold conditions toward summer and vice versa for warm conditions (Brunner et al. 2017).

Temperature anomalies in the spring season are of particular relevance as they can have devastating effects on vegetation in the early green-up phase and, hence, affect agriculture and economy. Continued research on extreme events, their impacts, and their drivers in the spring season is crucial in light of the disturbances due to continued climate change (e.g., Cassou and Cattiaux 2016).

# Part II.

# Published papers

Atmospheric
Chemistry
and Physics

# Exploring atmospheric blocking with GPS radio occultation observations

**Lukas Brunner**[1,2], **Andrea K. Steiner**[1,2,3], **Barbara Scherllin-Pirscher**[1,3], **and Martin W. Jury**[1]

[1]Wegener Center for Climate and Global Change (WEGC), University of Graz, Graz, Austria
[2]FWF-DK Climate Change, University of Graz, Graz, Austria
[3]Institute for Geophysics, Astrophysics, and Meteorology, Institute of Physics, University of Graz, Graz, Austria

*Correspondence to:* Lukas Brunner (lukas.brunner@uni-graz.at)

**Abstract.** Atmospheric blocking has been closely investigated in recent years due to its impact on weather and climate, such as heat waves, droughts, and flooding. We use, for the first time, satellite-based observations from Global Positioning System (GPS) radio occultation (RO) and explore their ability to resolve blocking in order to potentially open up new avenues complementing models and reanalyses. RO delivers globally available and vertically highly resolved profiles of atmospheric variables such as temperature and geopotential height (GPH). Applying a standard blocking detection algorithm, we find that RO data robustly capture blocking as demonstrated for two well-known blocking events over Russia in summer 2010 and over Greenland in late winter 2013. During blocking episodes, vertically resolved GPH gradients show a distinct anomalous behavior compared to climatological conditions up to 300 hPa and sometimes even further up into the tropopause. The accompanying increase in GPH of up to 300 m in the upper troposphere yields a pronounced tropopause height increase. Corresponding temperatures rise up to 10 K in the middle and lower troposphere. These results demonstrate the feasibility and potential of RO to detect and resolve blocking and in particular to explore the vertical structure of the atmosphere during blocking episodes. This new observation-based view is available globally at the same quality so that blocking in the Southern Hemisphere can also be studied with the same reliability as in the Northern Hemisphere.

## 1 Introduction

Weather and climate in the Northern Hemisphere (NH) midlatitudes are dominated by large-scale circulations of the atmosphere and ocean and by dynamical features including jet streams, storm tracks, and blocking. Blocking describes an atmospheric situation where a persistent and stationary high-pressure system blocks the climatological westerly flow for several days to weeks (Rex, 1950). It is often associated with anomalous weather patterns and extreme events (see, e.g., Cattiaux et al., 2010; Matsueda, 2011; Mattingly et al., 2015). The blocking over Russia in summer 2010, for instance, was one of the strongest blocking events in recent history, with impacts on large parts of Europe and Asia. It did not only lead to record-breaking temperatures in Russia but has also been associated with severe flooding in Pakistan at the same time (Matsueda, 2011; Galarneau Jr. et al., 2012). Severe impacts of these blocking-related extremes on society and the economy have increased the interest in investigating blocking evolution and impacts of climate change on blocking frequency and duration (Sillmann et al., 2011; Cohen et al., 2014; Shepherd, 2014; Gramling, 2015; Lhotka and Kyselý, 2015).

In the NH, blocking preferentially occurs near the northeastern ends of the Atlantic and Pacific storm tracks (Euro-Atlantic blocking and North Pacific blocking, respectively) (Doblas-Reyes et al., 2002; Barriopedro et al., 2010; IPCC, 2013). Blocking is connected to the North Atlantic oscillation and to jet stream variability (see, e.g., Scherrer et al., 2006; Davini et al., 2014a). A connection of blocking to stratospheric phenomena such as sudden stratospheric warming events has been suggested by several authors in the past

(e.g., Quiroz, 1986; Martius et al., 2009; Woollings et al., 2010; Barriopedro and Calvo, 2014). Recently, thermodynamic processes in the troposphere such as latent heating have also been found to be important for the formation of blocking (Pfahl et al., 2015).

In the Southern Hemisphere (SH) where the midlatitudes are mostly characterized by oceanic regions with very sparse human population, blocking has received less attention. Main blocking regions are located in the Australia–New Zealand area and in the southeast Pacific (Lejenäs, 1984; Mendes et al., 2008). The frequency and location of SH blocking are strongly influenced by the El Niño–Southern Oscillation (ENSO) and the southern annular mode (Wiedenmann et al., 2002; Oliveira et al., 2014). However, sparse coverage by classical observational systems in the SH introduces larger uncertainties into SH blocking research (Tibaldi et al., 1994; Marques and Rao, 2000).

Most blocking studies are based on climate model output or reanalysis data analyzing geopotential height (GPH) fields at a constant pressure level (see, e.g., Barriopedro et al., 2006, 2010; Barnes et al., 2014; Davini et al., 2014b). Other studies employed dynamical atmospheric parameters such as vertically averaged potential vorticity or potential temperature in the dynamical tropopause (e.g., Pelly and Hoskins, 2003; Schwierz et al., 2004). However, it has been shown that the blocking frequency exhibits considerable inter-model spread in current climate models (Anstey et al., 2013; IPCC, 2013) and blocking trends can differ depending on the reanalysis used (Barnes et al., 2014).

We use, for the first time, observations from Global Positioning System (GPS) radio occultation (RO) to detect blocking and inspect the atmospheric structure during blocking events. This study does not provide an analysis of blocking dynamics nor an extended comparison to model or reanalysis data. Our objective is to explore the feasibility of detecting blocking and to characterize its three-dimensional structure with RO observations. To this end we show blocking patterns and the vertically resolved structure of the troposphere and lower stratosphere during two well-known blocking events: the blocking over Russia in summer 2010 and the blocking over Greenland in winter 2013.

## 2 Radio occultation data

The analysis presented here is based on RO measurements. RO is a satellite-based limb sounding technique, delivering profiles of atmospheric parameters with global coverage and high vertical resolution of about 100 m in the troposphere to 1.5 km in the stratosphere (Kursinski et al., 1997; Gorbunov et al., 2004). The horizontal resolution ranges from about 60 to 300 km (Kursinski et al., 1997). RO data are of high quality. In the troposphere the accuracy of GPH is about 10 m and that of temperature is better than 1 K (Scherllin-Pirscher et al., 2011b), with averaged profiles exhibiting further sta-

tistical reduction of errors (Scherllin-Pirscher et al., 2011a). Structural uncertainty is low and data from different satellites are highly consistent and require no inter-satellite calibration (Foelsche et al., 2011; Ho et al., 2012; Steiner et al., 2013).

RO data are of great benefit for improving weather forecasts and atmospheric analyses (note that several weather prediction centers already assimilate RO data) as well as for monitoring atmospheric climate variability and changes (see, e.g., Anthes, 2011; Steiner et al., 2011; Gleisner et al., 2015; Randel and Wu, 2015). RO has been applied, so far, for a range of atmospheric dynamics studies, such as investigating the planetary boundary layer (e.g., von Engeln et al., 2005) and tropopause (Schmidt et al., 2008; Rieckh et al., 2014; Peevey et al., 2014), the ENSO (Scherllin-Pirscher et al., 2012; Sun et al., 2014), atmospheric tides (e.g., Pirscher et al., 2010), and waves, including the Quasi-Biennial Oscillation (Randel et al., 2003; Schmidt et al., 2005), Kelvin waves (e.g., Randel and Wu, 2005), and stratospheric gravity waves (e.g., de la Torre and Alexander, 2005; Tsuda, 2014). Recent studies also focused on tracing wind fields (Scherllin-Pirscher et al., 2014) and analyzing the thermodynamic structure of cyclones (Biondi et al., 2015).

RO data used in the present study were processed with the Wegener Center occultation processing system version 5.6 (OPSv5.6) (Schwärz et al., 2013). The full set of atmospheric variables derived from RO includes density, pressure, GPH, temperature, potential temperature, and tropospheric water vapor. Observations from several RO missions are exploited including from the CHAllenging Minisatellite Payload (CHAMP), the Gravity Recovery and Climate Experiment (GRACE), and the Constellation Observing System for Meteorology, Ionosphere, and Climate (COSMIC) for the period 2006 to 2013, where we focus on two well-known blocking events: over Russia in summer 2010 (Russian blocking) and over Greenland in late winter and early spring 2013 (Greenland blocking). During these time periods about 800 high-quality RO profiles are available per day in the NH.

We analyze GPH and temperature profiles as a function of pressure. The levels of the pressure grid have been calculated from $p_i(z_i) = p_0\exp(-\frac{z_i}{H})$, with $p_0 = 1013.25$ hPa (standard surface pressure), $H = 7000$ m (constant scale height), and altitude $z_i$ ranging from the surface to 16 km (corresponding to about 100 hPa) in equidistant 200 m steps.

We calculate daily fields on a $2.5° \times 2.5°$ longitude–latitude grid by applying a weighted average to the RO profiles:

$$x_{\text{grid}}(\lambda, \phi, d) = \frac{\sum_i w_i x_i(\lambda', \phi', d')}{\sum_i w_i},$$

where $x_{\text{grid}}(\lambda, \phi, d)$ is GPH or temperature at a specific grid point at longitude $\lambda$, latitude $\phi$, and day $d$. $x_i(\lambda', \phi', d')$ denotes an individual atmospheric profile at the RO event location $(\lambda', \phi')$ and day $(d')$. All RO events within $\pm 7.5°$ in longitude, $\pm 2.5°$ in latitude, and $\pm 2$ days are considered and

weighted with a Gaussian weighting function $w_i$ over longitude and time according to $w_i = \exp\left(-\left[\left(\frac{\Delta\lambda}{L}\right)^2 + \left(\frac{\Delta d}{D}\right)^2\right]\right)$, with $L = 7.5°$ and $D = 1$ day (adapted from Randel and Wu, 2005). This effective resolution has been chosen to minimize the number of bins in which no measurements exist, while still resolving most of the atmospheric variability. Sensitivity tests with data from the European Centre for Medium-range Weather Forecasts (ECMWF) reanalysis Interim (ERA-Interim) (Dee et al., 2011) showed only small differences ($< 100$ m in geopotential height) between mean fields obtained from this binning and native $2.5° \times 2.5°$ daily fields, confirming the robustness of our gridding strategy.

Figures 1a and 2a depict the distribution of RO profiles and the number of profiles contributing to each grid cell for 2 exemplary days during the Russian blocking in 2010 and the Greenland blocking in 2013. More than 80 % of all grid cells contain information of at least four RO profiles. Only near the equator and at very high latitudes does the number of profiles decrease, and some grid cells with no measurements exist.

Applying our gridding method, we are able to resolve synoptic-scale atmospheric variability on a daily basis as shown for GPH at the 500 hPa pressure level (Figs. 1b and 2b). At midlatitudes (between approximately 45 and 65° N), mean GPH fields reveal high-pressure systems over Scandinavia and the western part of Russia in summer 2010 (Russian blocking) and over the east Atlantic in winter and spring 2013 (Greenland blocking), representing typical blocking situations (Davini et al., 2014a).

These features are even more pronounced in GPH anomaly fields (Figs. 1c and 2c) which are calculated relative to the daily means averaged over 8 years (2006 to 2013). GPH anomalies are larger during the Greenland blocking ($> 300$ m) in winter than during the Russian blocking (mainly within 200 m) in summer. However, both anomalies are distinctively larger than the variability, shown as the standard deviation of the individual RO profiles in each grid cell in Figs. 1d and 2d for the Russian and Greenland blocking, respectively.

To provide information about uncertainty associated with discrete data sampling and our averaging method, Figs. 1e and 2e show the sampling error (SE). It is calculated as the difference between the mean field from co-located ECMWF analysis profiles applying the same averaging technique as for RO profiles (see above) and the daily mean ECMWF analysis field on a native $2.5° \times 2.5°$ resolution. For both blocking events, the SE is distinctively smaller than the GPH anomalies. It is slightly larger during the Greenland blocking than during the Russian blocking because (i) atmospheric variability is stronger in the winter season than in the summer season and (ii) the number of profiles is slightly smaller in 2013 than in 2010. However, the small magnitude of the SE (Figs. 1e and 2e) compared to blocking-related anomalies (Figs. 1c and 2c) as well as small standard deviation (Figs. 1d and 2d) underpins the fact that RO data sampling is sufficient

to capture atmospheric variability on a daily basis when applying a suitable averaging technique. RO data are therefore well suited for blocking detection.

## 3 Blocking detection

Blocking diagnosis is usually performed on a fixed pressure level (see, e.g., Barriopedro et al., 2006, 2010; Barnes et al., 2014; Davini et al., 2014b). To detect blocking episodes we utilize a frequently used blocking index based on GPH at 500 hPa (Tibaldi and Molteni, 1990; Scherrer et al., 2006; Davini et al., 2012, 2014b). Blocking is identified via three criteria.

First, the northern and southern GPH gradients, $\Delta Z_N$ and $\Delta Z_S$, are calculated as

$$\Delta Z_N(\lambda, \phi, p) = \frac{Z(\lambda, \phi + \Delta\phi, p) - Z(\lambda, \phi, p)}{\Delta\phi},$$

$$\Delta Z_S(\lambda, \phi, p) = \frac{Z(\lambda, \phi, p) - Z(\lambda, \phi - \Delta\phi, p)}{\Delta\phi},$$

where $\Delta\phi = 15°$. The computation is performed separately for each $2.5° \times 2.5°$ grid point from 50 to 65° N; thus, grid points are effectively used from 35 to 80° N over all longitudes. Following Davini et al. (2014a), *instantaneous blocking (IB)* is identified if both of the following conditions are met: $\Delta Z_S(\lambda, \phi, p') > 0$ m/° lat and $\Delta Z_N(\lambda, \phi, p')$ $< -10$ m/° lat at $p' = 500$ hPa. A positive southward gradient indicates the reversal of the meridional GPH gradient with easterlies equatorward of $\phi$. This is the essential condition for blocking. Additionally, the second condition indicates strong westerlies poleward of $\phi$. It rules out some synoptic cases which marginally satisfy condition one but are not blockings (Tibaldi and Molteni, 1990; Anstey et al., 2013).

The second blocking detection criterion is set to account only for large high-pressure systems. Thus, *extended IB* is identified at a grid point if all neighboring grid cells within $\pm7.5°$ longitude are instantaneously blocked.

The third criterion guarantees detecting only stationary high-pressure systems and filtering out fast-moving events. It specifies that a grid cell with extended IB is *blocked* if at least one grid cell with extended IB is found within a box of 10° longitude $\times$ 5° latitude on each of the neighboring $\pm2$ days.

Figure 3 shows the blocking occurrence and temporal evolution at the 500 hPa pressure level for the Russian and Greenland blocking. To demonstrate the influence of the three blocking criteria, Fig. 3 also includes IB and extended IB. Note the very similar patterns for all criteria, indicating that the gradient criterion (first criterion) is in principle sufficient for catching most of the blocking features.

Overall, the evolutions of the blocking patterns are different for the Russian blocking and the Greenland blocking. While the Russian blocking is more continuous, lasting for more than 6 weeks from the end of June to mid-August, the Greenland blocking is most pronounced only for about

www.atmos-chem-phys.net/16/4593/2016/ Atmos. Chem. Phys., 16, 4593–4604, 2016

47
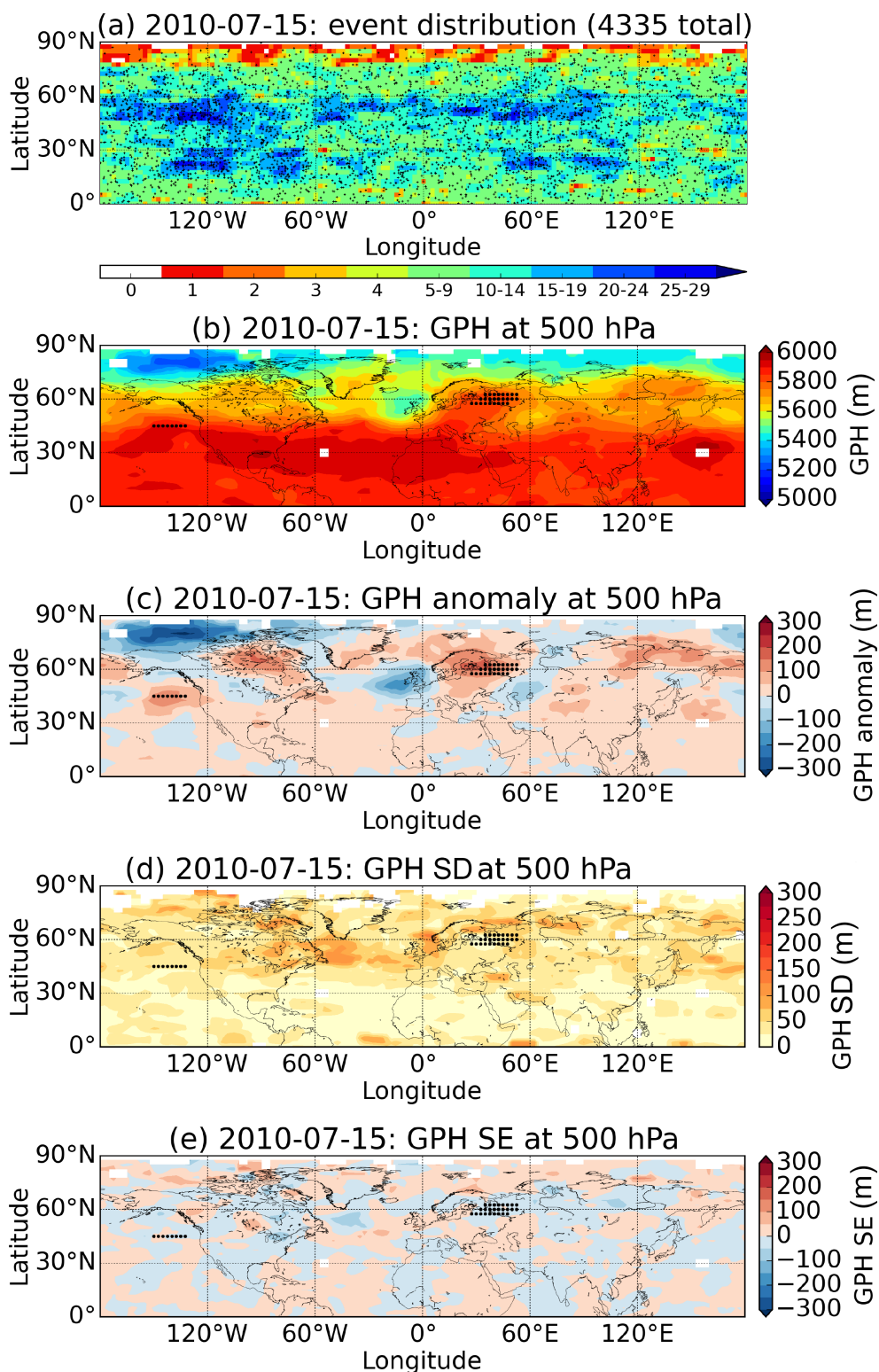
**Figure 1.** Panel **(a)**: RO event distribution (plus signs) in the NH for an exemplary day (±2 neighboring days) during the Russian blocking and number of events per grid cell (shading). Other panels: geographic maps at 500 hPa of **(b)** GPH, **(c)** GPH anomaly relative to the mean from 2006 to 2013, **(d)** standard deviation of individual profiles, and **(e)** sampling error. Blocked grid cells are indicated by dots; missing data are white.
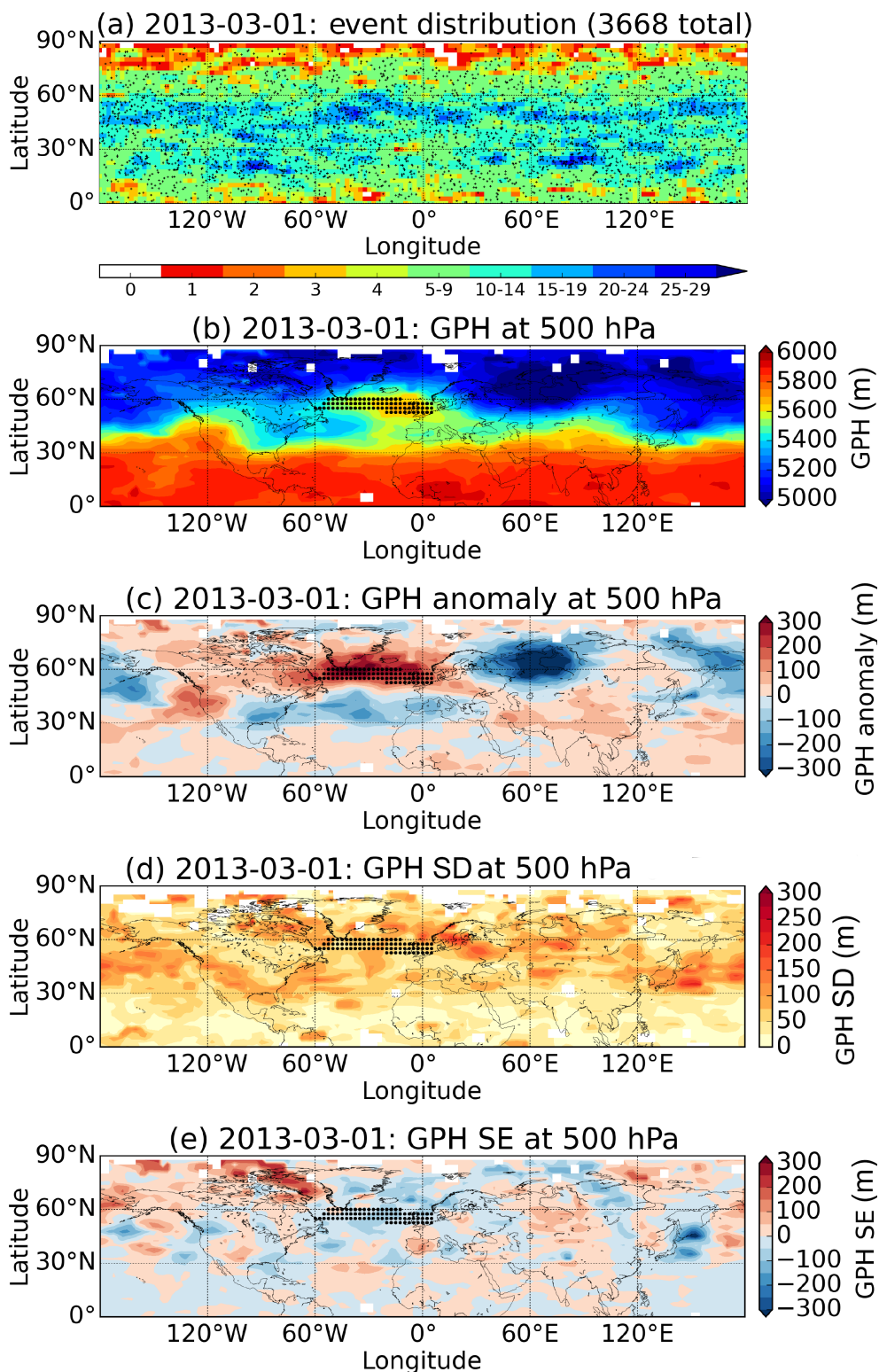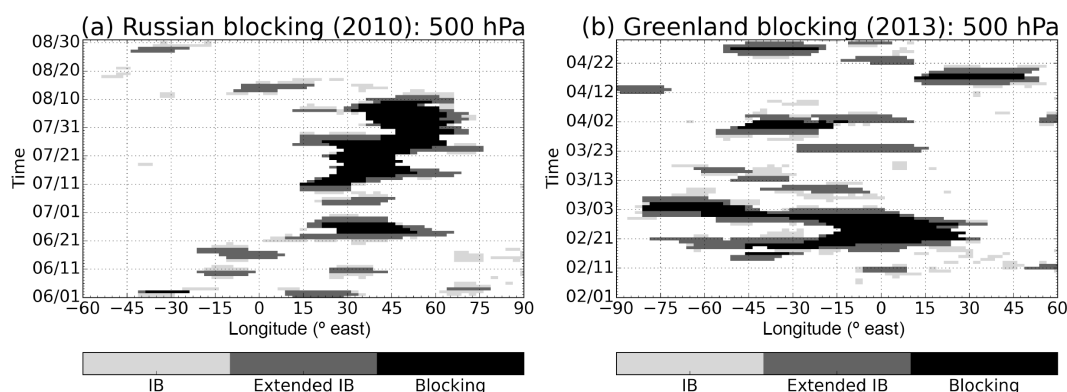
**Atmos. Chem. Phys., 16, 4593–4604, 2016**                    **www.atmos-chem-phys.net/16/4593/2016/**

48

**Figure 2.** Same layout as Fig. 1 but for an exemplary day during the Greenland blocking.

49

**Figure 3.** Hovmöller diagrams of observed blocking occurrence at 500 hPa over **(a)** Russia in June–July–August (JJA) 2010 and over **(b)** Greenland in February–March–April (FMA) 2013. Blocking is considered between 50 and 65° N. Shading indicates the three blocking detection steps: IB (light gray), extended IB (dark gray), and blocking (black).

2 weeks from mid-February to early March, with minor and less extended blockings taking place until mid-April 2013. The Russian blocking is smaller in longitudinal extent, ranging over 55°, while the Greenland blocking is twice as large, ranging over 100° in longitude.

We compared the resulting blocking patterns from RO observations to those from ERA-Interim data and found very good agreement (Brunner et al., 2015). The consistency of our results is also confirmed by comparison with existing literature (see, e.g., Matsueda, 2011, Fig. 1b). This again proves the feasibility of blocking detection with RO.

## 4 Vertically resolved blocking patterns

Tropospheric profiles of GPH gradients are shown in Fig. 4 for 2 exemplary days and regions for the Russian and Greenland blocking, respectively. Climatological GPH gradients in the same region are additionally shown for comparison. These climatological gradients $\Delta Z_S$ and $\Delta Z_N$ for June–July–August (JJA) and February–March–April (FMA) are obtained from averaging over all available years (2006 to 2013).
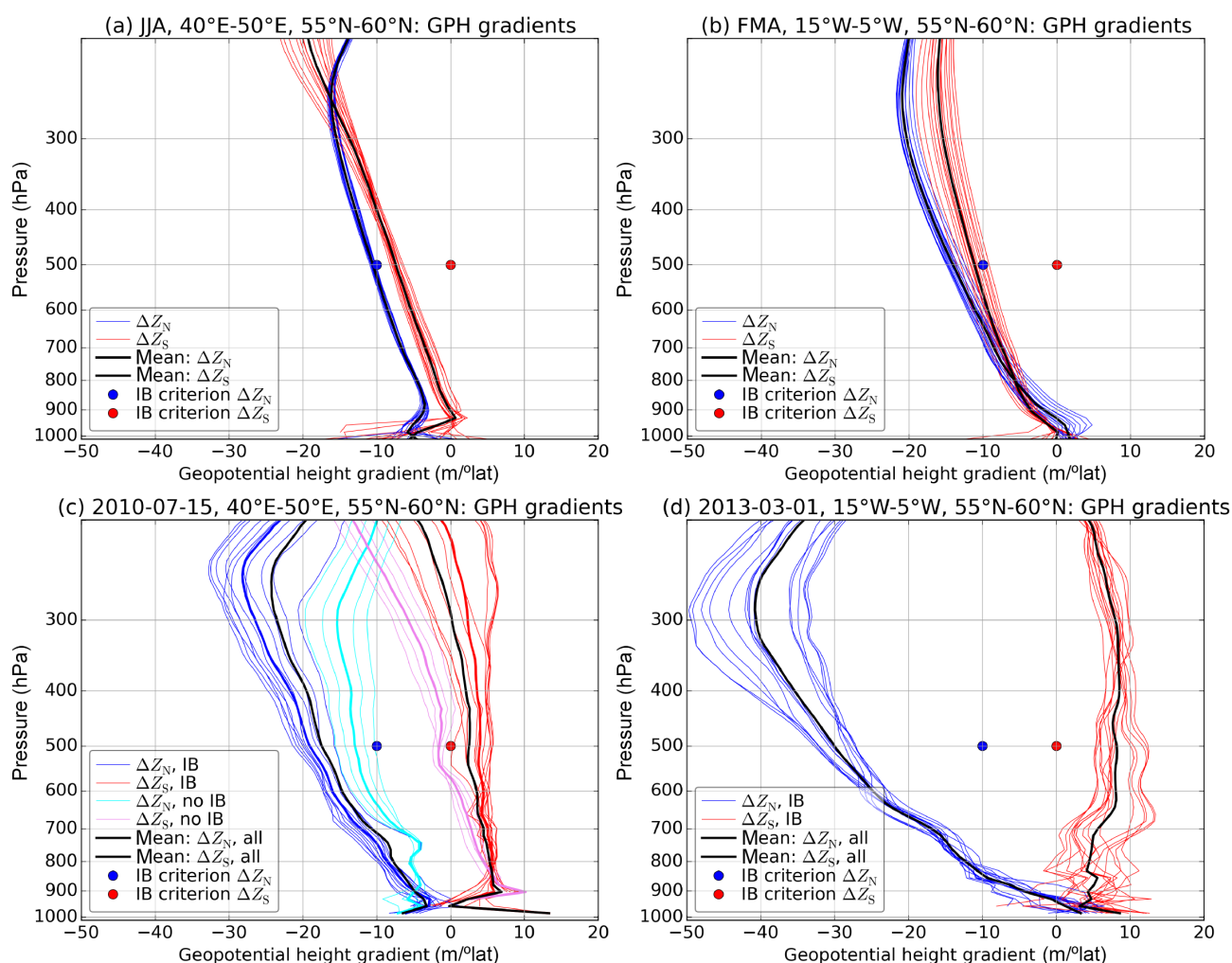
During normal, climatological conditions (Fig. 4a, b), all gradient profiles are close to each other. In the entire troposphere above the boundary layer GPH gradients are smaller than 0 m/° lat indicating the climatological westerly geostrophic flow at NH midlatitudes. In general, the climatological northern gradients are near to the blocking threshold ($-10$ m/° lat). For the inspected regions they are even found below the threshold.

A clear separation between the northern and southern gradients can be observed during blocking events as presented for 2 exemplary days and regions for the Russian and Greenland blocking, respectively (Fig. 4c, d). While the southern gradient becomes positive (i.e., easterly geostrophic flow equatorward of the depicted region), the northern gradient becomes distinctively more negative compared to the clima-

tology: at 500 hPa $\Delta Z_N$ exceeds $-20$ m/° lat over Russia in July and even $-30$ m/° lat over Greenland in March, further increasing upwards. Figure 4c also shows some $\Delta Z_S$ profiles which do not reach the IB criterion at some grid cells within the depicted region. However, the all-mean gradients $\Delta Z_S$ and $\Delta Z_N$ clearly represent instantaneously blocked conditions during these particular days.

The corresponding evolution of the GPH gradients over time is shown in Fig. 5 for exemplary grid cells during the Russian and Greenland blocking. Different temporal and vertical behavior of $\Delta Z_N$ (Fig. 5a, b) and $\Delta Z_S$ (Fig. 5c, d) is evident. $\Delta Z_N$ is always negative in JJA 2010 and meets the IB criterion during almost the entire period. During some days in February and March 2013, however, it is positive in the entire troposphere, indicating a potential high-pressure system at high northern latitudes (70 to 75° N). In JJA 2010, the southern gradient is positive for a couple of days by the end of June 2010 and for a longer time period from mid-July to mid-August 2010. In FMA 2013, positive $\Delta Z_S$ can be found for several days from mid-February to early March 2013 as well as for some days in early April 2013.

The comparison of the northern and the southern gradient and their combined use for IB detection based on the two blocking cases reveals that the $\Delta Z_S$ criterion is harder to meet than the $\Delta Z_N$ criterion, in particular during JJA 2010. During this time period two IB episodes can be identified over Russia: a short one at the end of June 2010 and a more persistent one from mid-July to mid-August 2010. Over Greenland, IB is found for mid-February to early March 2013 as well as for 3 days in early April 2013. Note that IB periods that are too short will no longer appear as blocking since additional blocking criteria become effective. Overall, blocking episodes show a distinct vertical extent of the GPH gradient up to 300 hPa (Russia) and even up to the tropopause at about 200 hPa (Greenland). Outside blocked episodes the gradients mainly show climatological behavior.

50

**Figure 4.** Vertical profiles of (blue) $\Delta Z_N$ and (red) $\Delta Z_S$ during climatological conditions in **(a)** JJA 2006 to 2013 within 40 to 50° E and 55 to 60° N and **(b)** FMA 2006 to 2013 within 15 to 5° W and 55 to 60° N. $\Delta Z_N$ and $\Delta Z_S$ are given for individual grid cells (thin lines) and the respective region mean (bold lines). IB blocking criteria at 500 hPa are shown for $\Delta Z_N$ (blue dot) and $\Delta Z_S$ (red dot). Vertical profiles of GPH gradients for an exemplary day during the **(c)** Russian blocking and **(d)** Greenland blocking; same area as **(a)** and **(b)**, respectively. Blocked profiles (blue, red) and those not meeting the blocking criteria (light blue, light red) are shown, as are mean (bold colored) and all-mean (bold black) $\Delta Z_N$ and $\Delta Z_S$ profiles. Note that the mean is identical with the "all-mean" for the Greenland blocking.

The vertical structure of blocking in GPH and temperature anomalies during the Russian and Greenland blocking is shown in Figs. 6 and 7, respectively. Meridional cross sections reveal the longitudinal extent of blockings with strong positive GPH anomalies during these events (Fig. 6a, b). The different characteristics in their temporal evolution are shown in Fig. 6c and d. Positive GPH anomalies extend into the stratosphere and show a maximum near the tropopause at approximately 200 hPa, exceeding 250 to 300 m during blocking episodes. The height of the lapse-rate tropopause correlates well with GPH maxima and minima. During the persistent Russian blocking, it stays almost constant (Fig. 6c) compared to its usual variations during unblocked conditions. Meridional cross sections of temperature anomalies (Fig. 7a,

b) reveal strong positive anomalies in the troposphere during blocking. These correspond to strong positive GPH anomalies and further result in a higher lapse-rate tropopause and in negative temperature anomalies in the stratosphere relative to climatological conditions. Strongest positive temperature anomalies of up to 10 K are found in the lower troposphere towards the surface during the Russian blocking (Fig. 7c). During the Greenland blocking, maximum temperature anomalies of up to 6 K are observed in the mid-troposphere (Fig. 7d).

www.atmos-chem-phys.net/16/4593/2016/ Atmos. Chem. Phys., 16, 4593–4604, 2016

51
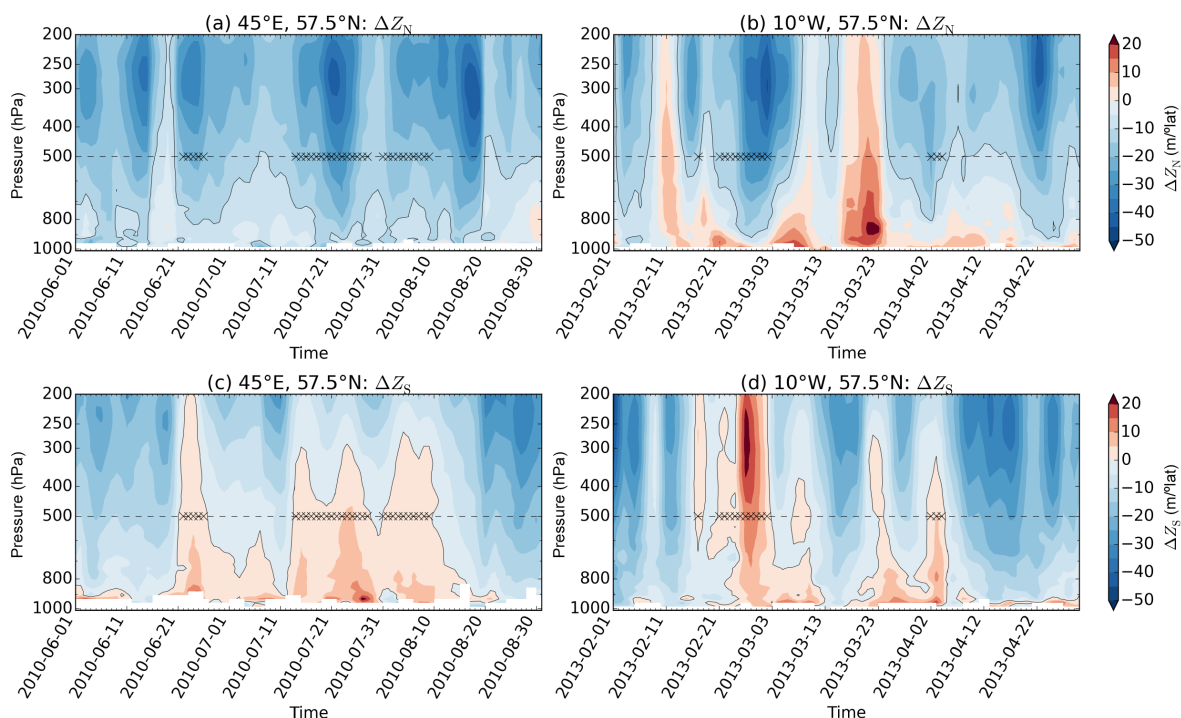
**Figure 5.** Temporal evolution of $\Delta Z_N$ and $\Delta Z_S$ during the **(a, c)** Russian and **(b, d)** Greenland blocking. Blocking criteria (solid black contours) are indicated at $-10\,\mathrm{m}/^\circ$ lat for $\Delta Z_N$ and $0\,\mathrm{m}/^\circ$ lat for $\Delta Z_S$. IB (crosses) is indicated at the $500\,\mathrm{hPa}$ pressure level (dashed black line).
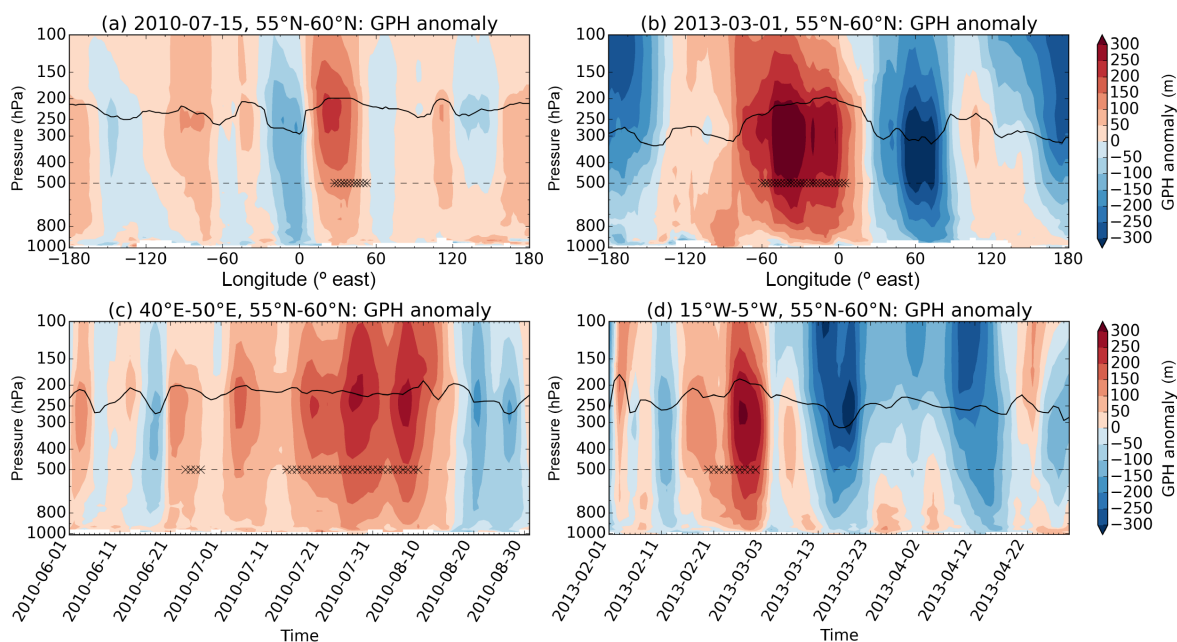


**Figure 6.** GPH anomalies during (left column) Russian blocking and (right column) Greenland blocking. Panels **(a, b)**: meridional cross sections of GPH for 2 exemplary days and regions as well as **(c, d)** temporal evolution of GPH for the same regions. Blocking (crosses) at the $500\,\mathrm{hPa}$ level (dashed line) is indicated if at least one grid cell in the averaged area is blocked. The solid line denotes the lapse-rate tropopause.

**Atmos. Chem. Phys., 16, 4593–4604, 2016** **www.atmos-chem-phys.net/16/4593/2016/**

52
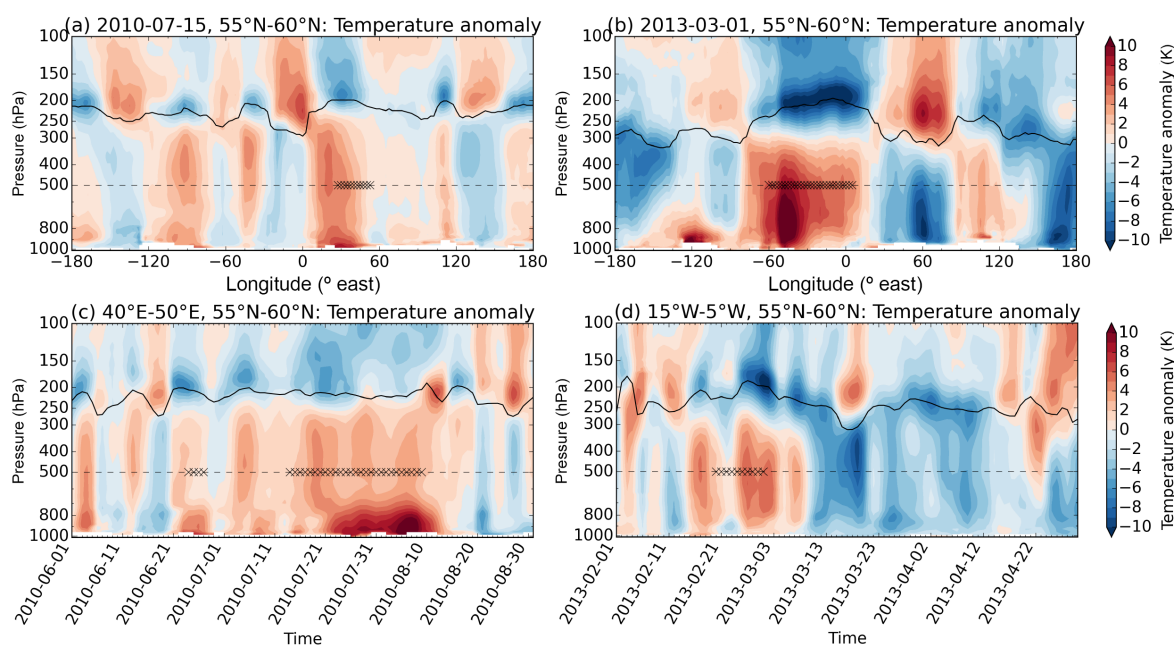
**Figure 7.** Same layout as Fig. 6 but for temperature anomalies.

## 5 Conclusions

We demonstrated the feasibility of atmospheric blocking detection in observations from radio occultation (RO). Utilizing about 800 profiles per day in the NH and applying an adequate gridding strategy, RO data are found to be dense enough to resolve atmospheric variability reasonably well on a daily basis as shown for geopotential height (GPH) fields and corresponding uncertainty measures.

For blocking detection we utilized a standard blocking detection algorithm based on GPH gradients at the 500 hPa pressure level. We analyzed two well-known blocking events over Russia in summer 2010 and over Greenland in late winter and early spring 2013. The resulting blocking pattern and temporal evolution in RO fields fully represent the characteristics of the events, consistent with existing literature.

Furthermore, we explored the vertically resolved atmospheric structure during blocking based on tropospheric profiles of GPH gradients. While GPH gradient profiles during climatological conditions are found to be smaller than 0 m/° lat in the entire troposphere above the boundary layer, indicating the westerly geostrophic flow at NH midlatitudes, a clear separation between the northern and southern gradients is observed during blocking episodes. The southern gradients become positive, indicating an easterly geostrophic flow equatorwards, while the northern gradients become distinctively more negative up to a few −10 m/° lat, depending on region and season. A distinct vertical extent of these features up to 300 hPa and even up to the tropopause is found.

During blocking, characteristic structures in GPH and temperature anomaly fields are found in the troposphere and

lower stratosphere. Strong positive GPH anomalies of up to 300 m in the upper troposphere yield a clear tropopause height increase. Corresponding temperature anomalies of up to 10 K are found in the middle and lower troposphere.

Overall, RO data are found to be very well suited for blocking detection and for providing information on the atmospheric structure during blocking episodes. They allow the detection and analysis of vertically resolved atmospheric blocking patterns in a comprehensive observation-based record and a set of atmospheric variables comprising density, pressure, GPH, temperature, potential temperature, and tropospheric water vapor.

RO observations from constellations such as COSMIC cover the entire Earth and can therefore provide a reliable data basis also in the Southern Hemisphere. They allow for comparisons of the atmospheric characteristics of both hemispheres without being affected by inhomogeneous data coverage. Since RO profiles also sample the lower stratosphere, they can, moreover, provide valuable information about the influence of stratospheric phenomena on blocking. RO could therefore complement ongoing research on the connection between sudden stratospheric warming events and blocking. Furthermore, combining RO observations in the free atmosphere with surface measurements will allow for a better understanding of the evolution of surface impacts, planned for future research.

www.atmos-chem-phys.net/16/4593/2016/ Atmos. Chem. Phys., 16, 4593–4604, 2016

53

## References

Anstey, J. A., Davini, P., Gray, L. J., Woollings, T. J., Butchart, N., Cagnazzo, C., Christiansen, B., Hardiman, S. C., Osprey, S. M., and Yang, S.: Multi-model analysis of Northern Hemisphere winter blocking: Model biases and the role of resolution, J. Geophys. Res., 118, 3956–3971, doi:10.1002/jgrd.50231, 2013.

Anthes, R. A.: Exploring Earth's atmosphere with radio occultation: contributions to weather, climate and space weather, Atmos. Meas. Tech., 4, 1077–1103, doi:10.5194/amt-4-1077-2011, 2011.

Barnes, E. A., Dunn-Sigouin, E., Masato, G., and Woollings, T.: Exploring recent trends in Northern Hemisphere blocking, Geophys. Res. Lett., 41, 638–644, doi:10.1002/2013GL058745, 2014.

Barriopedro, D. and Calvo, N.: On the Relationship between ENSO, Stratospheric Sudden Warmings, and Blocking, J. Climate, 27, 4704–4720, doi:10.1175/JCLI-D-13-00770.1, 2014.

Barriopedro, D., García-Herrera, R., Lupo, A. R., and Hernández, E.: A climatology of northern hemisphere blocking, J. Climate, 19, 1042–1063, doi:10.1175/JCLI3678.1, 2006.

Barriopedro, D., García-Herrera, R., and Trigo, R. M.: Application of blocking diagnosis methods to General Circulation Models. Part I: a novel detection scheme, Clim. Dynam., 35, 1373–1391, doi:10.1007/s00382-010-0767-5, 2010.

Biondi, R., Steiner, A. K., Kirchengast, G., and Rieckh, T.: Characterization of thermal structure and conditions for overshooting of tropical and extratropical cyclones with GPS radio occultation, Atmos. Chem. Phys., 15, 5181–5193, doi:10.5194/acp-15-5181-2015, 2015.

Brunner, L., Steiner, A. K., Scherllin-Pirscher, B., and Jury, M. W.: Feasibility of blocking detection in observations from radio occultation, Geophys. Res. Abstr., EGU2015–1519, EGU General Assembly 2015, Vienna, Austria, 2015.

Cattiaux, J., Vautard, R., Cassou, C., Yiou, P., Masson-Delmotte, V., and Codron, F.: Winter 2010 in Europe: A cold extreme in a warming climate, Geophys. Res. Lett., 37, L20704, doi:10.1029/2010GL044613, 2010.

Cohen, J., Screen, J. A., Furtado, J. C., Barlow, M., Whittleston, D., Coumou, D., Francis, J., Dethloff, K., Entekhabi, D., Overland, J., and Jones, J.: Recent Arctic amplification and extreme mid-latitude weather, Nat. Geosci., 7, 627–637, doi:10.1038/ngeo2234, 2014.

Davini, P., Cagnazzo, C., Gualdi, S., and Navarra, A.: Bidimensional diagnostics, variability, and trends of Northern Hemisphere blocking, J. Climate, 25, 6496–6509, doi:10.1175/JCLI-D-12-00032.1, 2012.

Davini, P., Cagnazzo, C., and Anstey, J. A.: A blocking view of the stratosphere-troposphere coupling, J. Geophys. Res., 119, 11 100–11 115, doi:10.1002/2014JD021703, 2014a.

Davini, P., Cagnazzo, C., Fogli, P. G., Manzini, E., Gualdi, S., and Navarra, A.: European blocking and Atlantic jet stream variability in the NCEP/NCAR reanalysis and the CMCC-CMS climate model, Clim. Dynam., 43, 71–85, doi:10.1007/s00382-013-1873-y, 2014b.

de la Torre, A. and Alexander, P.: Gravity waves above Andes detected from GPS radio occultation temperature profiles: Mountain forcing?, Geophys. Res. Lett., 32, L17815, doi:10.1029/2005GL022959, 2005.

Dee, D. P., Uppala, S. M., Simmons, A. J., Berrisford, P., Poli, P., Kobayashi, S., Andrae, U., Balmaseda, M. A., Balsamo, G., Bauer, P., Bechtold, P., Beljaars, A. C. M., van de Berg, L., Bidlot, J., Bormann, N., Delsol, C., Dragani, R., Fuentes, M., Geer, A. J., Haimberger, L., Healy, S. B., Hersbach, H., Hólm, E. V., Isaksen, L., Kållberg, P., Köhler, M., Matricardi, M., McNally, A. P., Monge-Sanz, B. M., Morcrette, J.-J., Park, B.-K., Peubey, C., de Rosnay, P., Tavolato, C., Thépaut, J.-N., and Vitart, F.: The ERA-Interim reanalysis: configuration and performance of the data assimilation system, Q. J. Roy. Meteor. Soc., 137, 553–597, doi:10.1002/qj.828, 2011.

Doblas-Reyes, F. J., Casado, M. J., and Pastor, M. A.: Sensitivity of the Northern Hemisphere blocking frequency to the detection index, J. Geophys. Res., 107, ACL 6-1–ACL 6-22, doi:10.1029/2000JD000290, 2002.

Foelsche, U., Scherllin-Pirscher, B., Ladstädter, F., Steiner, A. K., and Kirchengast, G.: Refractivity and temperature climate records from multiple radio occultation satellites consistent within 0.05 %, Atmos. Meas. Tech., 4, 2007–2018, doi:10.5194/amt-4-2007-2011, 2011.

Galarneau Jr., T. J., Hamill, T. M., Dole, R. M., and Perlwitz, J.: A Multiscale Analysis of the Extreme Weather Events over Western Russia and Northern Pakistan during July 2010, Mon. Weather Rev., 140, 1639–1664, doi:10.1175/MWR-D-11-00191.1, 2012.

Gleisner, H., Thejll, P., Christiansen, B., and Nielsen, J. K.: Recent global warming hiatus dominated by low-latitude temperature trends in surface and troposphere data, Geophys. Res. Lett., 42, 510–517, doi:10.1002/2014GL062596, 2015.

Gorbunov, M. E., Benzon, H.-H., Jensen, A. S., Lohmann, M. S., and Nielsen, A. S.: Comparative analysis of radio occultation processing approaches based on Fourier integral operators, Radio Sci., 39, RS6004, doi:10.1029/2003RS002916, 2004.

Gramling, C.: Arctic impact, Science, 347, 818–821, doi:10.1126/science.347.6224.818, 2015.

Ho, S.-P., Hunt, D., Steiner, A. K., Mannucci, A. J., Kirchengast, G., Gleisner, H., Heise, S., von Engeln, A., Marquardt, C., Sokolovskiy, S., Schreiner, W., Scherllin-Pirscher, B., Ao, C., Wickert, J., Syndergaard, S., Lauritsen, K., Leroy, S., Kursinski, E. R., Kuo, Y.-H., Foelsche, U., Schmidt, T., and Gorbunov, M.: Reproducibility of GPS radio occultation data for climate monitoring: Profile-to-profile inter-comparison of CHAMP climate records 2002 to 2008 from six data centers, J. Geophys. Res., 117, D18111, doi:10.1029/2012JD017665, 2012.

IPCC: Climate Change 2013: The Physical Science Basis. Contribution of Working Group I to the Fifth Assessment Report of the

Intergovernmental Panel on Climate Change, Cambridge University Press, Cambridge, United Kingdom and New York, NY, USA, 2013.

Kursinski, E. R., Hajj, G. A., Schofield, J. T., Linfield, R. P., and Hardy, K. R.: Observing Earth's atmosphere with radio occultation measurements using the Global Positioning System, J. Geophys. Res., 102, 23429–23465, doi:10.1029/97JD01569, 1997.

Lejenäs, H.: Characteristics of southern hemisphere blocking as determined from a time series of observational data, Q. J. Roy. Meteor. Soc., 110, 967–979, doi:10.1002/qj.49711046610, 1984.

Lhotka, O. and Kyselý, J.: Hot Central-European summer of 2013 in a long-term context, Int. J. Climatol., 35, 4399–4407, doi:10.1002/joc.4277, 2015.

Marques, R. d. F. C. and Rao, V. B.: Interannual variations of blockings in the southern hemisphere and their energetics, J. Geophys. Res., 105, 4625–4636, doi:10.1029/1999JD901066, 2000.

Martius, O., Polvani, L. M., and Davies, H. C.: Blocking precursors to stratospheric sudden warming events, Geophys. Res. Lett., 36, L14806, doi:10.1029/2009GL038776, 2009.

Matsueda, M.: Predictability of Euro-Russian blocking in summer of 2010, Geophys. Res. Lett., 38, L06801, doi:10.1029/2010GL046557, 2011.

Mattingly, K. S., McLeod, J. T., Knox, J. A., Shepherd, J. M., and Mote, T. L.: A climatological assessment of Greenland blocking conditions associated with the track of Hurricane Sandy and historical North Atlantic hurricanes, Int. J. Climatol., 35, 746–760, doi:10.1002/joc.4018, 2015.

Mendes, M. C. D. a., Trigo, R. M., Cavalcanti, I. F. A., and DaCamara, C. C.: Blocking Episodes in the Southern Hemisphere: Impact on the Climate of Adjacent Continental Areas, Pure Appl. Geophys., 165, 1941–1962, doi:10.1007/s00024-008-0409-4, 2008.

Oliveira, F. N. M., Carvalho, L. M. V., and Ambrizzi, T.: A new climatology for Southern Hemisphere blockings in the winter and the combined effect of ENSO and SAM phases, Int. J. Climatol., 34, 1676–1692, doi:10.1002/joc.3795, 2014.

Peevey, T. R., Gille, J. C., Homeyer, C. R., and Manney, G. L.: The double tropopause and its dynamical relationship to the tropopause inversion layer in storm track regions, J. Geophys. Res., 119, 10194–10212, doi:10.1002/2014JD021808, 2014.

Pelly, J. L. and Hoskins, B. J.: A new perspective on blocking, J. Atmos. Sci., 60, 743–755, doi:10.1175/1520-0469(2003)060<0743:ANPOB>2.0.CO;2, 2003.

Pfahl, S., Schwierz, C., Croci-Maspoli, M., Grams, C. M., and Wernli, H.: Importance of latent heat release in ascending air streams for atmospheric blocking, Nat. Geosci., 8, 610–614, doi:10.1038/ngeo2487, 2015.

Pirscher, B., Foelsche, U., Borsche, M., Kirchengast, G., and Kuo, Y.-H.: Analysis of migrating diurnal tides detected in FORMOSAT-3/COSMIC temperature data, J. Geophys. Res., 115, D14108, doi:10.1029/2009JD013008, 2010.

Quiroz, R. S.: The association of stratospheric warmings with tropospheric blocking, J. Geophys. Res., 91, 5277–5285, doi:10.1029/JD091iD04p05277, 1986.

Randel, W. J. and Wu, F.: Kelvin wave variability near the equatorial tropopause observed in GPS radio occultation measurements, J. Geophys. Res., 110, D03102, doi:10.1029/2004JD005006, 2005.

Randel, W. J. and Wu, F.: Variability of Zonal Mean Tropical Temperatures Derived from a Decade of GPS Radio Occultation Data, J. Atmos. Sci., 72, 1261–1275, doi:10.1175/JAS-D-14-0216.1, 2015.

Randel, W. J., Wu, F., and Ríos, W. R.: Thermal variability of the tropical tropopause region derived from GPS/MET observations, J. Geophys. Res., 108, 4024, doi:10.1029/2002JD002595, 2003.

Rex, D. F.: Blocking Action in the Middle Troposphere and its Effect upon Regional Climate I: An aerological study of blocking action, Tellus, 2, 196–211, doi:10.1111/j.2153-3490.1950.tb00331.x, 1950.

Rieckh, T., Scherllin-Pirscher, B., Ladstädter, F., and Foelsche, U.: Characteristics of tropopause parameters as observed with GPS radio occultation, Atmos. Meas. Tech., 7, 3947–3958, doi:10.5194/amt-7-3947-2014, 2014.

Scherllin-Pirscher, B., Kirchengast, G., Steiner, A. K., Kuo, Y.-H., and Foelsche, U.: Quantifying uncertainty in climatological fields from GPS radio occultation: an empirical-analytical error model, Atmos. Meas. Tech., 4, 2019–2034, doi:10.5194/amt-4-2019-2011, 2011a.

Scherllin-Pirscher, B., Steiner, A. K., Kirchengast, G., Kuo, Y.-H., and Foelsche, U.: Empirical analysis and modeling of errors of atmospheric profiles from GPS radio occultation, Atmos. Meas. Tech., 4, 1875–1890, doi:10.5194/amt-4-1875-2011, 2011b.

Scherllin-Pirscher, B., Deser, C., Ho, S.-P., Chou, C., Randel, W., and Kuo, Y.-H.: The vertical and spatial structure of ENSO in the upper troposphere and lower stratosphere from GPS radio occultation measurements, Geophys. Res. Lett., 39, L20801, doi:10.1029/2012GL053071, 2012.

Scherllin-Pirscher, B., Steiner, A. K., and Kirchengast, G.: Deriving dynamics from GPS radio occultation: Three-dimensional wind fields for monitoring the climate, Geophys. Res. Lett., 41, 7367–7374, doi:10.1002/2014GL061524, 2014.

Scherrer, S. C., Croci-Maspoli, M., Schwierz, C., and Appenzeller, C.: Two-dimensional indices of atmospheric blocking and their statistical relationship with winter climate patterns in the Euro-Atlantic region, Int. J. Climatol., 26, 233–249, doi:10.1002/joc.1250, 2006.

Schmidt, T., Heise, S., Wickert, J., Beyerle, G., and Reigber, C.: GPS radio occultation with CHAMP and SAC-C: global monitoring of thermal tropopause parameters, Atmos. Chem. Phys., 5, 1473–1488, doi:10.5194/acp-5-1473-2005, 2005.

Schmidt, T., Wickert, J., Beyerle, G., and Heise, S.: Global tropopause height trends estimated from GPS radio occultation data, Geophys. Res. Lett., 35, L11806, doi:10.1029/2008GL034012, 2008.

Schwärz, M., Scherllin-Pirscher, B., Kirchengast, G., Schwarz, J., Ladstädter, F., Fritzer, J., and Ramsauer, J.: Multi-Mission Validation by Satellite Radio Occultation, Final report for ESA/ESRIN No. 01/2013, WEGC, University of Graz, Austria, 2013.

Schwierz, C., Croci-Maspoli, M., and Davies, H. C.: Perspicacious indicators of atmospheric blocking, Geophys. Res. Lett., 31, L06125, doi:10.1029/2003GL019341, 2004.

Shepherd, T. G.: Atmospheric circulation as a source of uncertainty in climate change projections, Nat. Geosci., 7, 703–708, doi:10.1038/ngeo2253, 2014.

Sillmann, J., Croci-Maspoli, M., Kallache, M., and Katz, R. W.: Extreme Cold Winter Temperatures in Europe under the Influence of North Atlantic Atmospheric Blocking, J. Climate, 24, 5899–5913, doi:10.1175/2011JCLI4075.1, 2011.

55

Steiner, A. K., Lackner, B. C., Ladstädter, F., Scherllin-Pirscher, B., Foelsche, U., and Kirchengast, G.: GPS radio occultation for climate monitoring and change detection, Radio Sci., 46, RS0D24, doi:10.1029/2010RS004614, 2011.

Steiner, A. K., Hunt, D., Ho, S.-P., Kirchengast, G., Mannucci, A. J., Scherllin-Pirscher, B., Gleisner, H., von Engeln, A., Schmidt, T., Ao, C., Leroy, S. S., Kursinski, E. R., Foelsche, U., Gorbunov, M., Heise, S., Kuo, Y.-H., Lauritsen, K. B., Marquardt, C., Rocken, C., Schreiner, W., Sokolovskiy, S., Syndergaard, S., and Wickert, J.: Quantification of structural uncertainty in climate data records from GPS radio occultation, Atmos. Chem. Phys., 13, 1469–1484, doi:10.5194/acp-13-1469-2013, 2013.

Sun, D.-Z., Zhang, T., Sun, Y., and Yu, Y.: Rectification of El Niño-Southern Oscillation into Climate Anomalies of Decadal and Longer Time Scales: Results from Rorced Ocean GCM Experiments, J. Climate, 27, 2545–2561, doi:10.1175/JCLI-D-13-00390.1, 2014.

Tibaldi, S. and Molteni, F.: On the operational predictability of blocking, Tellus A, 42, 343–365, doi:10.1034/j.1600-0870.1990.t01-2-00003.x, 1990.

Tibaldi, S., Tosi, E., Navarra, A., and Pedulli, L.: Northern and southern hemisphere seasonal variability of blocking frequency and predictability, Mon. Weather Rev., 122, 1971–2003, doi:10.1175/1520-0493(1994)122<1971:NASHSV>2.0.CO;2, 1994.

Tsuda, T.: Characteristics of atmospheric gravity waves observed using the MU (Middle and Upper atmosphere) radar and GPS (Global Positioning System) radio occultation, P. Jpn. Acad. B-Phys., 90, 12–27, 2014.

von Engeln, A., Teixeira, J., Wickert, J., and Buehler, S. A.: Using CHAMP radio occultation data to determine the top altitude of the Planetary Boundary Layer, Geophys. Res. Lett., 32, L06815, doi:10.1029/2004GL022168, 2005.

Wiedenmann, J. M., Lupo, A. R., Mokhov, I. I., and Tikhonova, E. A.: The climatology of blocking anticyclones for the northern and southern hemispheres: block intensity as a diagnostic, J. Climate, 15, 3459–3473, doi:10.1175/1520-0442(2002)015<3459:TCOBAF>2.0.CO;2, 2002.

Woollings, T., Charlton-Perez, A., Ineson, S., Marshall, A. G., and Masato, G.: Associations between stratospheric variability and tropospheric blocking, J. Geophys. Res., 115, D06108, doi:10.1029/2009JD012742, 2010.

**Atmos. Chem. Phys., 16, 4593–4604, 2016**  www.atmos-chem-phys.net/16/4593/2016/

56

Atmospheric
Measurement
Techniques

# A global perspective on atmospheric blocking using GPS radio occultation – one decade of observations

**Lukas Brunner**[1,2] **and Andrea K. Steiner**[1,2,3]

[1]Wegener Center for Climate and Global Change (WEGC), University of Graz, Graz, Austria
[2]FWF-DK Climate Change, University of Graz, Graz, Austria
[3]Institute for Geophysics, Astrophysics, and Meteorology, Institute of Physics, University of Graz, Graz, Austria

*Correspondence to:* Lukas Brunner (lukas.brunner@uni-graz.at)

**Abstract.** Atmospheric blocking represents a weather pattern where a stationary high-pressure system weakens or reverses the climatological westerly flow at mid-latitudes for up to several weeks. It is closely connected to strong anomalies in key atmospheric variables such as geopotential height, temperature, and humidity. Here we provide, for the first time, a comprehensive, global perspective on atmospheric blocking and related impacts by using an observation-based data set from Global Positioning System (GPS) radio occultation (RO) from 2006 to 2016. The main blocking regions in both hemispheres and seasonal variations are found to be represented well in RO data. The effect of blocking on vertically resolved temperature and humidity anomalies in the troposphere and lower stratosphere is investigated for blocking regions in the Northern and Southern hemispheres, respectively. We find a statistically significant correlation of blocking with positive temperature anomalies, exceeding 3 K in the troposphere, and a reversal above the tropopause with negative temperature anomalies below −3 K in the lower stratosphere. Specific humidity is positively correlated with temperature throughout the troposphere with larger anomalies revealed in the Southern Hemisphere. At the eastern and equatorward side of the investigated blocking regions, a band of tropospheric cold anomalies reveals advection of cold air by anticyclonic motion around blocking highs, which is less distinct in the Southern Hemisphere due to stronger zonal flow. We find GPS RO to be a promising new data set for blocking research that gives insight into the vertical atmospheric structure, especially in light of the expected increase in data coverage that future missions will provide.

## 1 Introduction

Global weather and climate are determined by different processes such as the jet stream, the storm tracks, and blocking. Blocking is a particularly important feature in many regions at mid-latitudes (e.g. Woollings, 2010). It describes a synoptic situation, in which a strong and stationary high-pressure system weakens or reverses the climatological eastward flow at mid-latitudes (Rex, 1950; Trenberth and Mo, 1985; Tibaldi and Molteni, 1990; Pelly and Hoskins, 2003; Barriopedro et al., 2006; Croci-Maspoli et al., 2007; Oliveira et al., 2014). Due to its persistence of up to several weeks, atmospheric blocking significantly influences key atmospheric variables such as geopotential height (GPH), temperature, and humidity throughout the troposphere and lower stratosphere. Further impacts of blocking are surface extremes which can lead to severe damages on economy and society (e.g. García-Herrera et al., 2010; Gilbert, 2010; Rodrigues and Woollings, 2017).

In the Northern Hemisphere (NH), the main blocking regions are located over the North Atlantic and Europe (Euro–Atlantic blocking region) as well as over the North Pacific (also referred to as the Alaskan blocking region) (Barriopedro et al., 2010; Whan et al., 2016). The impact of blocking on surface temperature extremes is well established for both regions and different seasons (e.g. Favre and Gershunov, 2006; Buehler et al., 2011; Pfahl and Wernli, 2012; Bieli et al., 2015; Whan et al., 2016; Brunner et al., 2017). The connection to humidity, precipitation, and droughts has also been intensively investigated, especially in recent years (e.g. Carrera et al., 2004; Galarneau et al., 2012; Pfahl et al., 2015; Wise, 2016; Sousa et al., 2017).

In the Southern Hemisphere (SH), blocking occurs in the entire South Pacific between 160° E and 75° W. The highest frequencies are found in the south-eastern Pacific during winter (e.g. de Adana and Colucci, 2005; Berrisford et al., 2007; Parsons et al., 2016). However, in the SH blocking occurrence is considerably lower than in the NH. Furthermore, the impacts of blocking on populated areas are weaker compared to the NH (e.g. Lejenäs, 1984; de Adana and Colucci, 2005). Due to this imbalance comparably few studies investigate blocking in the SH, mostly focusing on impacts in Australia and New Zealand (Australian–New Zealand blocking region) and in South America (south-eastern Pacific blocking region) (e.g. Marques and Rao, 1999; Cowan et al., 2013; Pook et al., 2013; Parker et al., 2014). Several studies have also looked into the influence of other phenomena like the El Niño–Southern Oscillation (ENSO) or the Antarctic oscillation (also known as Southern Annular Mode) on SH blocking (Damião Mendes and Cavalcanti, 2014; Oliveira et al., 2014).

The systematic and global detection and analysis of atmospheric blocking as well as its impacts set demanding requirements of the data sets in use. Apart from global coverage, observations with high spatial and temporal resolution are needed. Hence, blocking research mainly relies on model output and reanalysis data rather than using direct observations. However, most models show only limited skill in blocking representation, as has been noted by many studies in the past (D'Andrea et al., 1998; Vial and Osborn, 2012; Barnes et al., 2012; Anstey et al., 2013; Christensen et al., 2013; Dunn-Sigouin and Son, 2013; Masato et al., 2013). Recently, Davini and D'Andrea (2016) showed that current climate models still underrepresent blocking occurrence by up to 50 %, particularly in the Euro–Atlantic blocking region. Reanalyses combine an atmospheric model with a range of observations from different measurement systems to approximate the atmospheric state as accurately as possible. Due to this data assimilation the accuracy of reanalyses is less well understood compared to observations (Parker, 2016). In addition, there can be significant differences between different reanalyses and the causes are not yet fully understood (Fujiwara et al., 2017). Brunner et al. (2016) demonstrated the potential of Global Positioning System (GPS) radio occultation (RO) to detect and analyse blocking in this observational data set, using two exemplary blocking cases in 2010 and 2013. GPS RO provides highly accurate measurements of atmospheric variables and has therefore the potential to complement models and reanalyses as data set for blocking research.

In this study we provide, for the first time, a global perspective on atmospheric blocking based on the RO record from September 2006 to August 2016 exploiting its good vertical resolution for investigating the atmospheric vertical structure in temperature and humidity during blocking events. In Sect. 2, we introduce the RO record as well as the reanalysis data sets used for comparison. Section 3 describes the blocking detection algorithm, the gridding method for RO, and the computation of anomalies, composites, and significance testing. We present the results of our study in Sect. 4 and conclude with a summary in Sect. 5.

## 2 Data

### 2.1 Radio occultation data

GPS RO is an active limb-sounding technique (Kursinski et al., 1997; Hajj et al., 2002). The measurements are characterised by global coverage, high vertical resolution, high accuracy, and no need for inter-satellite calibration (e.g. Foelsche et al., 2011; Ho et al., 2012; Steiner et al., 2013). The resolution reaches about 60 km horizontally and 100 m vertically in the lower troposphere and about 300 km horizontally and 1.5 km vertically in the lower stratosphere (Melbourne et al., 1994; Kursinski et al., 1997; Gorbunov et al., 2004). RO data have, so far, been used for a range of different applications in monitoring atmospheric variability and changes in Earth's climate (Anthes, 2011; Steiner et al., 2011; Gleisner et al., 2015; Randel and Wu, 2015). Significant improvement of weather forecasting (e.g. Healy and Thépaut, 2006; Cardinali, 2009) and atmospheric reanalyses (e.g. Poli et al., 2010; Simmons et al., 2014) has been made since RO observations can be assimilated without bias correction and act as anchor measurements. Including RO into reanalyses can reduce biases in the troposphere and stratosphere in both hemispheres (Poli et al., 2010). Several studies also used RO data to investigate dynamical features of the atmosphere such as waves (Randel and Wu, 2005; de la Torre and Alexander, 2005; Tsuda, 2014), the ENSO (Scherllin-Pirscher et al., 2012; Sun et al., 2014), tropopause characteristics (Schmidt et al., 2008; Rieckh et al., 2014; Peevey et al., 2014; Randel et al., 2003; Schmidt et al., 2005), and blocking (Brunner et al., 2016).

In this study we use RO data processed by the Wegener Center occultation processing system version 5.6 (OPSv5.6). Quality-controlled measurements (Angerer et al., 2017) for the 10-year period from September 2006 to August 2016 are selected, including data from CHAMP, FORMOSAT-3/COSMIC, C/NOFS, GRACE, SAC-C, and TerraSAR-X. A detailed description of the OPS retrieval is given by Schwärz et al. (2016, Appendix A therein). Error estimates are provided by Scherllin-Pirscher et al. (2017). The accuracy of the data is best in the upper troposphere and lower stratosphere with 0.7 K in temperature and 10 m in GPH for individual profiles (Scherllin-Pirscher et al., 2011b, 2017) and even better when averaging over a range of profiles (Scherllin-Pirscher et al., 2011a).

We compute daily fields at a regular 2.5° × 2.5° grid using a weighted average in space and time applied to the randomly distributed RO events, following

**Table 1.** Summary of reanalysis products, their resolution, assimilation of GPS RO data, and reference publications.

| Name | Provider | Downloaded resolution | RO assimilation | Reference |
|------|----------|----------------------|-----------------|-----------|
| ERA-Interim | ECMWF | 6 h, $2.5° \times 2.5°$ | Since 1 January 2001 | Poli et al. (2010), Dee et al. (2011) |
| JRA-55 | JMA | 6 h, $1.25° \times 1.25°$ | Since 1 January 2001 | Ebita et al. (2011), Kobayashi et al. (2015) |
| MERRA-2 | NASA | 6 h, $0.625° \times 0.5°$ | Since 15 July 2004 | McCarty et al. (2016), Gelaro et al. (2017) |

$$x_{\text{grid}}(\lambda, \phi, d) = \frac{\sum_i w_i x_i(\lambda', \phi', d')}{\sum_i w_i}, \tag{1}$$

where $x_{\text{grid}}(\lambda, \phi, d)$ represents a certain grid cell centred at longitude $\lambda$, latitude $\phi$, and day $d$. Each RO event $x_i(\lambda', \phi', d')$ within $\pm 7.5°$ in longitude, $\pm 2.5°$ in latitude, and $\pm 2$ days of the grid cell centre is considered and weighted with a Gaussian weighting function, $w_i$. The weighting function is given as

$$w_i = \exp\left(-\left[\left(\frac{\Delta\lambda}{L}\right)^2 + \left(\frac{\Delta d}{D}\right)^2\right]\right), \tag{2}$$

with $\Delta\lambda = \lambda - \lambda'$, $\Delta d = d - d'$, $L = 7.5°$, and $D = 1$ day. This effective resolution has been chosen to minimise the number of empty grid cells while maintaining most of the atmospheric variability. For more detailed information on the applied gridding method we refer to Brunner et al. (2016).

## 2.2 Reanalysis data

Different reanalyses have extensively been used to investigate blocking and to evaluate the model performance in blocking representation (e.g. Sinclair, 1996; Trigo et al., 2004; Sillmann et al., 2011; IPCC, 2013; Davini and D'Andrea, 2016; Schiemann et al., 2017). Here, we selected three of the more recent reanalyses (Table 1), which compare well against each other, e.g. in terms of temperature and zonal winds (e.g. Long et al., 2017), to investigate their representation of blocking in comparison to RO: the European Centre for Medium-Range Weather Forecasts (ECMWF) Reanalysis Interim (ERA-Interim), the Japanese 55-year Reanalysis (JRA-55) by the Japan Meteorological Agency (JMA), and the recently published second Modern-Era Retrospective analysis for Research and Applications (MERRA-2) by the National Aeronautics and Space Administration (NASA). We use GPH at the 500 hPa pressure level from September 2006 to August 2016, from ERA-Interim, JRA-55, and MERRA-2 for blocking detection. All three reanalyses have a native 6-hourly time resolution, which is averaged to daily fields. The varying spatial resolutions are interpolated to a consistent $2.5° \times 2.5°$ longitude–latitude grid.

All three reanalyses assimilate RO data. ERA-Interim includes measurements from CHAMP, FORMOSAT-3/COSMIC, GRACE, MetOp, and TerraSAR-X (Poli et al.,

2010; Dee et al., 2016); MERRA-2 additionally includes SAC-C (McCarty et al., 2016); and JRA-55 all the former plus C/NOFS (Kobayashi et al., 2015).

## 3 Methods

A blocking detection algorithm based on the reversal of 500 hPa GPH gradients is applied to the RO data between September 2006 and August 2016. Resulting blocking frequencies are investigated with regard to their horizontal and temporal evolution and compared to established reanalyses. Three main blocking regions in both hemispheres are selected and the vertical atmospheric structure of temperature and specific humidity anomalies during blocking in these regions is analysed. Statistically significant links between blocking and the anomalies in temperature and specific humidity are found via a Monte Carlo test.

## 3.1 Blocking detection in RO GPH fields

We use a standard 500 hPa GPH gradient algorithm (Tibaldi and Molteni, 1990; Scherrer et al., 2006; Davini et al., 2012, 2014), adapted to allow the simultaneous detection of blocking in the NH and SH. First, GPH gradients to the north ($\Delta Z_N$) and to the south ($\Delta Z_S$) are calculated for each grid cell:

$$\Delta Z_N(\lambda, \phi) = \frac{Z(\lambda, \phi + \Delta\phi) - Z(\lambda, \phi)}{\Delta\phi}, \tag{3}$$

$$\Delta Z_S(\lambda, \phi) = \frac{Z(\lambda, \phi - \Delta\phi) - Z(\lambda, \phi)}{\Delta\phi}, \tag{4}$$

with the longitude $\lambda$ running from $180° W$ to $177.5° E$ and the latitude $\phi$ running from $72.5° S$ to $72.5° N$. The gradient is calculated over a latitude width of $\Delta\phi = 15°$. By this definition the northern gradient $\Delta Z_N$ is positive if the GPH is higher to the north and equivalently $\Delta Z_S$ is positive if the GPH is higher to the south.

GPH-based blocking detection indices are usually restricted in latitude to avoid the detection of low-latitude atmospheric waves which are not considered as blocking in the classical sense (e.g. Scherrer et al., 2006; Barriopedro et al., 2006; Martineau et al., 2017). Particularly in hemispheric summer, the poleward shift of slow-moving atmospheric ridges can otherwise lead to very high blocking frequencies equatorward of $45°$ latitude (e.g. Davini et al.,

59

2014). In order to avoid the detection of low-latitude blocking and to ensure comparability of our results with existing literature, we introduce a third gradient towards the Equator ($\Delta Z_E$), following Davini et al. (2012):

$$\Delta Z_E(\lambda, \phi) = \frac{Z(\lambda, \phi \mp 2 \times \Delta\phi) - Z(\lambda, \phi \mp \Delta\phi)}{\Delta\phi}$$

$$\text{with} \begin{cases} - \text{ in the NH} \\ + \text{ in the SH,} \end{cases} \quad (5)$$

where the minus sign is valid in the NH and the plus sign is valid in the SH. To put it simply, $\Delta Z_E$ is defined positive at a certain grid cell if there is a clear trough in the GPH field towards the Equator and is used to prohibit the identification of slow-moving low-latitude ridges as blocking.

Instantaneous blocking (IB) is identified on a grid cell basis when the following three conditions are simultaneously met:

$$\Delta Z_N(\lambda, \phi) \begin{cases} < -10\,\text{m}\,(°\,\text{lat.})^{-1} \text{ in the NH} \\ < 0\,\text{m}\,(°\,\text{lat.})^{-1} \text{ in the SH,} \end{cases} \quad (6)$$

$$\Delta Z_S(\lambda, \phi) \begin{cases} < 0\,\text{m}\,(°\,\text{lat.})^{-1} \text{ in the NH} \\ < -10\,\text{m}\,(°\,\text{lat.})^{-1} \text{ in the SH,} \end{cases} \quad (7)$$

$$\Delta Z_E(\lambda, \phi) > 5\,\text{m}\,(°\,\text{lat.})^{-1} \text{ for both hemispheres.} \quad (8)$$

We only consider IB events with an extent of at least 15° in longitude and filter out smaller blocking systems. In a final step, we define blocking for a given day and grid cell when such a large-scale event is also persistent and stationary, requesting IB to be found within a $10° \times 5°$ longitude–latitude region in the neighbouring $\pm 2$ days. Reducing the longitude–latitude view, one-dimensional blocking frequencies consider a given longitude in the NH or SH as blocked if at least one latitude is blocked.

To investigate the effects of blocking on temperature and humidity we further define blocked days with respect to three selected regions. A blocked day is found if at least one grid point is blocked in such a region. The regions are chosen to cover the blocking maxima in both hemispheres. These main blocking regions are, in the following, referred to as the North Atlantic region (30° W to 10° E and 30 to 72.5° N), the North Pacific region (160° E to 160° W and 30 to 72.5° N), and the East Pacific region (150 to 90° W and 72.5 to 30° S). The coincidence of temperature and humidity anomalies during blocked days is tested statistically (see Sect. 3.3) in order to investigate the effects of blocking on the atmospheric temperature and humidity structure (see Sect. 4.2).

### 3.2 Anomaly computation in RO temperature and humidity fields

Anomalies of atmospheric temperature ($T_{Anom}$) and relative specific humidity ($q_{Anom}$) during blocked days $t$ are calcu-

lated for each location ($\lambda, \phi$) and pressure level $p$:

$$T_{Anom} = T - \overline{T}, \quad (9)$$

$$q_{Anom} = \frac{q - \overline{q}}{\overline{q}} \times 100\%, \quad (10)$$

with temperature $T = T(t, \lambda, \phi, p)$ and specific humidity $q = q(t, \lambda, \phi, p)$. Respective daily mean values $\overline{T} = \overline{T}(d, \lambda, \phi, p)$ and $\overline{q} = \overline{q}(d, \lambda, \phi, p)$ are calculated over the 10 years from September 2006 to August 2016 for each day of the year $d$. For specific humidity we show relative anomalies to allow easier comparison across different pressure levels due to its exponential decline with altitude. Composites of the temperature and specific humidity anomalies are then obtained by averaging over all blocked days $t$ of a certain region.

### 3.3 Statistical significance testing

Statistical significance of the composites is determined for each pressure level on a grid cell basis using a Monte Carlo test. Given $n$ blocked days in a certain region and period, 1000 samples of $n$ random days are drawn from the same period (e.g. season) and averaged. To conserve the autocorrelation, consecutive blocked days are clustered and lead to consecutive days in the random samples. Based on the 1000 random samples the probability density function (PDF) is calculated, with values below the 5th or above the 95th percentile of this PDF being considered statistically significant.

## 4 Results

### 4.1 Blocking climatologies from RO

Figure 1 shows annual mean blocking frequencies derived from the RO data set and the three reanalyses, ERA-Interim, JRA-55, and MERRA-2. All four data sets agree on the two main blocking regions in the NH (Fig. 1a). There is a clear maximum in the blocking frequency in the Euro–Atlantic blocking region between 50° W and 50° E and a smaller maximum in the North Pacific blocking region between 150° E and 150° W (compare IPCC, 2013, Box 14.2). In the Euro–Atlantic region, the maximum frequency is between about 10% for ERA-Interim and JRA-55 and about 10.5% for MERRA-2, while the maximum RO frequency is a bit lower with 8%. In addition, the RO maximum in this region is shifted by about 10° to the east compared to the reanalyses. All four data sets consistently place the minimum blocking frequency east of the Euro–Atlantic region at 100° E. RO shows frequencies of 2% here, ERA-Interim and JRA-55 are about 1% higher, and MERRA-2 is about 1.5% higher. In the North Pacific region, RO reaches a maximum frequency of about 6%, while the reanalyses show about 7 to 8%. The region with lowest blocking frequencies below 1% is found at 90° W across all data sets. In general, RO
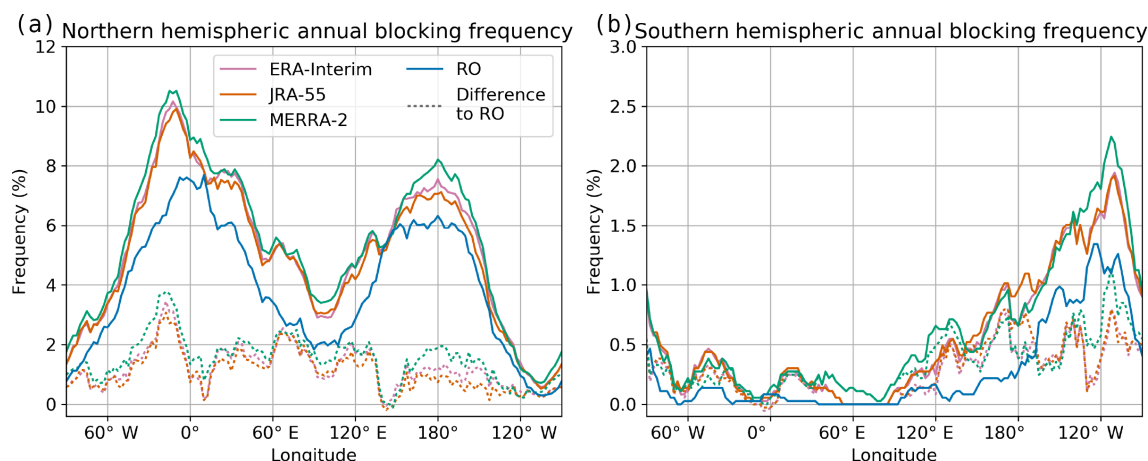
**Figure 1.** Annual mean blocking frequencies for the **(a)** Northern and **(b)** Southern Hemisphere in the period September 2006 to August 2016. Each coloured line represents a data set, the dashed lines show the respective differences of reanalyses to RO. Note the different *y*-axis ranges.

data show an underestimation of one-dimensional blocking frequencies. The absolute difference to the reanalyses stays below 2 % at most longitudes. Only near the maximum in the Euro–Atlantic blocking region the difference exceeds 3 %.

Figure 1b shows the SH blocking distribution. Again, all data sets agree on the main blocking region in the South Pacific, with RO again showing a slight underestimation of about 0.5 %. Highest frequencies are consistently found in the south-eastern Pacific between 150 and 100° W. MERRA-2 shows the highest maximum frequency with about 2.25 %, followed by ERA-Interim and JRA-55 with about 2 %, and RO with about 1.25 %. Eastward of the south-eastern Pacific region, RO shows hardly any blocking and all three reanalyses stay below 0.5 % blocking frequency as well (corresponding to about 2 blocked days per year on average). In the Australian–New Zealand region between 100° E and 150° W, RO blocking frequencies hardly exceed 0.5 % and the reanalyses hardly exceed 1 %.

The time evolution of blocking is presented in Fig. 2 for both hemispheres from September 2006 to August 2016. Both main blocking areas in the NH, as well as the South Pacific region in the SH are clearly recognisable in this view. A closer inspection reveals that a NH blocking has an average duration of 4 days and an average longitudinal extent of about 34°. The most persistent and continuous blocking cases in the NH occurred in March–April 2007 (27 days), in December–January 2009/2010 (28 days), and in February 2015 (23 days). All three cases were connected to unusual temperature anomalies, as e.g. discussed by Cattiaux et al. (2010) for winter 2009/2010 with severe cold spells hitting Europe.

Note that blocking can show considerable fluctuations in intensity during its evolution so that blocking cases may be interrupted by a few unblocked days and are not regarded as continuous signal. An example is the sequence of blockings

in summer 2010 (see e.g. Brunner et al., 2016, Fig. 3) leading to a severe heat wave in Russia (e.g. Barriopedro et al., 2011).

In the SH, an average blocking only lasts 2.5 days and has an extent of 23° in longitude. There, the most persistent blocking cases are found in May–June 2012 (12 days), in July–August 2014 (8 days), and in September 2015 (8 days). In general, blocking in the SH is by far weaker and less frequent than in the NH.

Taking a closer look into the characteristic blocking features, we further investigate the distribution of blocking frequencies in longitude and latitude for different seasons. Figure 3 shows horizontally resolved blocking frequencies for all seasons in the NH for RO and ERA-Interim. A comparison of blocking frequencies with JRA-55 and MERRA-2 is not shown as they are highly consistent and agree within 0.2 % annual mean blocking frequency to ERA-Interim. RO resolves all the main features in the NH blocking distribution. Annual mean frequencies from RO show the main blocking regions over the North Atlantic and Europe (Euro–Atlantic blocking region) as well as a maximum over the North Pacific. In the seasonally resolved analysis, RO detects the highest blocking frequencies over the Euro–Atlantic region during winter (DJF) and spring (MAM) consistent with ERA-Interim. Blocking occurrence in the North Pacific region is high during the entire year, with fewest blockings in fall (SON). In general, RO and ERA-Interim agree very well on the location of the blocking regions in all seasons. Larger differences exceeding 2 % are only found in NH summer (JJA), where RO does not fully capture the frequency maxima over northern Russia. In winter, RO shows slightly higher blocking frequencies than ERA-Interim in the North Atlantic and over Scandinavia.

One possible reason for the generally lower blocking frequencies in the RO record is the measurement density of the RO events. As described in Sect. 2, RO data are aver-

www.atmos-meas-tech.net/10/4727/2017/     Atmos. Meas. Tech., 10, 4727–4745, 2017

61
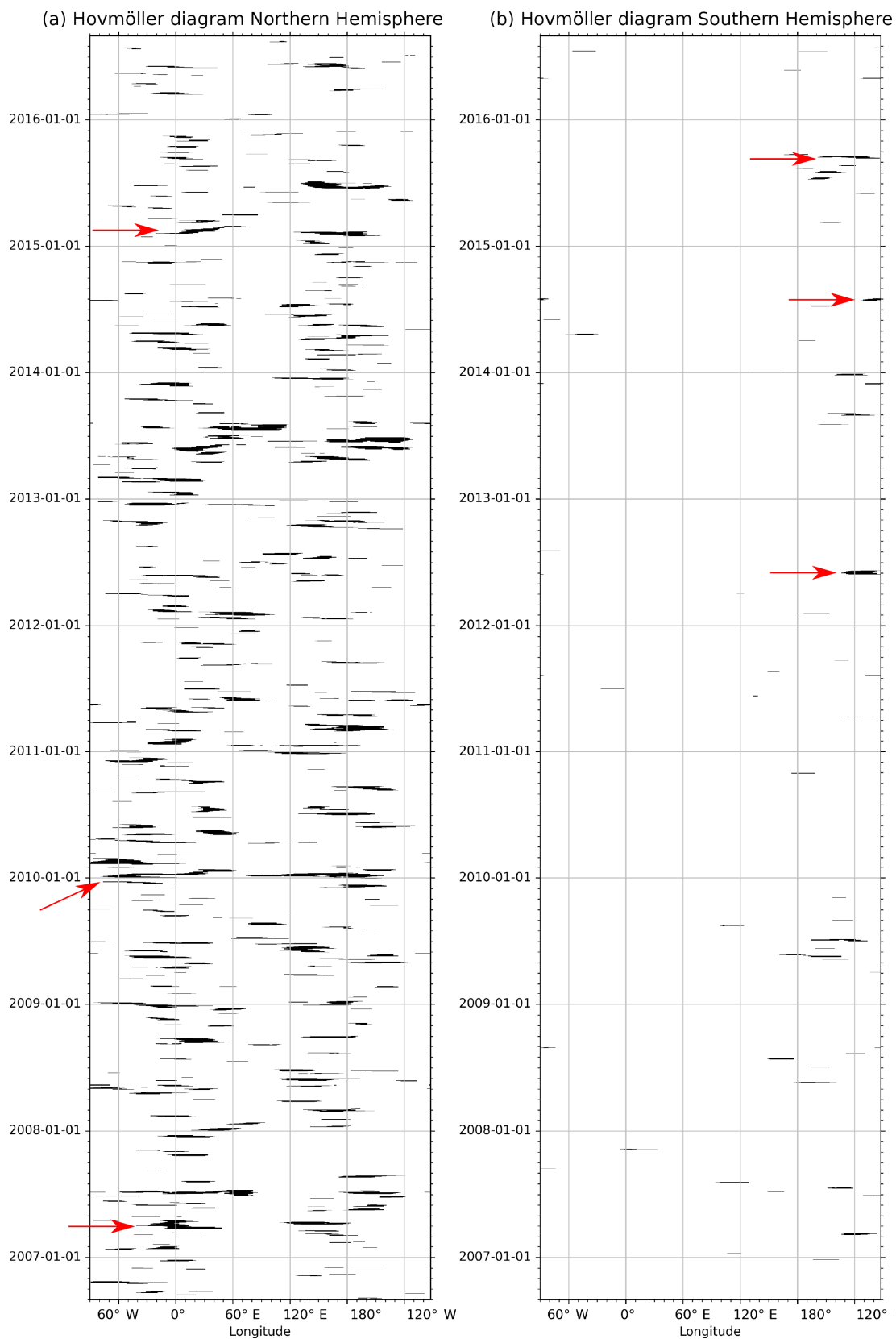
**Figure 2.** Hovmöller diagram of blocking as function of time over longitudes for the **(a)** Northern and **(b)** Southern Hemisphere based on the RO record for the period September 2006 to August 2016. Red arrows mark the three longest blocking events in each hemisphere.

**Atmos. Meas. Tech., 10, 4727–4745, 2017**     **www.atmos-meas-tech.net/10/4727/2017/**

62
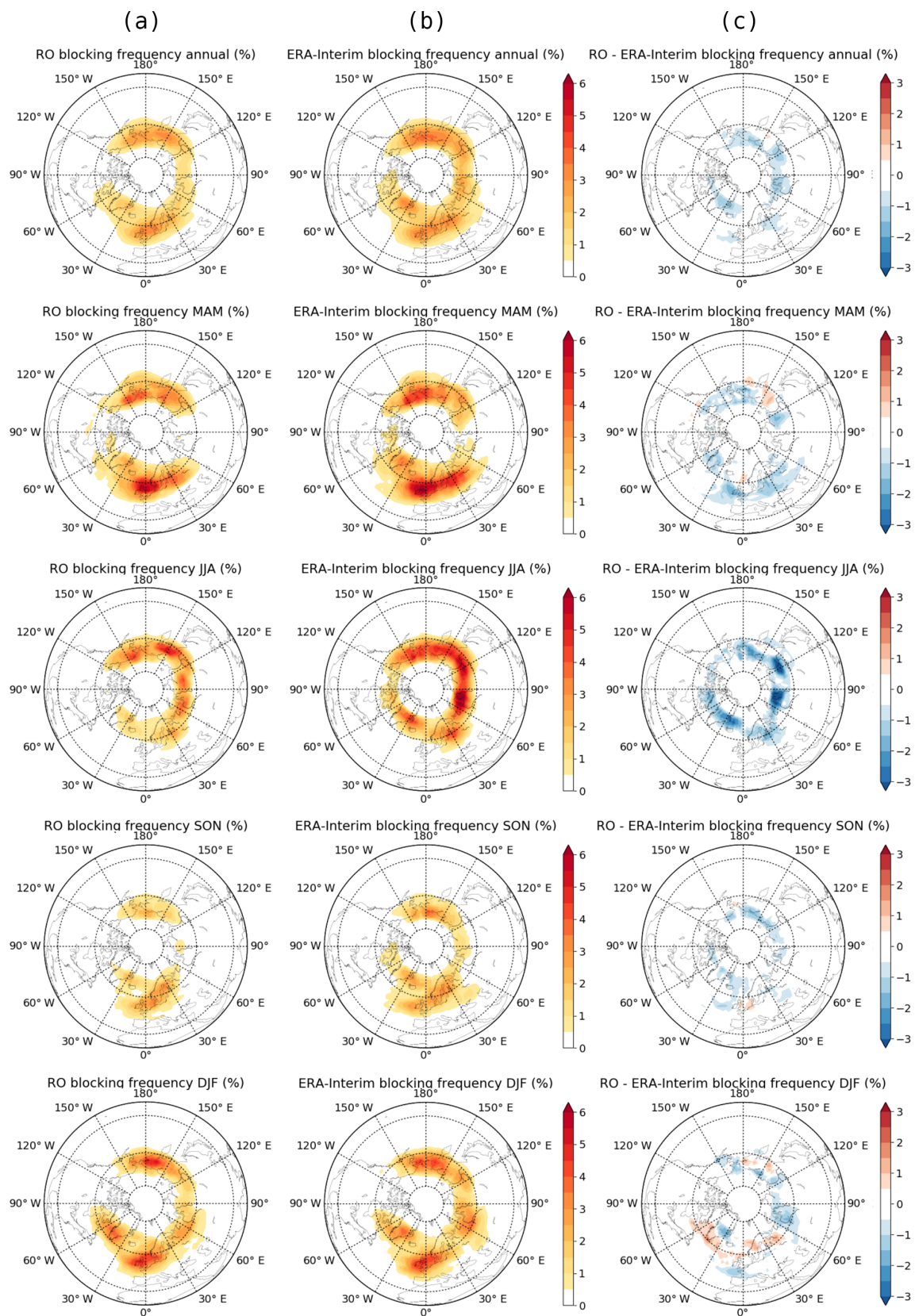
**Figure 3.** Blocking frequencies for the Northern Hemisphere in the period September 2006 to August 2016. Frequencies are shown for **(a)** RO, **(b)** ERA-Interim, and **(c)** RO minus ERA-Interim for (from top to bottom) the annual mean and seasonal means, spring, summer, fall, and winter.

63

aged from the randomly distributed measurements to a regular daily grid using a weighted mean. Due to the random distribution of observations, some grid cells may not have any contributing RO events (see also Brunner et al., 2016, for a detailed analysis). Such empty grid cells can artificially lower the blocking frequency if they appear at the location of a blocking.

We tested the effect of the weighted averaging in the gridding of RO data and applied the same weighted averaging in space and time to ERA-Interim data. Comparing then blocking frequencies from the similarly weighted ERA-Interim fields to RO yields slightly reduced differences in blocking frequency and shows that about 0.5 % in difference can be explained by the weighted averaging.

In the SH, the overall blocking frequency is notably lower compared to the NH. It has been argued that the stronger zonal flow at mid-latitudes in the SH leads to less persistent blocking conditions (e.g. Trenberth and Mo, 1985). Oliveira et al. (2014) suggest a 3-day stationarity criterion for blocking detection in the SH as opposed to the typical 5-day criterion in the NH to account for the stronger westerlies. However, we here aim at a consistent comparison of blocking in both hemispheres and therefore use the 5-day criterion globally. This approach allows a direct comparison of blocking anticyclones and their impacts in both hemispheres.

In the SH, blocking is almost exclusively found in the South Pacific (Fig. 4). Normally two sub-regions are distinguished mainly with regard to the impact on populated areas: blocking in the south-western Pacific (often referred to as the Australian–New Zealand blocking region) and blocking in the south-eastern Pacific region (influencing populated areas in South America; referenced to as the East Pacific region). In contrast to the NH, SH blocking is mainly constraint to the southern winter (JJA) season, where two-dimensional frequencies can reach 2 %. RO and ERA-Interim consistently show this seasonal development. Differences between the two data sets stay mostly below 0.25 % annually and below 0.5 % seasonally. Largest differences are found during the blocking maximum in SH winter.

## 4.2 Atmospheric temperature and specific humidity response to blocking

In the following we investigate the atmospheric structure of vertically resolved temperature and relative specific humidity anomalies in the troposphere and lower stratosphere during blocked days. The effects of blocking are shown for three regions (two in the NH, one in the SH) and for five selected pressure levels: 850, 500, 270, 200, and 100 hPa. These levels represent (bottom to top) regions of main blocking influence in the lower- and middle-tropospheric region, the tropopause region, the region of main blocking influence in the lowest stratosphere and of decreasing influence in the stratosphere above.

Winter and summer seasons are compared in Figs. 5 and 6 for temperature and relative specific humidity anomalies during blocked days over the North Atlantic region showing extended winter (NDJFM) and extended summer (MJJAS), respectively. During winter a clear and statistically significant positive temperature anomaly dominates most of the blocking region throughout the troposphere up to about 300 hPa (Fig. 5a). The anomalies reach about 2 K in the lower troposphere and exceed 3 K at their maximum at about 500 hPa. At upper levels, the positive anomalies decrease towards the tropopause. Beginning near 300 hPa, the decrease is accompanied by a shift to the north. The temperature anomalies are smallest at about 270 hPa, where they change from positive to negative. In the lower stratosphere, increasingly negative temperature anomalies, falling below −3 K at 200 hPa, are the dominating feature. At higher altitudes, the influence of blocking on the temperature weakens and the anomalies decrease. A noticeable feature is also that the temperature anomalies are not centred in the blocking region in the troposphere near 500 hPa but appear to be shifted to the west. This asymmetry disappears at higher altitudes and especially the lower-stratospheric cold anomalies are perfectly centred in the blocking region.

In the troposphere the central positive temperature anomaly is surrounded by a cold anomaly on the northern, eastern, and southern flanks. This anomaly, which is considerably weaker in summer (see Fig. 6), hints at the influence of the circulation during blocked conditions. The anticyclonic motion of air around stationary high-pressure systems in the investigated region favours the advection of cold air from the north towards central Europe. The cold anomalies are stronger in the lower regions of the troposphere, falling below −2 K at 850 hPa. At 500 hPa a band of cold air with composite temperatures below −1 K is still visible to the east and south of the positive anomaly which change above the tropopause at the 200 and 100 hPa level into positive anomalies of about 0.5 to 1.5 K, especially north and south of the central cold anomaly.

The analysis of relative specific humidity anomaly composites (Fig. 5b) reveals a clear correlation with temperature in most of the troposphere: positive temperature anomalies are accompanied by positive specific humidity anomalies and negative temperature anomalies are accompanied by negative specific humidity anomalies. However, dry anomalies are mostly restricted to the European continent, especially in the lower troposphere. In contrast to temperature, specific humidity anomalies do not change sign in the tropopause region. The strongest anomalies, exceeding 30 %, are found at the altitude of weakest temperature anomalies (near 270 hPa). In the (generally) very dry stratosphere the specific humidity anomalies decrease rapidly and no statistically significant signal of blocking is found above about 150 hPa.

For extended summer, temperature and relative specific humidity anomaly composites during blocked days in the
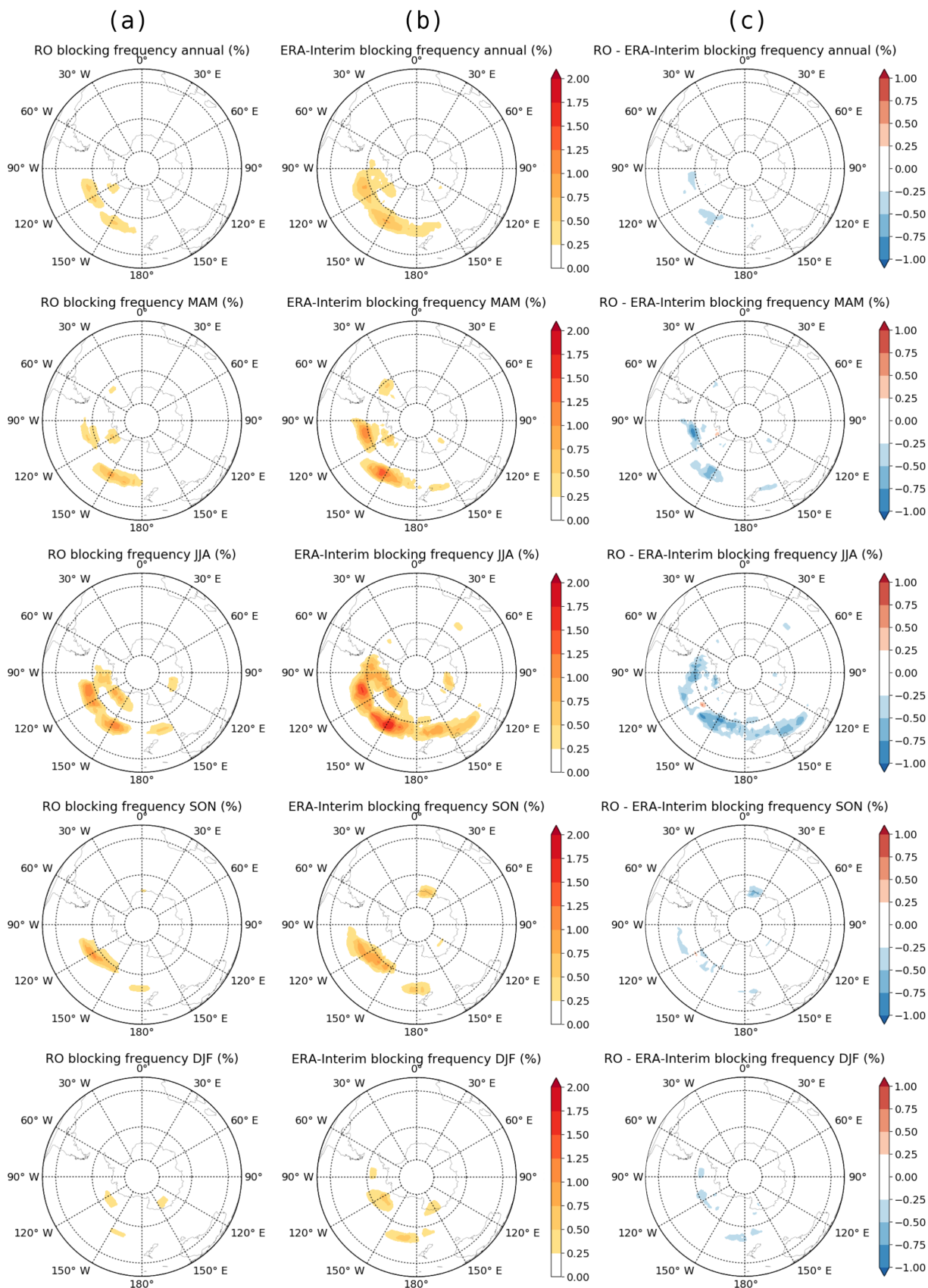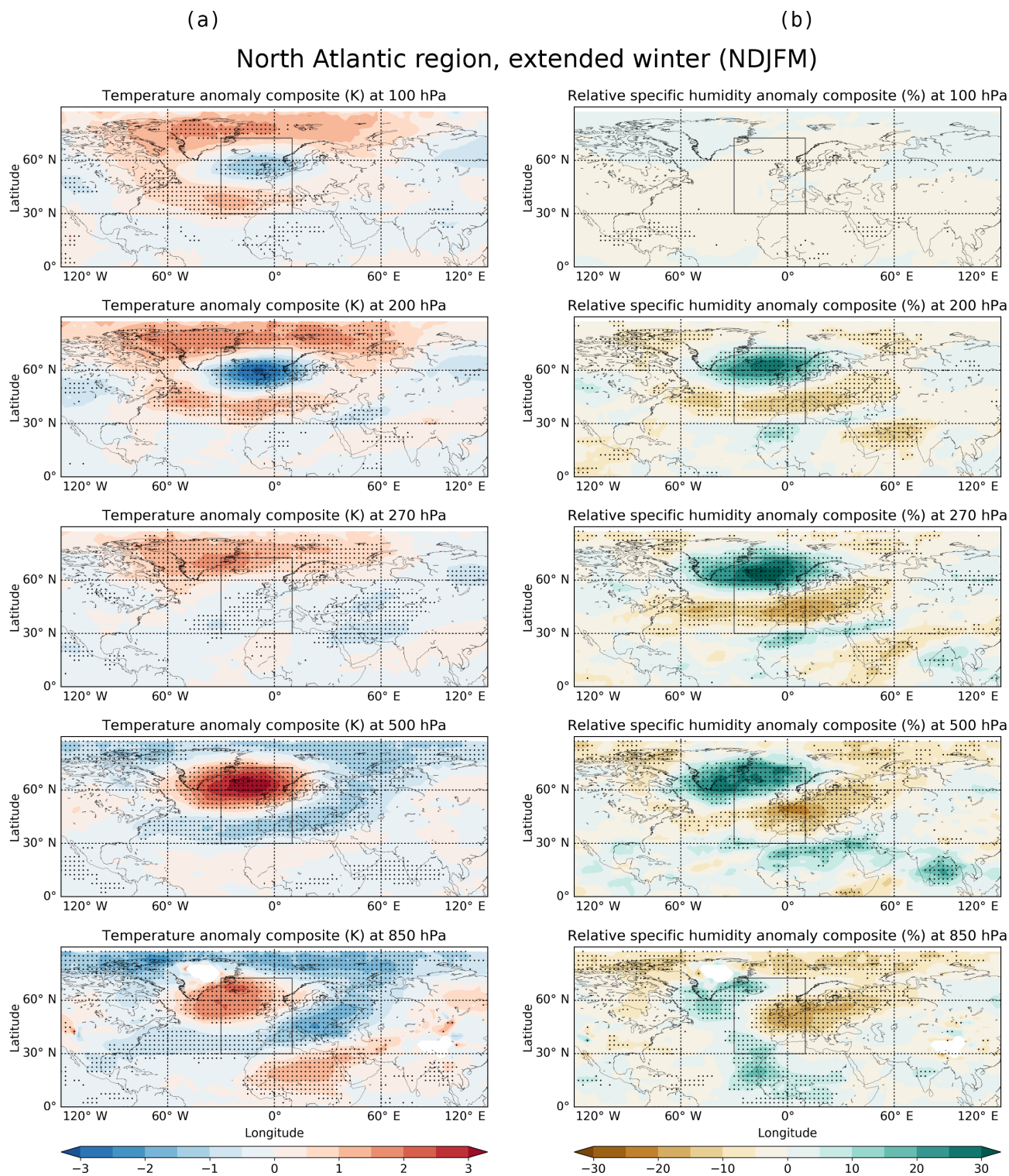
**Figure 4.** As Fig. 3 but for the Southern Hemisphere. Note the different colour bar ranges compared to Fig. 3.

www.atmos-meas-tech.net/10/4727/2017/                    Atmos. Meas. Tech., 10, 4727–4745, 2017

65

(a)

(b)

## North Atlantic region, extended winter (NDJFM)



**Figure 5.** Composites of **(a)** temperature anomalies and **(b)** relative specific humidity anomalies during blocked days in the North Atlantic region between 30° W–10° E and 30–72.5° N (grey box; 267 days in total). Shown is the northern hemispheric extended winter (NDJFM) season. Hatched regions denote statistical significance at the 5th and 95th percentile levels.

(a)                                                                                                (b)

## North Atlantic region, extended summer (MJJAS)
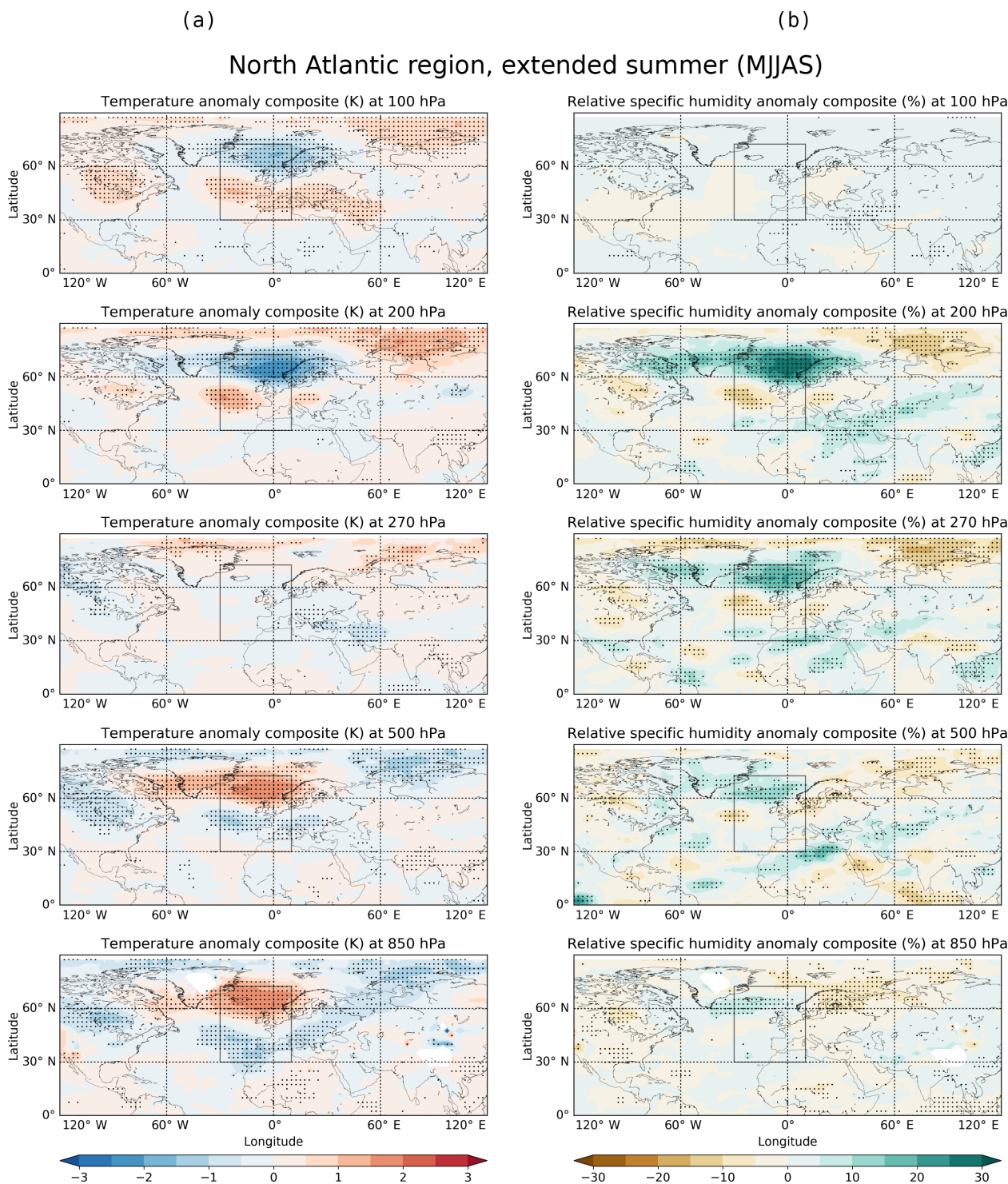


**Figure 6.** As Fig. 5 but for the extended summer (MJJAS) season (186 days in total).

Euro–Atlantic region (Fig. 6) are about 1 K and 10 % lower compared to respective anomalies in winter. Moreover, the band of cold air surrounding the central warm anomaly is less distinct in summer. At 500 hPa, where the feature is clearest in winter, large regions, especially over north-eastern Eu-

rope, are not statistically significantly colder during blocked conditions. This indicates that cold advection from the north is less important during summer blocking. Specific humidity anomalies during summer blocking in this region are not statistically significant in most of the troposphere. Stronger

67

(a)                                                                    (b)

## North Pacific region, extended winter (NDJFM)
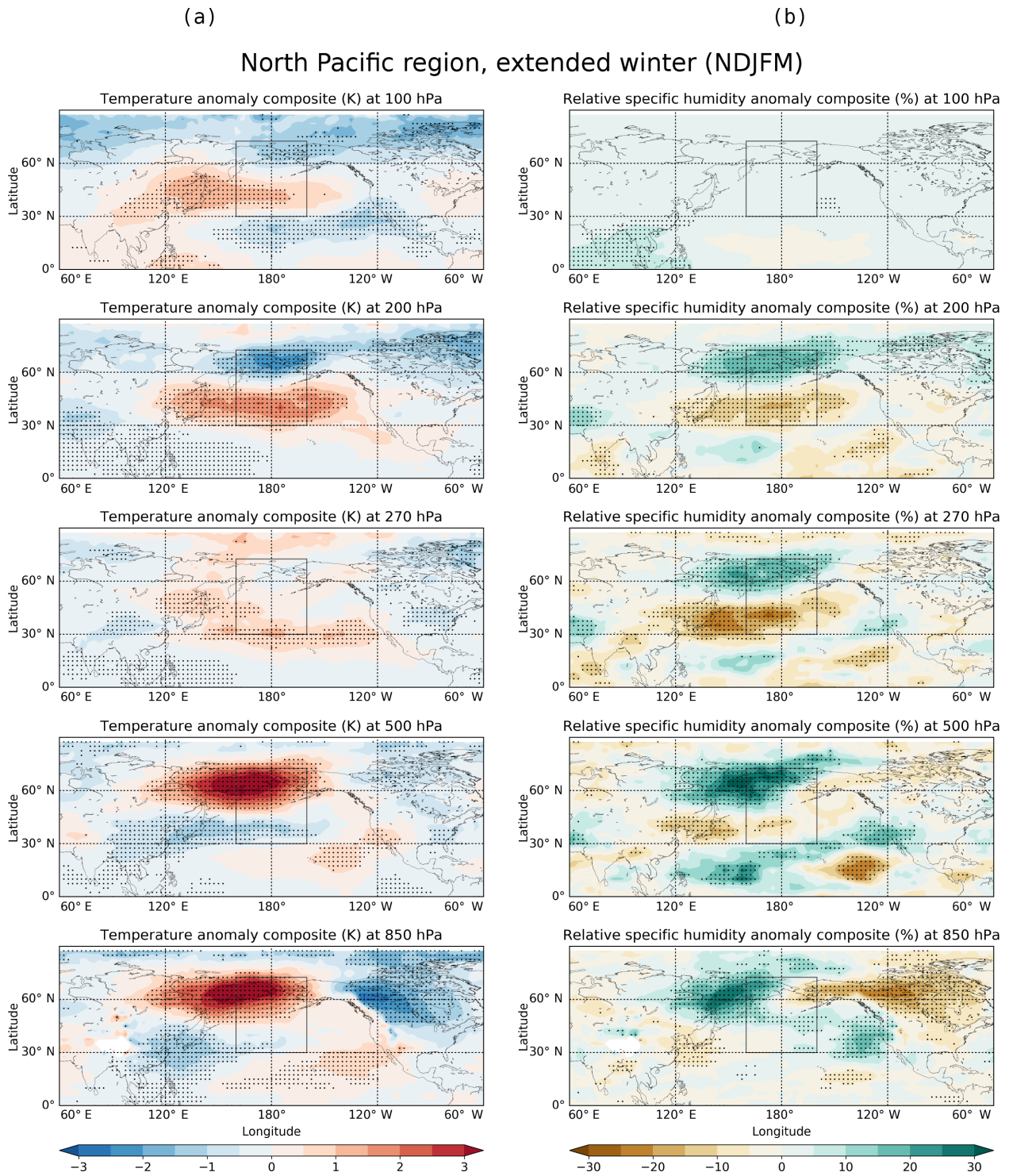


**Figure 7.** As Fig. 5 but for blocking in the North Pacific region between 160° E–160° W and 30–72.5° N (191 days in total).

anomalies are only visible near the tropopause and above, between 270 and 200 hPa.

In the North Pacific blocking region during extended winter (Fig. 7), the main feature in temperature is again a strong positive anomaly in the troposphere. Compared to the North

Atlantic region the anomaly is stronger in the lower troposphere below 500 hPa, while the negative anomaly in the lower stratosphere is slightly weaker. The tropospheric cold anomalies are limited to east and south-west of the blocking region with the coldest temperatures found over the north-

west of the North American continent. In the lower stratosphere the warm anomaly is limited to the south of the blocking region, creating a distinct dipole feature near the 200 hPa pressure level.

Specific humidity anomalies are strongest in the lower and middle troposphere between 850 and 500 hPa and about 10 % lower than in the North Atlantic region between 270 and 200 hPa. At 270 and 200 hPa a clear dipole similar to the 200 hPa temperature anomaly can be found. Above 200 hPa the influence of blocking on atmospheric humidity decreases and hardly any significant signal is found.

For the SH (Fig. 8) we show blocking effects in the East Pacific region. Similar to the NH, both temperature and specific humidity anomalies are clearly shifted to the west of the blocking region in the lower troposphere. The strongest temperature anomalies during blocking, clearly exceeding 3 K, are found in the lowermost part of the troposphere. Towards the tropopause the anomalies decrease and again change sign near 270 hPa. The lowest temperature anomalies below −3 K are located near 200 hPa, similar to the NH. Above, the influence of blocking on temperature decreases. The tropospheric cold anomalies surrounding the blocking region are less distinct in the SH. These results suggest that cold advection plays a less important role in the SH due to the stronger zonal flow. A clear band of negative temperature anomalies is only visible at 500 hPa, while at 850 hPa the strongest cold anomalies are restricted to downstream of the blocking region. Compared to the NH a stronger second temperature maximum appears north-east of the blocking region.

Specific humidity anomalies in the SH show notably more variation than in the NH. Throughout the entire troposphere relative wet and dry anomalies exceed 30 %. The anomalies spread in a wave-like pattern from the blocking region to the north-east, which is most distinct near the tropopause at about 270 hPa. In the lower stratosphere the specific humidity anomalies again decrease rapidly.

In summary, we find similar effects of blocking on atmospheric temperature and specific humidity anomalies in the different investigated regions in both hemispheres. Largest differences in amplitude appear between the seasons, while the SH shows a more complex signature of blocking, especially in specific humidity. For all cases strong positive temperature anomalies are found in the lower to middle troposphere and a maximum negative anomaly in the lower stratosphere at about 200 hPa. Specific humidity anomalies are strongest higher up between 270 and 200 hPa except in the North Pacific region, where the largest anomalies are found at the 500 hPa level.

## 5   Summary, conclusions, and outlook

We presented the first comprehensive analysis of global atmospheric blocking based on GPS RO observations. We used one decade of RO measurements from September 2006 to August 2016 to derive blocking climatologies and to investigate blocking impacts on vertically resolved atmospheric temperature and specific humidity fields. We investigated the representation of main blocking regions in the NH and SH for different seasons. The impact of blocking on vertically resolved temperature and humidity was examined based on anomaly composites and its significance was tested.

Our results show that RO data are well suited for blocking detection. RO correctly resolves the blocking regions in both hemispheres, also capturing the seasonal blocking variability. Average blocking episodes in the NH are found to persist for 4 days and have a longitudinal extent of 34°. In the SH blocking is less persistent and lasts on average 2.5 days, with a typical extent of 23° in longitude.

The impact of blocking on temperature and specific humidity is found to be statistically significant throughout the troposphere and lower stratosphere in both hemispheres. During extended winter a strong positive temperature anomaly exceeding 3 K is found in the centre of the blocking area, slightly shifted to the west at lower altitudes. Above about 500 hPa this anomaly decreases until it changes sign above the climatological tropopause near 270 hPa. In the lower stratosphere, blocking leads to a negative temperature anomaly below −3 K near 200 hPa. Higher up the influence of blocking on temperature decreases. In the troposphere, cold anomalies surround the central warm anomaly, indicating the effect of advection of cold air from the polar region by the anticyclonic motion around blocking highs, which is in general agreement with findings by Bieli et al. (2015). In the lower stratosphere this anomaly also changes sign and appears as anomalously warm region equatorward of the block. Summer temperature anomalies are similar to those in winter but notably weaker in amplitude of up to 50 %. In addition, the advection of cold air plays a less important role, leading to less distinct negative anomalies in the troposphere.

Specific humidity anomalies show a similar behaviour as temperature in the troposphere. In the North Atlantic region, a central wet anomaly is surrounded by dry anomalies on the eastern and equatorward side. However, the anomalies do not change sign at the tropopause, leading to inverse patterns of temperature and specific humidity anomalies in the lower stratosphere. This behaviour of temperature and specific humidity at the tropopause level has recently also been noted by Sitnov et al. (2017). Above about 200 hPa, the influence of blocking on specific humidity is found to decrease rapidly. In the south-east Pacific region, specific humidity anomalies are generally stronger than in the NH and show a wave-like pattern with positive and negative anomalies alternating from the south-west to the north-east due to a stronger zonal flow.

Our findings highlight the main blocking regions in both hemispheres and the effect of blocking in these regions on atmospheric temperature and specific humidity using GPS RO observations. The slight underestimation of blocking frequencies in RO compared to three different reanalyses, ERA-Interim, JRA-55, and MERRA-2, is most probably due

(a)                                                                    (b)

## East Pacific region, extended winter (MJJAS)
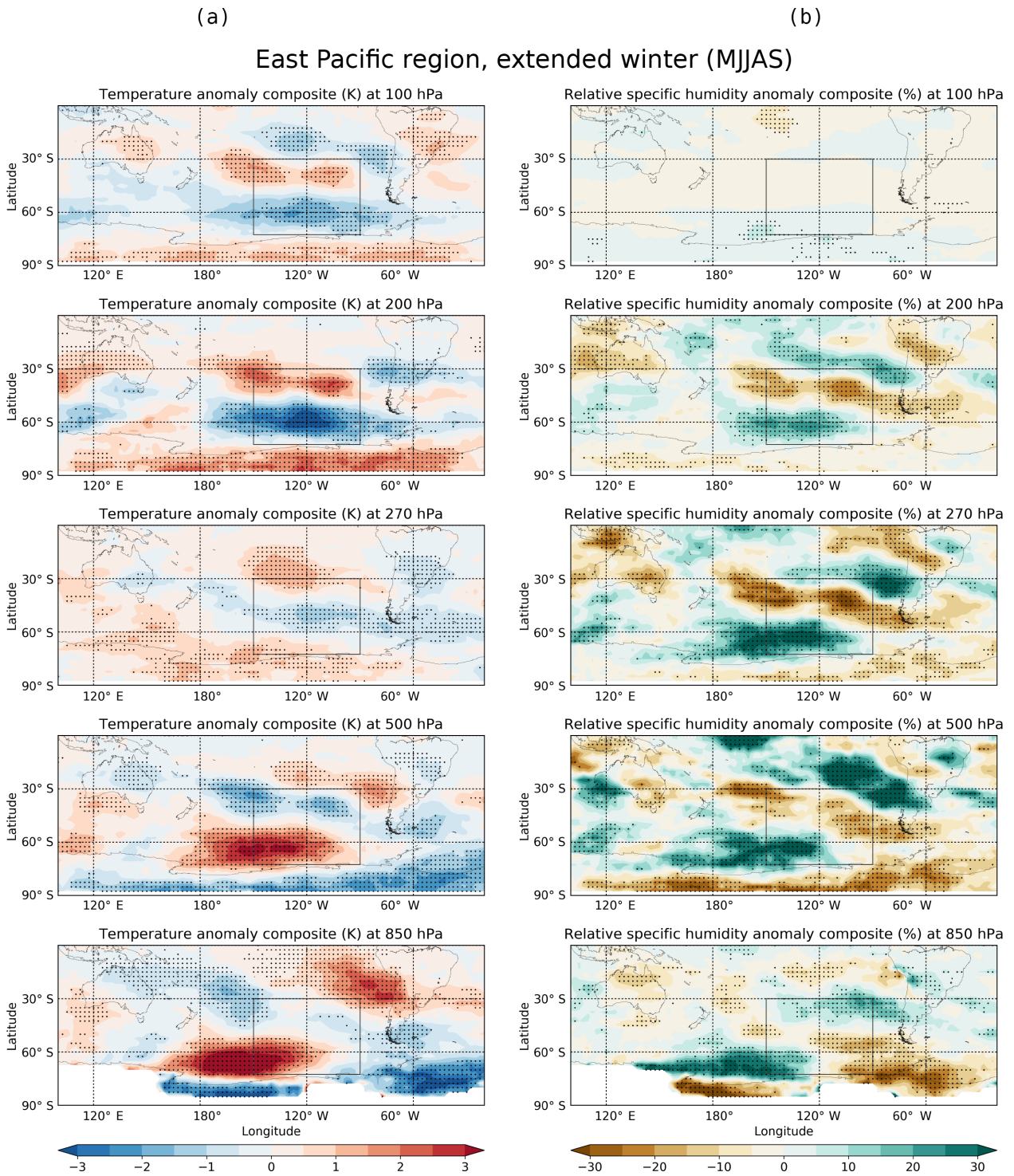


**Figure 8.** As Fig. 5 but for the southern hemispheric extended winter (MJJAS) shown for blocking in the East Pacific region between 150–90° W and 72.5–30° S (81 days in total).

to a too-sparse measurement density. Future RO missions, like the FORMOSAT-7/COSMIC-2 constellation, and the exploitation of signals from more Global Navigation Satellite System (GNSS) constellations, like the European Galileo, the Russian GLONASS, and the Chinese BeiDou, are expected to significantly increase the number of RO events, promising to overcome this undersampling and allowing an

even better performance of RO data in blocking representation (Yue et al., 2014).

RO measurements provide a mostly independent, comprehensive observation-based record of known accuracy (Parker, 2016) for the detection and analysis of atmospheric blocking complementing reanalyses and models. The high vertical resolution of the RO measurements makes them ideal for investigating the atmospheric structure during blocking episodes. This will allow to gain a better understanding of the development of blocking related extreme events, like heat waves and cold spells, flooding, or droughts, in the future.

# References

Angerer, B., Ladstädter, F., Scherllin-Pirscher, B., Schwärz, M., Steiner, A. K., Foelsche, U., and Kirchengast, G.: Quality Aspects of the Wegener Center Multi-Satellite GPS Radio Occultation Record OPSv5.6, Atmos. Meas. Tech. Discuss., https://doi.org/10.5194/amt-2017-225, in review, 2017.

Anstey, J. A., Davini, P., Gray, L. J., Woollings, T. J., Butchart, N., Cagnazzo, C., Christiansen, B., Hardiman, S. C., Osprey, S. M., and Yang, S.: Multi-model analysis of Northern Hemisphere winter blocking: Model biases and the role of resolution, J. Geophys. Res., 118, 3956–3971, https://doi.org/10.1002/jgrd.50231, 2013.

Anthes, R. A.: Exploring Earth's atmosphere with radio occultation: contributions to weather, climate and space weather, Atmos. Meas. Tech., 4, 1077–1103, https://doi.org/10.5194/amt-4-1077-2011, 2011.

Barnes, E. A., Slingo, J., and Woollings, T.: A methodology for the comparison of blocking climatologies across indices, models and climate scenarios, Clim. Dynam., 38, 2467–2481, https://doi.org/10.1007/s00382-011-1243-6, 2012.

Barriopedro, D., García-Herrera, R., Lupo, A. R., and Hernández, E.: A climatology of northern hemisphere blocking, J. Climate, 19, 1042–1063, https://doi.org/10.1175/JCLI3678.1, 2006.

Barriopedro, D., García-Herrera, R., and Trigo, R. M.: Application of blocking diagnosis methods to General Circulation Models. Part I: a novel detection scheme, Clim. Dynam., 35, 1373–1391, https://doi.org/10.1007/s00382-010-0767-5, 2010.

Barriopedro, D., Fischer, E. M., Luterbacher, J., Trigo, R. M., and García-Herrera, R.: The Hot Summer of 2010: Redrawing the Temperature Record Map of Europe, Science, 332, 220–224, https://doi.org/10.1126/science.1201224, 2011.

Berrisford, P., Hoskins, B. J., and Tyrlis, E.: Blocking and Rossby Wave Breaking on the Dynamical Tropopause in the Southern Hemisphere, J. Atmos. Sci., 64, 2881–2898, https://doi.org/10.1175/JAS3984.1, 2007.

Bieli, M., Pfahl, S., and Wernli, H.: A Lagrangian investigation of hot and cold temperature extremes in Europe, Q. J. Roy. Meteor. Soc., 141, 98–108, https://doi.org/10.1002/qj.2339, 2015.

Brunner, L., Steiner, A. K., Scherllin-Pirscher, B., and Jury, M. W.: Exploring atmospheric blocking with GPS radio occultation observations, Atmos. Chem. Phys., 16, 4593–4604, https://doi.org/10.5194/acp-16-4593-2016, 2016.

Brunner, L., Hegerl, G. C., and Steiner, A. K.: Connecting atmospheric blocking to European temperature extremes in spring,

www.atmos-meas-tech.net/10/4727/2017/ **Atmos. Meas. Tech., 10, 4727–4745, 2017**

71

J. Climate, 30, 585–594, https://doi.org/10.1175/JCLI-D-16-0518.1, 2017.

Buehler, T., Raible, C. C., and Stocker, T. F.: The relationship of winter season North Atlantic blocking frequencies to extreme cold or dry spells in the ERA-40, Tellus A, 63, 212–222, https://doi.org/10.1111/j.1600-0870.2010.00492.x, 2011.

Cardinali, C.: Monitoring the observation impact on the short-range forecast, Q. J. Roy. Meteor. Soc., 135, 239–250, https://doi.org/10.1002/qj.366, 2009.

Carrera, M., Higgins, R., and Kousky, V.: Downstream Weather Impacts Associated with Atmospheric Blocking over the Northeast Pacific, J. Climate, 17, 4823–4839, https://doi.org/10.1175/JCLI-3237.1, 2004.

Cattiaux, J., Vautard, R., Cassou, C., Yiou, P., Masson-Delmotte, V., and Codron, F.: Winter 2010 in Europe: A cold extreme in a warming climate, Geophys. Res. Lett., 37, L20704, https://doi.org/10.1029/2010GL044613, 2010.

Christensen, J. H., Kumar, K. K., Aldrian, E., An, S.-I., Cavalcanti, I., de Castro, M., Dong, W., Goswami, P., Hall, A., Kanyanga, J., Kitoh, A., Kossin, J., Lau, N.-C., Renwick, J., Stephenson, D., Xie, S.-P., and Zhou, T.: Climate Phenomena and their Relevance for Future Regional Climate Change, in: Climate Change 2013: The Physical Science Basis. Contribution of Working Group I to the Fifth Assessment Report of the Intergovernmental Panel on Climate Change, edited by: Stocker, T., Qin, D., Plattner, G.-K., Tignor, M., Allen, S., Boschung, J., Nauels, A., Xia, Y., Bex, V., and Midgley, P., 1217–1308, Cambridge University Press, Cambridge, UK and New York, NY, USA, 2013.

Cowan, T., van Rensch, P., Purich, A., and Cai, W.: The Association of Tropical and Extratropical Climate Modes to Atmospheric Blocking across Southeastern Australia, J. Climate, 26, 7555–7569, https://doi.org/10.1175/JCLI-D-12-00781.1, 2013.

Croci-Maspoli, M., Schwierz, C., and Davies, H. C.: A Multifaceted Climatology of Atmospheric Blocking and Its Recent Linear Trend, J. Climate, 20, 633–649, https://doi.org/10.1175/JCLI4029.1, 2007.

Damião Mendes, M. C. and Cavalcanti, I. F. A.: The relationship between the Antarctic oscillation and blocking events over the South Pacific and Atlantic Oceans, Int. J. Climatol., 34, 529–544, https://doi.org/10.1002/joc.3729, 2014.

D'Andrea, F., Tibaldi, S., Blackburn, M., Boer, G., Déqué, M., Dix, M. R., Dugas, B., Ferranti, L., Iwasaki, T., Kitoh, A., Pope, V., Randall, D., Roeckner, E., Strauss, D., Stern, W., Van den Dool, H., and Williamson, D.: Northern Hemisphere atmospheric blocking as simulated by 15 atmospheric general circulation models in the period 1979–1988, Clim. Dynam., 14, 385–407, https://doi.org/10.1007/s003820050230, 1998.

Davini, P. and D'Andrea, F.: Northern Hemisphere Atmospheric Blocking Representation in Global Climate Models: Twenty Years of Improvements?, J. Climate, 29, 8823–8840, https://doi.org/10.1175/JCLI-D-16-0242.1, 2016.

Davini, P., Cagnazzo, C., Gualdi, S., and Navarra, A.: Bidimensional diagnostics, variability, and trends of Northern Hemisphere blocking, J. Climate, 25, 6496–6509, https://doi.org/10.1175/JCLI-D-12-00032.1, 2012.

Davini, P., Cagnazzo, C., Fogli, P. G., Manzini, E., Gualdi, S., and Navarra, A.: European blocking and Atlantic jet stream variability in the NCEP/NCAR reanalysis and the

CMCC-CMS climate model, Clim. Dynam., 43, 71–85, https://doi.org/10.1007/s00382-013-1873-y, 2014.

de Adana, F. J. S. and Colucci, S. J.: Southern Hemisphere Blocking Onsets Associated with Upper-Tropospheric Divergence Anomalies, J. Atmos. Sci., 62, 1614–1625, https://doi.org/10.1175/JAS3421.1, 2005.

Dee, D. P., Uppala, S. M., Simmons, A. J., Berrisford, P., Poli, P., Kobayashi, S., Andrae, U., Balmaseda, M. A., Balsamo, G., Bauer, P., Bechtold, P., Beljaars, A. C. M., van de Berg, L., Bidlot, J., Bormann, N., Delsol, C., Dragani, R., Fuentes, M., Geer, A. J., Haimberger, L., Healy, S. B., Hersbach, H., Hólm, E. V., Isaksen, L., Kållberg, P., Köhler, M., Matricardi, M., McNally, A. P., Monge-Sanz, B. M., Morcrette, J.-J., Park, B.-K., Peubey, C., de Rosnay, P., Tavolato, C., Thépaut, J.-N., and Vitart, F.: The ERA-Interim reanalysis: configuration and performance of the data assimilation system, Q. J. Roy. Meteor. Soc., 137, 553–597, https://doi.org/10.1002/qj.828, 2011.

Dee, D. P., Fasullo, J., Shea, D., Walsh, J., and National Center for Atmospheric Research Staff: The Climate Data Guide: Atmospheric Reanalysis: Overview & Comparison Tables, available at: https://climatedataguide.ucar.edu/climate-data/atmospheric-reanalysis-overview-comparison-tables (last access: 15 November 2017), 2016.

de la Torre, A. and Alexander, P.: Gravity waves above Andes detected from GPS radio occultation temperature profiles: Mountain forcing?, Geophys. Res. Lett., 32, L17815, https://doi.org/10.1029/2005GL022959, 2005.

Dunn-Sigouin, E. and Son, S.-W.: Northern Hemisphere blocking frequency and duration in the CMIP5 models, J. Geophys. Res.-Atmos, 118, 1179–1188, https://doi.org/10.1002/jgrd.50143, 2013.

Ebita, A., Kobayashi, S., Ota, Y., Moriya, M., Kumabe, R., Onogi, K., Harada, Y., Yasui, S., Miyaoka, K., Takahashi, K., Kamahori, H., Kobayashi, C., Endo, H., Soma, M., Oikawa, Y., and Ishimizu, T.: The Japanese 55-year Reanalysis "JRA-55": An Interim Report, SOLA, 7, 149–152, https://doi.org/10.2151/sola.2011-038, 2011.

European Centre for Medium-Range Weather Forecasts (ECMWF): ERA-Interim: ECMWF Reanalysis Interim, available at: http://apps.ecmwf.int/datasets/data/interim-full-daily/levtype=pl/, last access: 1 March 2017.

Favre, A. and Gershunov, A.: Extra-tropical cyclonic/anticyclonic activity in North-Eastern Pacific and air temperature extremes in Western North America, Clim. Dynam., 26, 617–629, https://doi.org/10.1007/s00382-005-0101-9, 2006.

Foelsche, U., Scherllin-Pirscher, B., Ladstädter, F., Steiner, A. K., and Kirchengast, G.: Refractivity and temperature climate records from multiple radio occultation satellites consistent within 0.05 %, Atmos. Meas. Tech., 4, 2007–2018, https://doi.org/10.5194/amt-4-2007-2011, 2011.

Fujiwara, M., Wright, J. S., Manney, G. L., Gray, L. J., Anstey, J., Birner, T., Davis, S., Gerber, E. P., Harvey, V. L., Hegglin, M. I., Homeyer, C. R., Knox, J. A., Krüger, K., Lambert, A., Long, C. S., Martineau, P., Molod, A., Monge-Sanz, B. M., Santee, M. L., Tegtmeier, S., Chabrillat, S., Tan, D. G. H., Jackson, D. R., Polavarapu, S., Compo, G. P., Dragani, R., Ebisuzaki, W., Harada, Y., Kobayashi, C., McCarty, W., Onogi, K., Pawson, S., Simmons, A., Wargan, K., Whitaker, J. S., and Zou, C.-Z.: Introduction to the SPARC Reanalysis Intercomparison

**Atmos. Meas. Tech., 10, 4727–4745, 2017**                                    **www.atmos-meas-tech.net/10/4727/2017/**

72

Project (S-RIP) and overview of the reanalysis systems, Atmos. Chem. Phys., 17, 1417–1452, https://doi.org/10.5194/acp-17-1417-2017, 2017.

Galarneau Jr., T. J., Hamill, T. M., Dole, R. M., and Perlwitz, J.: A Multiscale Analysis of the Extreme Weather Events over Western Russia and Northern Pakistan during July 2010, Mon. Weather Rev., 140, 1639–1664, https://doi.org/10.1175/MWR-D-11-00191.1, 2012.

García-Herrera, R., Diaz, J., Trigo, R. M., Luterbacher, J., and Fischer, E. M.: A Review of the European Summer Heat Wave of 2003, Crit. Rev. Env. Sci. Tec., 40, https://doi.org/10.1080/10643380802238137, 2010.

Gelaro, R., McCarty, W., Suárez, M. J., Todling, R., Molod, A., Takacs, L., Randles, C., Darmenov, A., Bosilovich, M. G., Reichle, R., Wargan, K., Coy, L., Cullather, R., Draper, C., Akella, S., Buchard, V., Conaty, A., da Silva, A., Gu, W., Kim, G.-K., Koster, R., Lucchesi, R., Merkova, D., Nielsen, J. E., Partyka, G., Pawson, S., Putman, W., Rienecker, M., Schubert, S. D., Sienkiewicz, M., and Zhao, B.: The Modern-Era Retrospective Analysis for Research and Applications, Version 2 (MERRA-2), J. Climate, 30, 5419–5454, https://doi.org/10.1175/JCLI-D-16-0758.1, 2017.

Gilbert, N.: Russia counts environmental cost of wildfires, Nature News: Briefing, https://doi.org/10.1038/news.2010.404, 2010.

Gleisner, H., Thejll, P., Christiansen, B., and Nielsen, J. K.: Recent global warming hiatus dominated by low-latitude temperature trends in surface and troposphere data, Geophys. Res. Lett., 42, 510–517, https://doi.org/10.1002/2014GL062596, 2015.

Global Modeling and Assimilation Office (GMAO): MERRA-2 inst6_3d_ana_Np: 3d, 6-Hourly, Instantaneous, Pressure-Level, Analysis, Analyzed Meteorological Fields V5.12.4, Greenbelt, MD, USA, Goddard Earth Sciences Data and Information Services Center (GES DISC), https://doi.org/10.5067/A7S6XP56VZWS, (last access: 18 November 2016), 2015.

Gorbunov, M. E., Benzon, H.-H., Jensen, A. S., Lohmann, M. S., and Nielsen, A. S.: Comparative analysis of radio occultation processing approaches based on Fourier integral operators, Radio Sci., 39, RS6004, https://doi.org/10.1029/2003RS002916, 2004.

Hajj, G. A., Kursinski, E. R., Romans, L. J., Bertiger, W. I., and Leroy, S. S.: A technical description of atmospheric sounding by GPS occultation, J. Atmos. Sol.-Terr. Phy., 64, 451–469, https://doi.org/10.1016/S1364-6826(01)00114-6, 2002.

Healy, S. B. and Thépaut, J. N.: Assimilation experiments with CHAMP GPS radio occultation measurements, Q. J. Roy. Meteor. Soc., 132, 605–623, https://doi.org/10.1256/qj.04.182, 2006.

Ho, S.-P., Hunt, D., Steiner, A. K., Mannucci, A. J., Kirchengast, G., Gleisner, H., Heise, S., von Engeln, A., Marquardt, C., Sokolovskiy, S., Schreiner, W., Scherllin-Pirscher, B., Ao, C., Wickert, J., Syndergaard, S., Lauritsen, K., Leroy, S., Kursinski, E. R., Kuo, Y.-H., Foelsche, U., Schmidt, T., and Gorbunov, M.: Reproducibility of GPS radio occultation data for climate monitoring: Profile-to-profile inter-comparison of CHAMP climate records 2002 to 2008 from six data centers, J. Geophys. Res., 117, D18111, https://doi.org/10.1029/2012JD017665, 2012.

IPCC: Climate Change 2013: The Physical Science Basis. Contribution of Working Group I to the Fifth Assessment Report of the Intergovernmental Panel on Climate Change, edited by: Stocker,

T. F., Qin, D., Plattner, G.-K., Tignor, M., Allen, S. K., Boschung, J., Nauels, A., Xia, Y., Bex, V., and Midgley, P. M., Cambridge, UK and New York, NY, USA, 1535 pp., 2013.

Japan Meteorological Agency (JMA): JRA-55: Japanese 55-year Reanalysis, available at: http://jra.kishou.go.jp/JRA-55/index_en.html, last access: 27 January 2017.

Kobayashi, S., Ota, Y., Harada, Y., Ebita, A., Moriya, M., Onoda, H., Onogi, K., Kamahori, H., Kobayashi, C., Endo, H., Miyaoka, K., and Takahashi, K.: The JRA-55 Reanalysis: General Specifications and Basic Characteristics, J. Meteorol. Soc. Jpn., 93, 5–48, https://doi.org/10.2151/jmsj.2015-001, 2015.

Kursinski, E. R., Hajj, G. A., Schofield, J. T., Linfield, R. P., and Hardy, K. R.: Observing Earth's atmosphere with radio occultation measurements using the Global Positioning System, J. Geophys. Res., 102, 23429–23465, https://doi.org/10.1029/97JD01569, 1997.

Lejenäs, H.: Characteristics of southern hemisphere blocking as determined from a time series of observational data, Q. J. Roy. Meteor. Soc., 110, 967–979, https://doi.org/10.1002/qj.49711046610, 1984.

Long, C. S., Fujiwara, M., Davis, S., Mitchell, D. M., and Wright, C. J.: Climatology and Interannual Variability of Dynamic Variables in Multiple Reanalyses Evaluated by the SPARC Reanalysis Intercomparison Project (S-RIP), Atmos. Chem. Phys. Discuss., https://doi.org/10.5194/acp-2017-289, in review, 2017.

Marques, R. d. F. C. and Rao, V. B.: A Diagnosis of a Long-Lasting Blocking Event over the Southeast Pacific Ocean, Mon. Weather Rev., 127, 1761–1776, https://doi.org/10.1175/1520-0493(1999)127<1761:ADOALL>2.0.CO;2, 1999.

Martineau, P., Chen, G., and Burrows, D. A.: Wave events: climatology, trends, and relationship to Northern Hemisphere winter blocking and weather extremes, J. Climate, 30, 5675–5697, https://doi.org/10.1175/JCLI-D-16-0692.1, 2017.

Masato, G., Hoskins, B. J., and Woollings, T.: Winter and Summer Northern Hemisphere Blocking in CMIP5 Models, J. Climate, 26, 7044–7059, https://doi.org/10.1175/JCLI-D-12-00466.1, 2013.

McCarty, W., Coy, L., Gelaro, R., Huang, A., Merkova, D., Smith, E. B., Sienkiewicz, M., and Wargan, K.: MERRA-2 Input Observations: Summary and Assessment, available at: https://gmao.gsfc.nasa.gov/pubs/docs/McCarty885.pdf (last access: 6 March 2017), 2016.

Melbourne, W. G., Davis, E. S., Duncan, C. B., Hajj, G. A., Hardy, K. R., Kursinski, E. R., Meehan, T. K., Young, L. E., and Yunck, T. P.: The application of spaceborne GPS to atmospheric limb sounding and global change monitoring, JPL Publication, 94–18, 147, 1994.

Oliveira, F. N. M., Carvalho, L. M. V., and Ambrizzi, T.: A new climatology for Southern Hemisphere blockings in the winter and the combined effect of ENSO and SAM phases, Int. J. Climatol., 34, 1676–1692, https://doi.org/10.1002/joc.3795, 2014.

Parker, T. J., Berry, G. J., and Reeder, M. J.: The Structure and Evolution of Heat Waves in Southeastern Australia, J. Climate, 27, 5768–5785, https://doi.org/10.1175/JCLI-D-13-00740.1, 2014.

Parker, W. S.: Reanalyses and Observations: What's the Difference?, B. Am. Meteorol. Soc., 97, 1565–1572, https://doi.org/10.1175/BAMS-D-14-00226.1, 2016.

Parsons, S., Renwick, J. A., and McDonald, A. J.: An Assessment of Future Southern Hemisphere Blocking Using CMIP5

73

Projections from Four GCMs, J. Climate, 29, 7599–7611, https://doi.org/10.1175/JCLI-D-15-0754.1, 2016.

Peevey, T. R., Gille, J. C., Homeyer, C. R., and Manney, G. L.: The double tropopause and its dynamical relationship to the tropopause inversion layer in storm track regions, J. Geophys. Res., 119, 10194–10212, https://doi.org/10.1002/2014JD021808, 2014.

Pelly, J. L. and Hoskins, B. J.: A new perspective on blocking, J. Atmos. Sci., 60, 743–755, https://doi.org/10.1175/1520-0469(2003)060<0743:ANPOB>2.0.CO;2, 2003.

Pfahl, S. and Wernli, H.: Quantifying the relevance of atmospheric blocking for co-located temperature extremes in the Northern Hemisphere on (sub-)daily time scales, Geophys. Res. Lett., 39, L12807, https://doi.org/10.1029/2012GL052261, 2012.

Pfahl, S., Schwierz, C., Croci-Maspoli, M., Grams, C. M., and Wernli, H.: Importance of latent heat release in ascending air streams for atmospheric blocking, Nat. Geosci., 8, 610–614, https://doi.org/10.1038/ngeo2487, 2015.

Poli, P., Healy, S. B., and Dee, D. P.: Assimilation of Global Positioning System radio occultation data in the ECMWF ERA-Interim reanalysis, Q. J. Roy. Meteor. Soc., 136, 1972–1990, https://doi.org/10.1002/qj.722, 2010.

Pook, M. J., Risbey, J. S., McIntosh, P. C., Ummenhofer, C. C., Marshall, A. G., and Meyers, G. A.: The Seasonal Cycle of Blocking and Associated Physical Mechanisms in the Australian Region and Relationship with Rainfall, Mon. Weather Rev., 141, 4534–4553, https://doi.org/10.1175/MWR-D-13-00040.1, 2013.

Randel, W. J. and Wu, F.: Kelvin wave variability near the equatorial tropopause observed in GPS radio occultation measurements, J. Geophys. Res., 110, D03102, https://doi.org/10.1029/2004JD005006, 2005.

Randel, W. J. and Wu, F.: Variability of Zonal Mean Tropical Temperatures Derived from a Decade of GPS Radio Occultation Data, J. Atmos. Sci., 72, 1261–1275, https://doi.org/10.1175/JAS-D-14-0216.1, 2015.

Randel, W. J., Wu, F., and Ríos, W. R.: Thermal variability of the tropical tropopause region derived from GPS/MET observations, J. Geophys. Res., 108, 4024, https://doi.org/10.1029/2002JD002595, 2003.

Rex, D. F.: Blocking Action in the Middle Troposphere and its Effect upon Regional Climate I: An aerological study of blocking action, Tellus, 2, 196–211, https://doi.org/10.1111/j.2153-3490.1950.tb00331.x, 1950.

Rieckh, T., Scherllin-Pirscher, B., Ladstädter, F., and Foelsche, U.: Characteristics of tropopause parameters as observed with GPS radio occultation, Atmos. Meas. Tech., 7, 3947–3958, https://doi.org/10.5194/amt-7-3947-2014, 2014.

Rodrigues, R. R. and Woollings, T.: Impact of Atmospheric Blocking on South America in Austral Summer, J. Climate, 30, 1821–1837, https://doi.org/10.1175/JCLI-D-16-0493.1, 2017.

Scherllin-Pirscher, B., Kirchengast, G., Steiner, A. K., Kuo, Y.-H., and Foelsche, U.: Quantifying uncertainty in climatological fields from GPS radio occultation: an empirical-analytical error model, Atmos. Meas. Tech., 4, 2019–2034, https://doi.org/10.5194/amt-4-2019-2011, 2011a.

Scherllin-Pirscher, B., Steiner, A. K., Kirchengast, G., Kuo, Y.-H., and Foelsche, U.: Empirical analysis and modeling of errors of atmospheric profiles from GPS radio occultation, Atmos. Meas.

Tech., 4, 1875–1890, https://doi.org/10.5194/amt-4-1875-2011, 2011b.

Scherllin-Pirscher, B., Deser, C., Ho, S.-P., Chou, C., Randel, W., and Kuo, Y.-H.: The vertical and spatial structure of ENSO in the upper troposphere and lower stratosphere from GPS radio occultation measurements, Geophys. Res. Lett., 39, L20801, https://doi.org/10.1029/2012GL053071, 2012.

Scherllin-Pirscher, B., Steiner, A. K., Kirchengast, G., Schwaerz, M., and Leroy, S. S.: The power of vertical geolocation of atmospheric profiles from GNSS radio occultation, J. Geophys. Res.-Atmos., 122, 1595–1616, https://doi.org/10.1002/2016JD025902, 2017.

Scherrer, S. C., Croci-Maspoli, M., Schwierz, C., and Appenzeller, C.: Two-dimensional indices of atmospheric blocking and their statistical relationship with winter climate patterns in the Euro-Atlantic region, Int. J. Climatol., 26, 233–249, https://doi.org/10.1002/joc.1250, 2006.

Schiemann, R., Demory, M.-E., Shaffrey, L. C., Jane, S., Vidale, P. L., Mizielinski, M. S., Roberts, M. J., Matsueda, M., Wehner, M. F., and Thomas, J.: The Resolution Sensitivity of Northern Hemisphere Blocking in Four 25-km Atmospheric Global Circulation Models, J. Climate, 30, 337–358, https://doi.org/10.1175/JCLI-D-16-0100.1, 2017.

Schmidt, T., Heise, S., Wickert, J., Beyerle, G., and Reigber, C.: GPS radio occultation with CHAMP and SAC-C: global monitoring of thermal tropopause parameters, Atmos. Chem. Phys., 5, 1473–1488, https://doi.org/10.5194/acp-5-1473-2005, 2005.

Schmidt, T., Wickert, J., Beyerle, G., and Heise, S.: Global tropopause height trends estimated from GPS radio occultation data, Geophys. Res. Lett., 35, L11806, https://doi.org/10.1029/2008GL034012, 2008.

Schwärz, M., Kirchengast, G., Scherllin-Pirscher, B., Schwarz, J., Ladstädter, F., and Angerer, B.: Multi-Mission Validation by Satellite Radio Occultation – Extension Project, Final report for ESA/ESRIN No. 01/2016, WEGC, University of Graz, Graz, Austria, 2016.

Sillmann, J., Croci-Maspoli, M., Kallache, M., and Katz, R. W.: Extreme Cold Winter Temperatures in Europe under the Influence of North Atlantic Atmospheric Blocking, J. Climate, 24, 5899–5913, https://doi.org/10.1175/2011JCLI4075.1, 2011.

Simmons, A. J., Poli, P., Dee, D. P., Berrisford, P., Hersbach, H., Kobayashi, S., and Peubey, C.: Estimating low-frequency variability and trends in atmospheric temperature using ERA-Interim, Q. J. Roy. Meteor. Soc., 140, 329–353, https://doi.org/10.1002/qj.2317, 2014.

Sinclair, M. R.: A Climatology of Anticyclones and Blocking for the Southern Hemisphere, Mon. Weather Rev., 124, 245–264, https://doi.org/10.1175/1520-0493(1996)124<0245:ACOAAB>2.0.CO;2, 1996.

Sitnov, S., Mokhov, I., and Lupo, A.: Ozone, water vapor, and temperature anomalies associated with atmospheric blocking events over Eastern Europe in spring–summer 2010, Atmos. Environ., 164, 180–194, https://doi.org/10.1016/j.atmosenv.2017.06.004, 2017.

Sousa, P. M., Trigo, R. M., Barriopedro, D., Soares, P. M. M., Ramos, A. M., and Liberato, M. L. R.: Responses of European precipitation distributions and regimes to different blocking locations, Clim. Dynam., 48, 1141–1160, https://doi.org/10.1007/s00382-016-3132-5, 2017.

**Atmos. Meas. Tech., 10, 4727–4745, 2017** **www.atmos-meas-tech.net/10/4727/2017/**

74

Steiner, A. K., Lackner, B. C., Ladstädter, F., Scherllin-Pirscher, B., Foelsche, U., and Kirchengast, G.: GPS radio occultation for climate monitoring and change detection, Radio Sci., 46, RS0D24, https://doi.org/10.1029/2010RS004614, 2011.

Steiner, A. K., Hunt, D., Ho, S.-P., Kirchengast, G., Mannucci, A. J., Scherllin-Pirscher, B., Gleisner, H., von Engeln, A., Schmidt, T., Ao, C., Leroy, S. S., Kursinski, E. R., Foelsche, U., Gorbunov, M., Heise, S., Kuo, Y.-H., Lauritsen, K. B., Marquardt, C., Rocken, C., Schreiner, W., Sokolovskiy, S., Syndergaard, S., and Wickert, J.: Quantification of structural uncertainty in climate data records from GPS radio occultation, Atmos. Chem. Phys., 13, 1469–1484, https://doi.org/10.5194/acp-13-1469-2013, 2013.

Sun, D.-Z., Zhang, T., Sun, Y., and Yu, Y.: Rectification of El Niño–Southern Oscillation into Climate Anomalies of Decadal and Longer Time Scales: Results from Forced Ocean GCM Experiments, J. Climate, 27, 2545–2561, https://doi.org/10.1175/JCLI-D-13-00390.1, 2014.

Tibaldi, S. and Molteni, F.: On the operational predictability of blocking, Tellus A, 42, 343–365, https://doi.org/10.1034/j.1600-0870.1990.t01-2-00003.x, 1990.

Trenberth, K. F. and Mo, K. C.: Blocking in the Southern Hemisphere, Mon. Weather Rev., 113, 3–21, https://doi.org/10.1175/1520-0493(1985)113<0003:BITSH>2.0.CO;2, 1985.

Trigo, R. M., Trigo, I. F., DaCamara, C. C., and Osborn, T. J.: Climate impact of the European winter blocking episodes from the NCEP/NCAR Reanalyses, Clim. Dynam., 23, 17–28, https://doi.org/10.1007/s00382-004-0410-4, 2004.

Tsuda, T.: Characteristics of atmospheric gravity waves observed using the MU (Middle and Upper atmosphere) radar and GPS (Global Positioning System) radio occultation, Proc. Jpn. Acad. Ser. B, 90, 12–27, 2014.

Vial, J. and Osborn, T. J.: Assessment of atmosphere-ocean general circulation model simulations of winter northern hemisphere atmospheric blocking, Clim. Dynam., 39, 95–112, https://doi.org/10.1007/s00382-011-1177-z, 2012.

Whan, K., Zwiers, F., and Sillmann, J.: The Influence of Atmospheric Blocking on Extreme Winter Minimum Temperatures in North America., J. Climate, 29, 4361–4381, https://doi.org/10.1175/JCLI-D-15-0493.1, 2016.

Wise, E. K.: Five centuries of U.S. West Coast drought: Occurrence, spatial distribution, and associated atmospheric circulation patterns, Geophys. Res. Lett., 43, 4539–4546, https://doi.org/10.1002/2016GL068487, 2016.

Woollings, T.: Dynamical influences on European climate: an uncertain future, Philos. T. Roy. Soc. A, 368, 3733–3756, https://doi.org/10.1098/rsta.2010.0040, 2010.

Yue, X., Schreiner, W. S., Pedatella, N., Anthes, R. A., Mannucci, A. J., Straus, P. R., and Liu, J.-Y.: Space Weather Observations by GNSS Radio Occultation: From FORMOSAT-3/COSMIC to FORMOSAT-7/COSMIC-2, Space Weather, 12, 616–621, https://doi.org/10.1002/2014SW001133, 2014.

75

# Connecting Atmospheric Blocking to European Temperature Extremes in Spring

LUKAS BRUNNER

*Wegener Center for Climate and Global Change (WEGC), Institute for Geophysics, Astrophysics, and Meteorology/Institute of Physics, and Fonds zur Förderung der wissenschaftlichen Forschung—Doktoratskolleg (FWF-DK) Climate Change, University of Graz, Graz, Austria*

GABRIELE C. HEGERL

*School of Geosciences, University of Edinburgh, Edinburgh, United Kingdom*

ANDREA K. STEINER

*Wegener Center for Climate and Global Change (WEGC), Institute for Geophysics, Astrophysics, and Meteorology/Institute of Physics, and Fonds zur Förderung der wissenschaftlichen Forschung—Doktoratskolleg (FWF-DK) Climate Change, University of Graz, Graz, Austria*

## ABSTRACT

Atmospheric blocking is an important contributor to European temperature variability. It can trigger cold and warm spells, which is of specific relevance in spring because vegetation is particularly vulnerable to extreme temperatures in the growing season. The spring season is investigated as a transition period from predominant connections of blocking with cold spells in winter to predominant connections of blocking with warm spells in summer. Extreme temperatures are termed cold or warm spells if temperature stays outside the 10th to 90th percentile range for at least six consecutive days. Cold and warm spells in Europe over 1979–2014 are analyzed in observations from the European daily high-resolution gridded dataset (E-OBS) and the connection to blocking is examined in geopotential height fields from ERA-Interim. A highly significant link between blocking and cold and warm spells is found that changes during spring. Blocking over the northeastern Atlantic and Scandinavia is correlated with the occurrence of cold spells in Europe, particularly early in spring, whereas blocking over central Europe is associated with warmer conditions, particularly from March onward. The location of the block also impacts the spatial distribution of temperature extremes. More than 80% of cold spells in southeastern Europe occur during blocking whereas warm spells are correlated with blocking mainly in northern Europe. Over the analysis period, substantial interannual variability is found but also a decrease in cold spells and an increase in warm spells. The long-term change to a warmer climate holds the potential for even higher vulnerability to spring cold extremes.

## 1. Introduction

European weather and climate are strongly influenced by large-scale circulation patterns such as the Atlantic storm tracks, the jet stream, and atmospheric blocking (e.g., Woollings 2010). Atmospheric blocking describes a meteorological situation in which a persistent and stationary high pressure system blocks the climatological westerly flow at midlatitudes for several days to weeks (Rex 1950; Tibaldi and Molteni 1990; Pelly and Hoskins 2003; Barriopedro et al. 2006; Croci-Maspoli et al. 2007).

Extremes on both ends of the temperature distribution are especially closely connected to atmospheric blocking. Increased cold spell frequency is found during blocked conditions in European winter (Buehler et al. 2011) and up to 80% of summer hot temperature extremes in northern Europe are associated with a collocated blocking (Pfahl and Wernli 2012). Atmospheric blocking has also been identified as main contributor to specific extreme events

---

ᵃ Denotes Open Access content.

*Corresponding author e-mail*: lukas.brunner@uni-graz.at

---

such as the cold European winter in 2010 (Cattiaux et al. 2010) and the Russian heatwave in summer 2010 (Matsueda 2011).

Surface temperatures can be impacted by atmospheric blocking via radiative forcing or advection. Radiative effects are mainly constrained to the center of the block where clear-sky conditions favor positive temperature anomalies. The anticyclonic circulation of the block affects temperatures especially on the eastern and southern flanks by advection of cold air from the north and east (e.g., Trigo et al. 2004; Bieli et al. 2015). A range of studies have focused on either the predominant cooling effect of blocking in winter (Trigo et al. 2004; Barriopedro et al. 2008; Cattiaux et al. 2010; Buehler et al. 2011; Sillmann et al. 2011; Whan et al. 2016) or the warming effect in summer (Xoplaki et al. 2003; Cassou et al. 2005; Pfahl and Wernli 2012; Stefanon et al. 2012). Recently, Cassou and Cattiaux (2016) showed that the transition from blocking being linked to anomalously cold conditions in winter to blocking being linked to warm conditions in summer has shifted by a few days because of climate warming.

Here we investigate the link between atmospheric blocking and European cold and warm spells during spring to provide better insight into the shifting role of blocking for extremes during this transition period. Spring temperature extremes are of special relevance because vegetation during this season is particularly vulnerable to abnormal temperatures. Late spring frost can severely harm or even destroy fresh leaves, subsequently requiring considerable additional resource use by plants. Correspondingly, warm spells in early spring can lead to premature greening onset (Hufkens et al. 2012; Menzel et al. 2015, and references therein). Ma et al. (2016) showed the potential of earlier spring green-up to also impact European warm spells via feedback processes. In this study we analyze the connection of blocking and extreme temperature occurrences, noting their spatial distribution and change over the last decades. We focus on spring on a month-by-month basis but also show results for the seasonal mean of other seasons. We describe data and methods in section 2. Results are presented in section 3 and a summary is given in section 4.

## 2. Data and methods

The detection of temperature extremes is based on the European daily high-resolution gridded dataset (E-OBS), version 12.0 (Haylock et al. 2008), an observational land-only dataset for Europe. It comprises measurements from a network of more than 2000 irregularly distributed meteorological stations interpolated to a regular grid (Klok and Klein Tank 2009). In this study we investigate daily minimum temperature $T_{min}$ and daily maximum

temperature $T_{max}$ on a $0.25° \times 0.25°$ longitude–latitude grid between 1979 and 2014. We detect cold and warm spells over mainland Europe and the British Isles ($35°$–$72.5°$N, $12.5°$W–$30°$E). First, the daily linear trend from 1979 to 2014 is subtracted from each grid point in the E-OBS temperatures to remove the long-term temperature trend. Daily 10th and 90th percentiles of $T_{min}$ and $T_{max}$ are computed, respectively, over the 36-yr period using a 21-day sliding window. A grid point with $T_{min}$ below the 10th percentile or $T_{max}$ above the 90th percentile for at least six consecutive days is identified as a cold or warm extreme, respectively. This study focuses on large-scale events on a daily basis. Therefore we define a cold spell day (CSD) or warm spell day (WSD) if at least 400 grid points (i.e., a $5° \times 5°$ region) simultaneously are found to be exposed to a cold or warm extreme criterion on a given day. Resulting cold and warm spells are found to be spatially highly coherent, so no separate adjacency criterion was applied.

The detection of blocking is based on daily geopotential height (GPH) fields from ERA-Interim (Dee et al. 2011) at a $2.5° \times 2.5°$ longitude–latitude grid, which is available from 1979 onward. We apply a standard algorithm utilizing the reversal of midlatitude 500-hPa GPH gradients (Tibaldi and Molteni 1990; Scherrer et al. 2006; Davini et al. 2012, 2014), detailed in Brunner et al. (2016). The blocking detection algorithm identifies high pressure systems associated with an overturning of the flow and selects extended and persistent events of at least five days duration. Therefore this classical approach covers stationary and isolated high pressure systems northward of $45°$N. We compute blocking frequencies on a grid point basis for climatological conditions as well as for CSDs and WSDs. We subsequently define a blocked day if blocking is found anywhere in the Euro-Atlantic blocking region ($45°$–$72.5°$N, $30°$W–$45°$E) (Barriopedro et al. 2010; IPCC 2013) on a certain day. We then also investigate the relative frequency of CSDs and WSDs on a grid point basis during blocked and unblocked days. This approach allows us to simultaneously investigate the local and remote effects of blocking on CSDs and WSDs.

In addition, we analyze selected subdomains and investigate the importance of the location of cold and warm spells and blocking for their connection. For selection of CSDs and WSDs in subdomains we adjust the spatial criterion to consider CSDs and WSDs with more than half of their grid points in the selected subdomain. For selection of blocking in subdomains we consider blocks with at least one blocked grid point in the selected subdomain.

To test any co-occurrence of CSDs and WSDs and blocked days for significance we perform a Monte Carlo test. Given $N$ CSDs or WSDs in a period (i.e., month or season), we draw 1000 random samples of $N$ days from the same period. To ensure that each random sample yields the same autocorrelation at all lags the samples
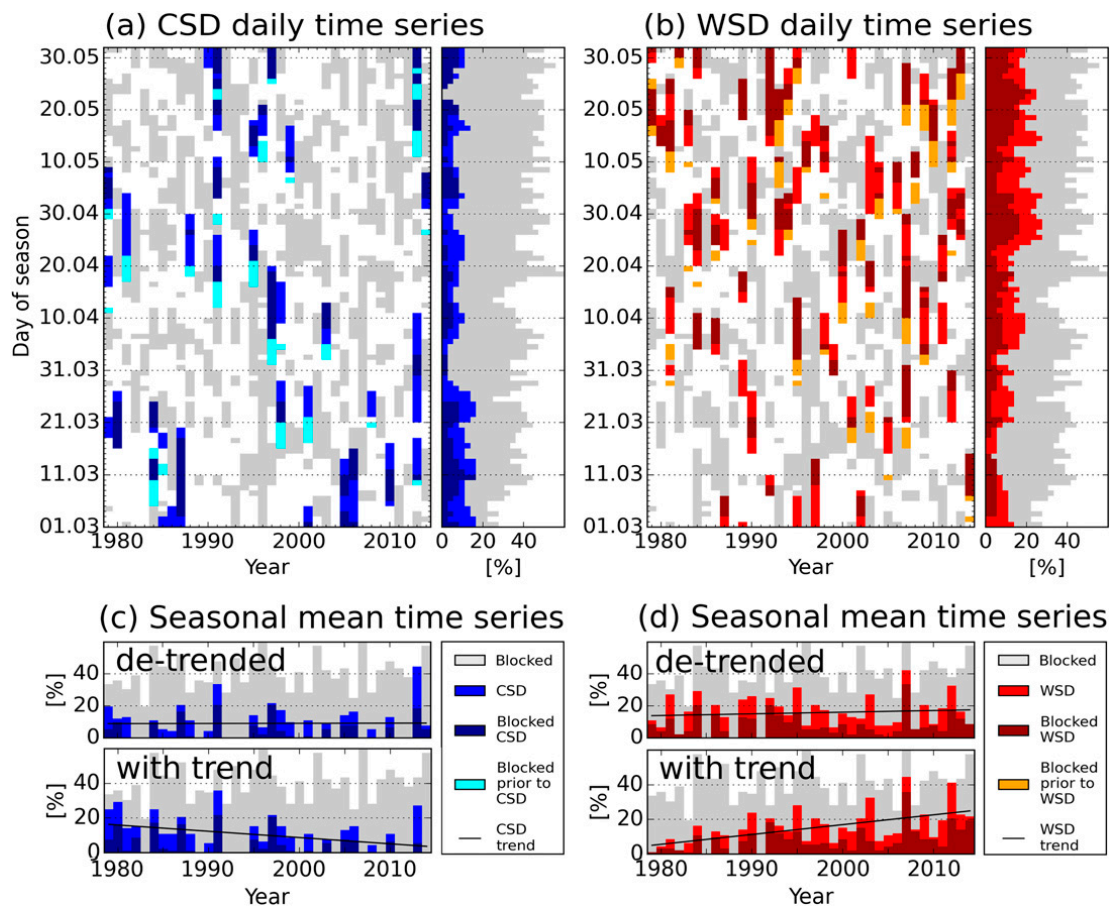
FIG. 1. Time evolution of blocking for (a) CSDs and (b) WSDs in European spring based on detrended data. The left panels in (a),(b) show blocked days in gray, cold (warm) spell days in blue (red), blocked cold (warm) spell days in dark blue (dark red), and blocking within 5 days before a cold (warm) spell day in turquoise (orange). The right panels in (a),(b) show percentages for each day during spring based on 36 years from 1979 to 2014. The seasonal mean time series are shown for (c) CSDs and (d) WSDs where the trend was removed (top plots) and not removed (bottom plots) from the underlying temperature time series.

are drawn as clusters of days similar as represented in the original dataset. We then calculate for each random sample of N days the blocking frequency on a grid point basis as well as the occurrence of blocked days in the blocking region. The correlation between blocking and CSDs or WSDs is considered statistically significant if the blocking frequency during CSDs and WSDs on a grid point or if the number of blocked CSDs or WSDs is smaller than the 5th percentile or larger than the 95th percentile of the joined probability density function (PDF) established over all 1000 random samples, respectively. The same considerations are made for the statistical significance of CSDs and WSDs given the number of blocked days in each period.

## 3. Results

The time evolution of blocked and extreme days is presented in Fig. 1. Over the spring season (MAM), a

decrease in the number of CSDs (both generally and also if restricted to blocked days) is found toward late spring (Fig. 1a, right). Over 1979–2014, the seasonal mean time series (Fig. 1c, top) shows periods with less or more CSDs, pointing at significant interannual variability. A considerable number of CSDs exhibit blocking several days before their onset, indicating that a certain amount of time is necessary to lower the temperature sufficiently for a cold spell to develop (Fig. 1a, left), consistent with findings of Buehler et al. (2011). If the trend in the underlying temperature time series is not removed (Fig. 1c, bottom) we find more CSDs at the beginning of the period and a lack of CSDs at the end of the period, indicating that extended cold periods are constrained to winter in a warming climate. However, some lack of cold spells also occurs after detrending (Fig. 1c, top), pointing at the role of internal variability.

Over the spring season, the number of WSDs and with it the number of blocked WSDs increases toward

TABLE 1. Overview on statistics of CSDs, WSDs, and blocked days. Columns from left to right: Period name and number of total days per (top) season and (bottom) month, number of blocked days (percentage of total days), number of CSDs (percentage of total days), number of WSDs (percentage of total days), number of blocked CSDs (percentage of blocked days/percentage of CSDs), and number of blocked WSDs (percentage of blocked days/percentage of WSDs). Entries with the number of blocked CSDs and WSDs above (below) the 95th (5th) percentile are indicated in boldface (italics).

| Period | Days | Blocked days | CSDs | WSDs | Blocked CSDs | Blocked WSDs |
|--------|------|--------------|------|------|--------------|--------------|
| MAM | 3312 | 1363 (41.15%) | 299 (9.03%) | 519 (15.67%) | 139 (10.20%/46.49%) | **280 (20.54%/53.95%)** |
| JJA | 3312 | 961 (29.02%) | 81 (2.45%) | 565 (17.06%) | *11 (1.14%/13.58%)* | **301 (31.32%/53.27%)** |
| SON | 3276 | 1025 (31.29%) | 308 (9.40%) | 421 (12.85%) | 116 (11.32%/37.66%) | 138 (13.46%/32.78%) |
| DJF | 3240 | 1176 (36.30%) | 554 (17.10%) | 361 (11.14%) | **297 (25.26%/53.61%)** | *102 (8.67%/28.25%)* |
| | | | | | | |
| Feb | 1008 | 423 (41.96%) | 157 (15.58%) | 103 (10.22%) | **93 (21.99%/59.24%)** | *24 (5.67%/23.30%)* |
| Mar | 1116 | 395 (35.39%) | 135 (12.10%) | 105 (9.41%) | 61 (15.44%/45.19%) | 46 (11.65%/43.81%) |
| Apr | 1080 | 449 (41.57%) | 80 (7.41%) | 183 (16.94%) | 27 (6.01%/33.75%) | **99 (22.05%/54.10%)** |
| May | 1116 | 519 (46.51%) | 84 (7.53%) | 231 (20.70%) | 51 (9.83%/60.71%) | **135 (26.01%/58.44%)** |
| Jun | 1080 | 393 (36.39%) | 30 (2.78%) | 181 (16.76%) | *4 (1.02%/13.33%)* | **111 (28.24%/61.33%)** |

summer (Fig. 1b, right). Over the analysis period, the seasonal mean time series also show considerable interannual variability for WSDs (Fig. 1d, top). If the trend is not removed from the underlying temperature time series (Fig. 1d, bottom) an increase of the number of WSDs (both, generally and if restricted to blocked conditions) in the investigated period from 1979 to 2014 is evident, consistent with the detection of changes in the number of temperature extremes in Europe (Zwiers et al. 2011; IPCC 2013; Morak et al. 2013). Note that all subsequent discussions refer exclusively to the detrended data.

A complete summary of statistics for CSDs and WSDs in spring and all individual months of the extended spring season (February–June) is shown in Table 1. We also included results for the summer (JJA), fall (SON), and winter (DJF) seasons for comparison. Our results generally indicate that blocking plays a strong role in spring–summer warm spells and in fall–winter cold spells, consistent with the literature (e.g., Cassou and Cattiaux 2016). In total about 46% of CSDs in spring are blocked days and about 10% of blocked spring days coincide with a CSD. A statistically significant link is found in the extended spring season in February (correlation) and June (anticorrelation) as well as in winter (correlation) and in summer (anticorrelation; cf. Table 1). Regarding WSDs in spring, a statistically significant fraction of 54% is blocked and about 21% blocked spring days coincide with a WSD. Also, most individual months of the extended spring show a significant correlation with blocking (as do summer months); however, February on the transition from winter to spring exhibits a significant anticorrelation (as do winter months; cf. Table 1).

Analyzing blocking on a grid point basis, the climatological blocking frequency in the Euro-Atlantic region is generally between 2% and 6% of spring days. The blocking frequency coinciding with CSDs in spring is depicted in Fig. 2a. Three distinct regions are revealed: west of the British Isles (region 1) and over northern Scandinavia (region 2) the blocking frequency is up to 3 times higher for CSDs than for climatological conditions and differs statistically significantly from the random sample. This is consistent with cold advection during such blocks into central and western Europe. Over central and eastern Europe (region 3) there is significantly less blocking during CSDs (<2%) than in the climatology since blocking occurring there tends to lead to warmer, fair-weather conditions.

A closer investigation of the extended spring season based on monthly frequencies reveals how the role of blocking associated with CSDs changes through spring (Figs. 2b–f). February and March show significantly increased blocking frequency northward of 60°N (exceeding 16% and 12%, respectively), indicating a strong link of blocking in this region to cold conditions in Europe in late winter–early spring. Between March and April a distinct change is obvious such that maximum blocking frequencies shift from northern Europe to the west of the British Isles. This change may be founded in the temperature seasonality over the European continent: in winter the continent is still relatively cold, such that easterly flow is sufficient to lead to CSDs, while northerly advection with blocking to the west is necessary as the continent warms up in later spring. The CSD blocking frequency in central and eastern Europe is lowered during all spring months, highlighting the anticorrelation between cold conditions and blocking in this region. In June where only about 3% of total days are associated with a cold spell (cf. Table 1) no significant relationship with blocking is found.

The blocking frequency coinciding with WSDs in spring is found to be up to 3 times higher than during climatological conditions (Fig. 3a) and statistically
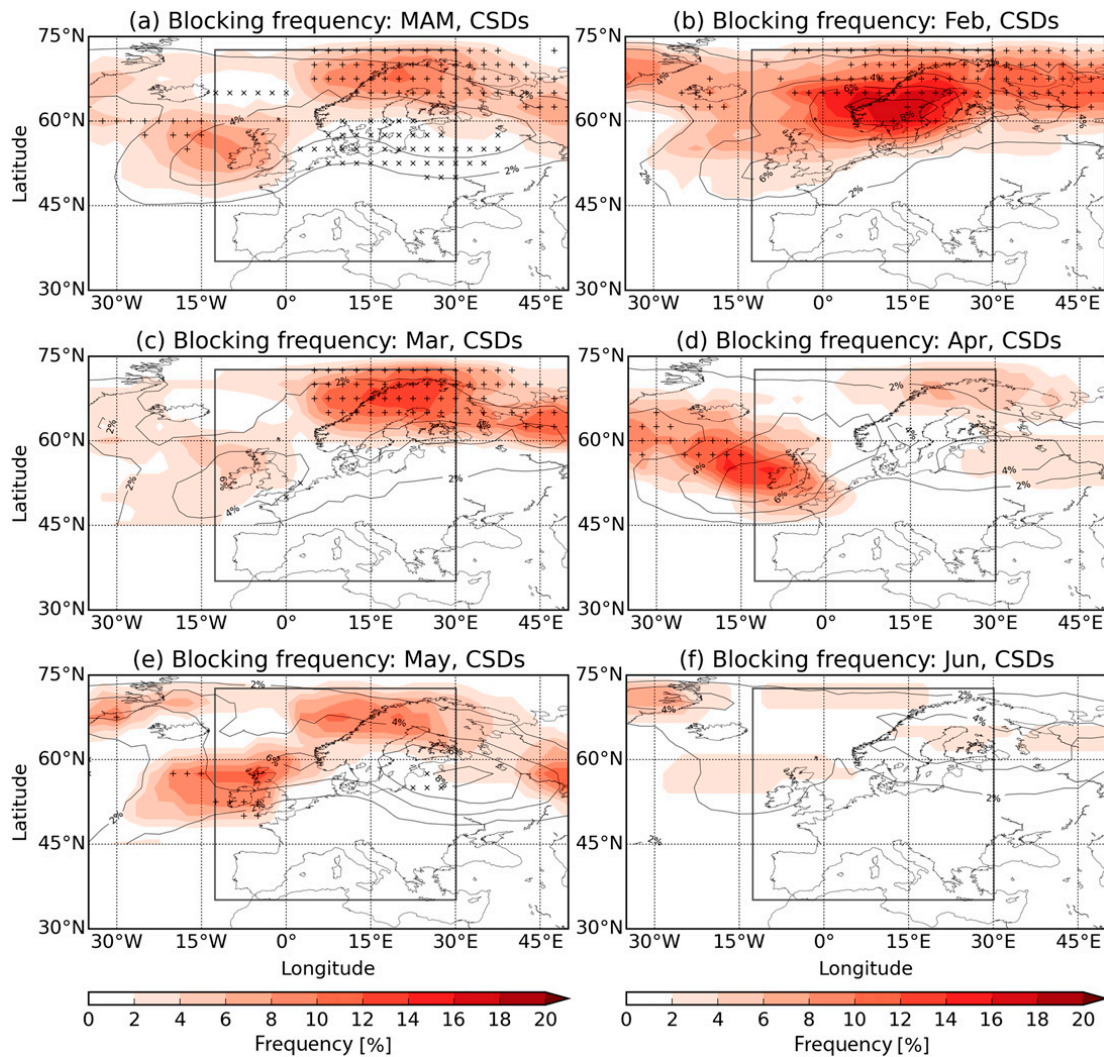
FIG. 2. Blocking frequency per grid point (shading) coinciding with CSDs in the European region (gray box) for (a) spring (MAM), (b) February, (c) March, (d) April, (e) May, and (f) June. Values that are statistically significantly larger than the number of blocks from random days (above 95th percentile) are marked with a plus sign and values that are statistically significantly lower (below 5th percentile) are marked with a multiplication sign. The climatological blocking frequency is indicated by black contour lines.

significantly different from the random sample in most of Europe. Blocks linked to warm spells are distributed across Europe, whereas there are fewer than average blocking days associated with WSDs west of the British Isles. The anticyclonic motion of blocking highs in the latter area would favor cold advection into Europe, consistent with the results for CSDs (Fig. 2).

Resolving individual months (Figs. 3b–f) reveals that in February the link between blocking and WSDs is mostly negative. Over the entire winter season, a significant and widespread anticorrelation is found between warm spells and blocking in the west and north of the Euro-Atlantic blocking region (not shown). However, over central Europe increased blocking frequencies on WSDs can be found in February and in

winter, indicating that fair-weather conditions connected with blocking highs can lead to winter warm spells here. From March onward the WSD blocking frequency shows a strong increase and is significantly higher than the climatological mean. The maximum of the frequency shifts slightly to the north toward summer.

Having analyzed the distribution of blocking frequencies, we now reversely investigate the spatial distribution of grid points contributing to CSDs and WSDs (termed CSDs and WSDs per grid point) in the European region. Figures 4a and 4b show the number of CSDs and WSDs per grid point over 36 springs from 1979 to 2014, respectively. The fraction of CSDs and WSDs per grid point during 1363 blocked days in spring
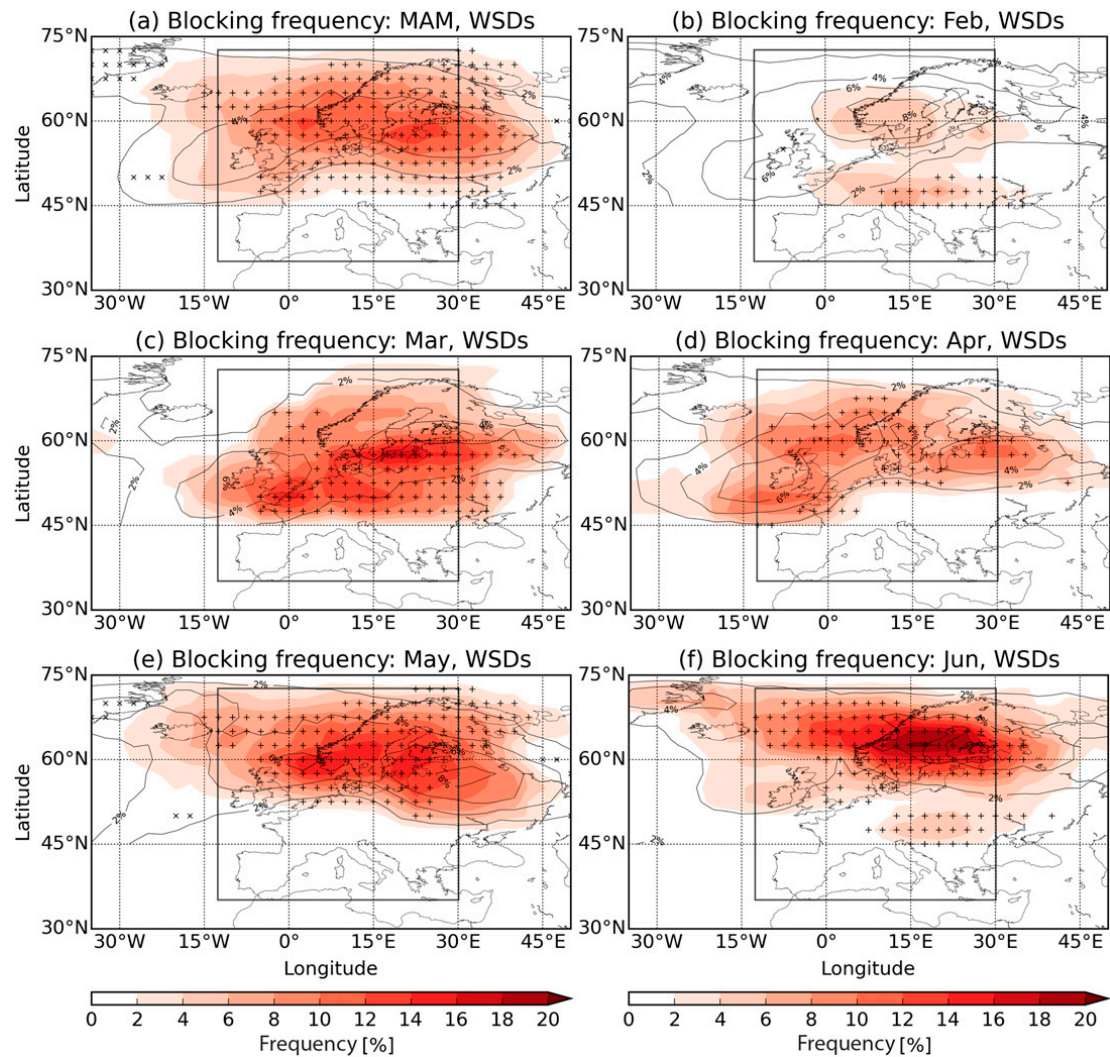
FIG. 3. As in Fig. 2, but for blocking frequency per grid point coinciding with WSDs.

(Figs. 4c,d) reveals a distinct dipole pattern for both cases. While in total about 46% of CSDs are blocked in spring (cf. Table 1), in southeastern Europe more than 80% of CSDs per grid point are blocked. In contrast, a strong anticorrelation is found over the British Isles and in Scandinavia, where less than 30% of CSDs per grid point coincide with blocking. For WSDs per grid point the opposite picture arises with locally more than 80% associated with blocking northward of 50°N. In southeastern Europe statistically significant anticorrelation is found with less than 40% of WSDs per grid point connected to blocking. This is consistent with the preferential location of blocks during WSDs, which is largely limited to northern Europe (Fig. 3), particularly later in spring. Differences for $T_{\min}$ and $T_{\max}$ composites of blocked minus unblocked CSDs and WSDs show a similar dipole pattern: both CSDs and WSDs with a blocking anywhere in the blocking region are warmer in

Scandinavia and colder in mainland Europe than without a blocking.

For a closer investigation of the dipole feature we divide Europe into two subdomains for CSDs and WSDs: northern (>50°N) and southern (<50°N) Europe (cf. Figs. 4c,d). Selecting only CSDs and WSDs in these subdomains we show the corresponding blocking frequency in Fig. 5. For the 163 CSDs in northern Europe hardly any blocking is found in the entire Euro-Atlantic blocking region (Fig. 5a), indicating that blocking tends to counteract CSDs here. CSDs (136 days) in southern Europe (Fig. 5c) are clearly linked to the blocking regions west of the British Isles and over Scandinavia indicated by distinct maximum blocking frequencies exceeding 18%. Considering conversely only blocking west of the British Isles (cf. Fig. 2a), we consistently find correlation predominantly with CSDs in southeastern Europe. Considering only
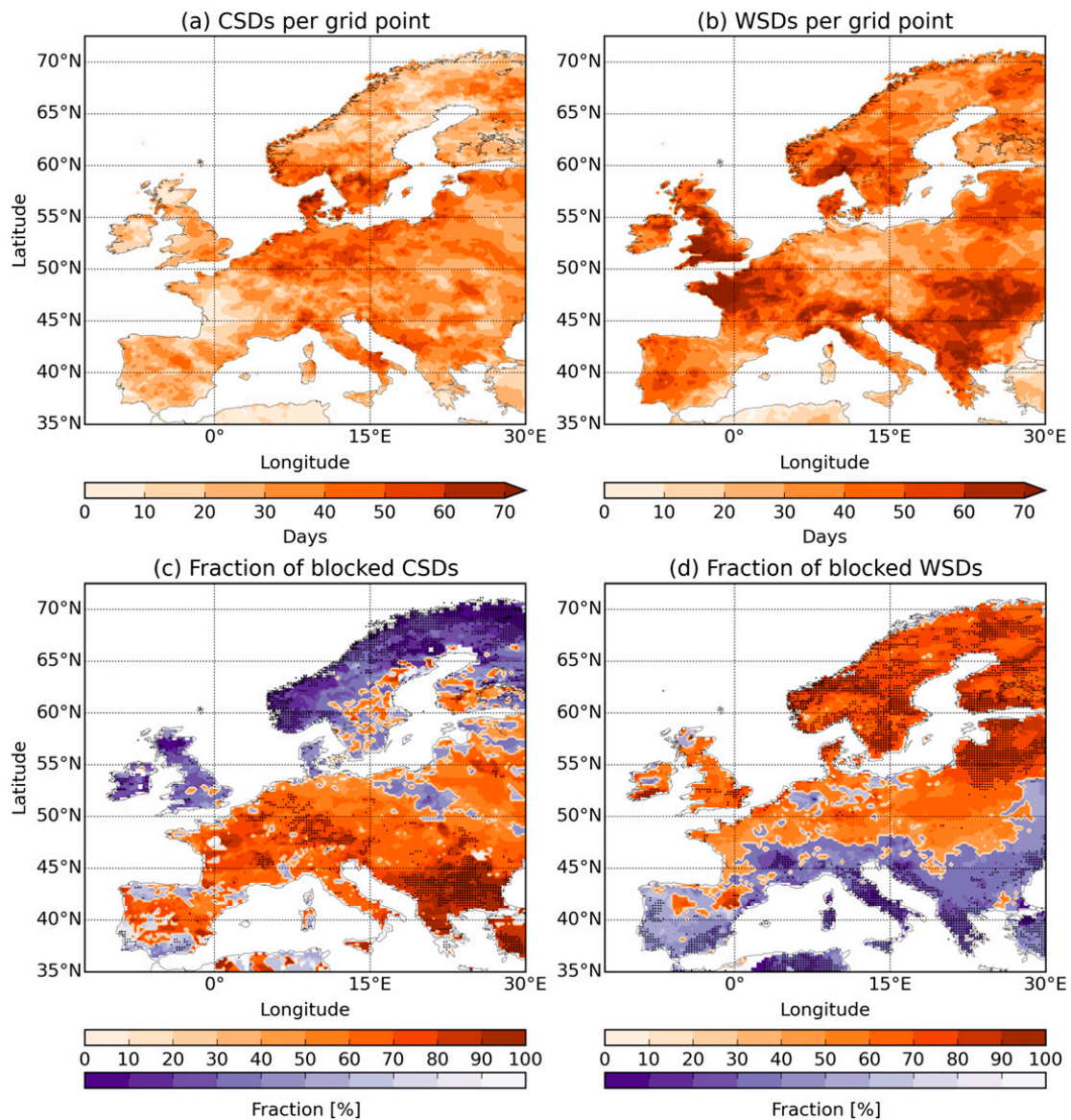
FIG. 4. Number of (a) CSDs and (b) WSDs per grid point in the European region over 36 springs from 1979 to 2014. Fraction of (c) CSDs and (d) WSDs per grid point during blocked days. Grid points where the fraction is above (below) the mean value of randomly drawn days are shown in orange (blue) shading. Grid points where the fraction is statistically significantly higher (above 95th percentile) or lower (below 5th percentile) than the random sample are marked with a dot.

blocking in northern Scandinavia (cf. Fig. 2a) leads to statistically significantly increased CSDs per grid point in most of central and eastern Europe (not shown).

WSDs in northern Europe (247 days) are found to be clearly connected to blocking over Scandinavia, with highest blocking frequencies exceeding 20% (Fig. 5b). Consistently, blocking over Scandinavia is correlated with increased frequency of WSDs in most of northern Europe in spring. In contrast, WSDs in southern Europe are connected to reduced blocking frequencies northward of 60°N (Fig. 5d). These results show the importance of the location of blocking and are consistent

with a strong role of cold advection at the edges of blocks for CSDs and increased solar radiation leading to WSDs in blocked regions.

## 4. Summary and discussion

We analyzed the relationship between blocking occurrence and temperature extremes in European spring for the period 1979–2014. Our results show statistically significant correlations of blocking frequency and the occurrence of cold spells and warm spells throughout the spring season, with sensitivity to the location of the
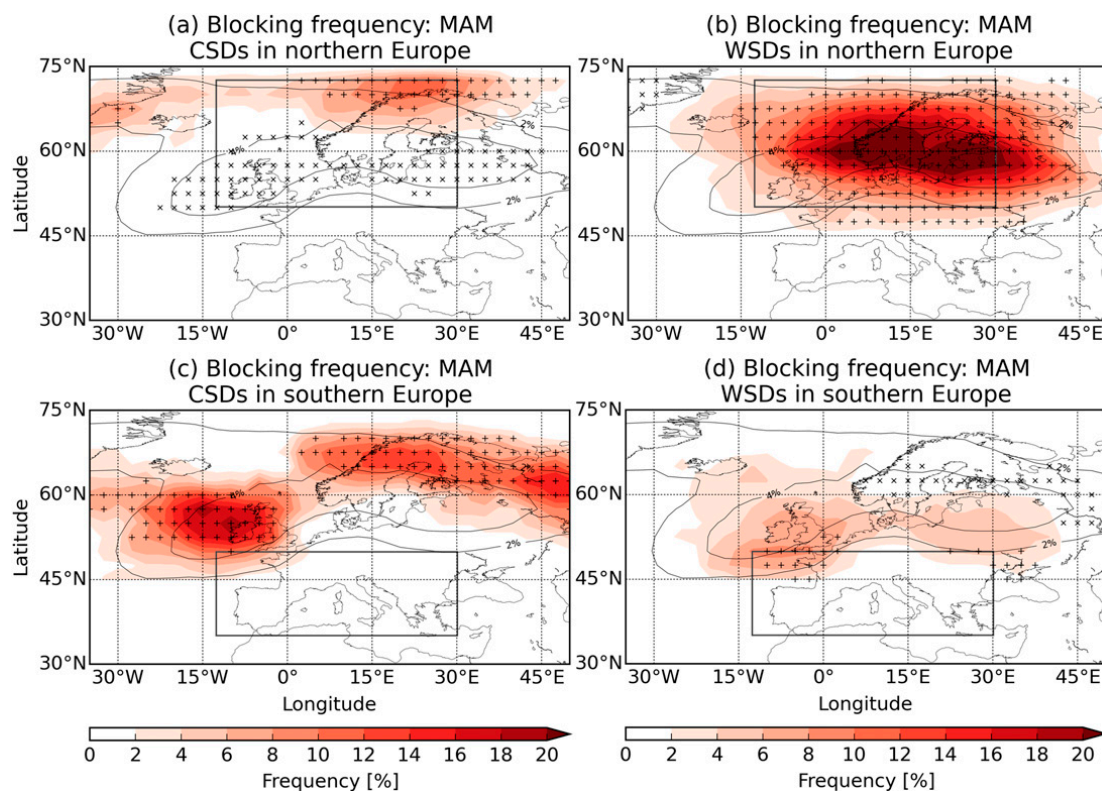
FIG. 5. Blocking frequency per grid point (shading) coinciding with (a),(c) CSDs and (b),(d) WSDs that occur over (top) northern and (bottom) southern Europe. The north–south split is at 50°N as indicated by the gray boxes. Values that are statistically significantly larger than the number of blocks from random days (above 95th percentile) are marked with a plus sign and values that are statistically significantly lower (below 5th percentile) are marked with a multiplication sign. The climatological blocking frequency is indicated by black contour lines.

block. We found blocking in winter and early spring to be stronger connected to cold conditions whereas blocking in late spring and summer is stronger connected to warm conditions. Blocked days in February show a statistically significant correlation with cold spell days whereas blocking in April is statistically significantly correlated to warm spell days, suggesting that on average the blocking–temperature relationship changes sign during this time.

Over the spring season, the number of cold spell days decreases toward late spring whereas the number of warm spell days increases. Over the analysis period, the seasonal mean time series shows considerable interannual variability for both cold and warm spells. If the trend is not removed from the underlying temperature time series, a lack of cold spell days and a clustering of warm spell days in late spring in the last 15 years of the investigated period suggest that the underlying long-term global warming trend also influences the frequency of cold spell days and warm spell days. In contrast, there is no apparent trend in the number of blocked days, suggesting that the trend is due to large-scale warming rather than a change in circulation. The

shift in probability of less cold extremes toward a higher probability of warm extremes, particularly in late spring, is consistent with recent findings on the earlier onset of summer and disruption of the European seasonal clock (Cassou and Cattiaux 2016). In such a warmer climate the occurrence of a cold spell in spring becomes even more critical and detrimental to vegetation, as just recently happened in Europe. After exceptionally warm spring temperatures, central and southeastern Europe were affected by a cold spell in late April 2016 that caused great damage to crops, orchards, and vineyards, especially in Austria, Slovenia, Slovakia, and Croatia (AGRI4CAST 2016). Our findings lay the basis for further research into these changes, including the atmospheric dynamics driving the relationship of blocking and temperature extremes and potential contributions to improved seasonal forecasting.

The location of the block is also found to be essential for its impact on European extreme temperatures. Blocking west of the British Isles and over northern Scandinavia is clearly connected with cold spells in southern Europe whereas blocking over central Europe and southern Scandinavia is associated with warm spells

in northern Europe. This is consistent with the role of cold advection at the edges of blocks leading to cold spells outside blocked regions and with increased solar radiation leading to warm spells in blocked regions.

The spatial distribution of cold and warm spells during blocking reveals a distinct dipole pattern. Cold spells in southeastern Europe are found to be highly correlated with blocking, and more than 80% of cold spell days co-occur with a blocking. In contrast, cold spells in northern Scandinavia and blocking are anticorrelated with regionally less than 30% co-occurrence. Warm spells show the opposite relationship with locally more than 80% of warm spell days in northern Europe co-occurring with blocking, but anticorrelation in southern Europe. An increased occurrence of both warm and cold spells during blocked conditions is found around 50°N, indicating that blocking increases the probability for both high and low temperature extremes here.

The occurrence of atmospheric blocking in the European region is found to be crucial for the development of both extended cold and warm spells in spring. We provide insight into the changing role of blocking in spring as its connection to cold conditions decreases and the connection to warm conditions increases. Our findings furthermore underline the importance of the location of blocking for its correlation with either cold or warm spells, highlighting in particular the remote effects of blocking on European temperatures.

## REFERENCES

AGRI4CAST, 2016: JRC MARS Bulletin—Crop monitoring in Europe. European Commission/Joint Research Centre, 41 pp. [Available online at https://ec.europa.eu/jrc/sites/default/files/jrc-mars-bulletin-vol24-no5.pdf.]

Barriopedro, D., R. García-Herrera, A. R. Lupo, and E. Hernández, 2006: A climatology of Northern Hemisphere blocking. *J. Climate*, **19**, 1042–1063, doi:10.1175/JCLI3678.1.

——, ——, and R. Huth, 2008: Solar modulation of Northern Hemisphere winter blocking. *J. Geophys. Res.*, **113**, D14118, doi:10.1029/2008JD009789.

——, ——, and R. M. Trigo, 2010: Application of blocking diagnosis methods to general circulation models. Part I: A novel detection scheme. *Climate Dyn.*, **35**, 1373–1391, doi:10.1007/s00382-010-0767-5.

Bieli, M., S. Pfahl, and H. Wernli, 2015: A Lagrangian investigation of hot and cold temperature extremes in Europe. *Quart. J. Roy. Meteor. Soc.*, **141**, 98–108, doi:10.1002/qj.2339.

Brunner, L., A. K. Steiner, B. Scherllin-Pirscher, and M. W. Jury, 2016: Exploring atmospheric blocking with GPS radio occultation observations. *Atmos. Chem. Phys.*, **16**, 4593–4604, doi:10.5194/acp-16-4593-2016.

Buehler, T., C. C. Raible, and T. F. Stocker, 2011: The relationship of winter season North Atlantic blocking frequencies to extreme cold or dry spells in the ERA-40. *Tellus*, **63A**, 212–222, doi:10.1111/j.1600-0870.2010.00492.x.

Cassou, C., and J. Cattiaux, 2016: Disruption of the European climate seasonal clock in a warming world. *Nat. Climate Change*, **6**, 589–594, doi:10.1038/nclimate2969.

——, L. Terray, and A. S. Phillips, 2005: Tropical Atlantic influence on European heat waves. *J. Climate*, **18**, 2805–2811, doi:10.1175/JCLI3506.1.

Cattiaux, J., R. Vautard, C. Cassou, P. Yiou, V. Masson-Delmotte, and F. Codron, 2010: Winter 2010 in Europe: A cold extreme in a warming climate. *Geophys. Res. Lett.*, **37**, L20704, doi:10.1029/2010GL044613.

Croci-Maspoli, M., C. Schwierz, and H. C. Davies, 2007: A multifaceted climatology of atmospheric blocking and its recent linear trend. *J. Climate*, **20**, 633–649, doi:10.1175/JCLI4029.1.

Davini, P., C. Cagnazzo, S. Gualdi, and A. Navarra, 2012: Bidimensional diagnostics, variability, and trends of Northern Hemisphere blocking. *J. Climate*, **25**, 6496–6509, doi:10.1175/JCLI-D-12-00032.1.

——, ——, P. G. Fogli, E. Manzini, S. Gualdi, and A. Navarra, 2014: European blocking and Atlantic jet stream variability in the NCEP/NCAR reanalysis and the CMCC-CMS climate model. *Climate Dyn.*, **43**, 71–85, doi:10.1007/s00382-013-1873-y.

Dee, D. P., and Coauthors, 2011: The ERA-Interim reanalysis: Configuration and performance of the data assimilation system. *Quart. J. Roy. Meteor. Soc.*, **137**, 553–597, doi:10.1002/qj.828.

Haylock, M. R., N. Hofstra, A. M. G. Klein Tank, E. J. Klok, P. D. Jones, and M. New, 2008: A European daily high-resolution gridded data set of surface temperature and precipitation for 1950–2006. *J. Geophys. Res.*, **113**, D20119, doi:10.1029/2008JD010201.

Hufkens, K., M. A. Friedl, T. F. Keenan, O. Sonnentag, A. Bailey, J. O'Keefe, and A. D. Richardson, 2012: Ecological impacts of a widespread frost event following early spring leaf-out. *Global Change Biol.*, **18**, 2365–2377, doi:10.1111/j.1365-2486.2012.02712.x.

IPCC, 2013: *Climate Change 2013: The Physical Science Basis*. T. F. Stocker et al., Eds., Cambridge University Press, 1535 pp.

Klok, E. J., and A. M. G. Klein Tank, 2009: Updated and extended European dataset of daily climate observations. *Int. J. Climatol.*, **29**, 1182–1191, doi:10.1002/joc.1779.

Ma, S., A. J. Pitman, R. Lorenz, J. Kala, and J. Srbinovsky, 2016: Earlier green-up and spring warming amplification over Europe. *Geophys. Res. Lett.*, **43**, 2011–2018, doi:10.1002/2016GL068062.

Matsueda, M., 2011: Predictability of Euro-Russian blocking in summer of 2010. *Geophys. Res. Lett.*, **38**, L06801, doi:10.1029/2010GL046557.

Menzel, A., R. Helm, and C. Zang, 2015: Patterns of late spring frost leaf damage and recovery in a European beech (*Fagus sylvatica* L.) stand in south-eastern Germany based on repeated digital photographs. *Front. Plant Sci.*, **6**, 110, doi:10.3389/fpls.2015.00110.

Morak, S., G. C. Hegerl, and N. Christidis, 2013: Detectable changes in the frequency of temperature extremes. *J. Climate*, **26**, 1561–1574, doi:10.1175/JCLI-D-11-00678.1.

Pelly, J. L., and B. J. Hoskins, 2003: A new perspective on blocking. *J. Atmos. Sci.*, **60**, 743–755, doi:10.1175/1520-0469(2003)060<0743:ANPOB>2.0.CO;2.

Pfahl, S., and H. Wernli, 2012: Quantifying the relevance of atmospheric blocking for co-located temperature extremes in the Northern Hemisphere on (sub-)daily time scales. *Geophys. Res. Lett.*, **39**, L12807, doi:10.1029/2012GL052261.

Rex, D. F., 1950: Blocking action in the middle troposphere and its effect upon regional climate I: An aerological study of blocking action. *Tellus*, **2**, 196–211, doi:10.1111/j.2153-3490.1950.tb00331.x.

Scherrer, S. C., M. Croci-Maspoli, C. Schwierz, and C. Appenzeller, 2006: Two-dimensional indices of atmospheric blocking and their statistical relationship with winter climate patterns in the Euro-Atlantic region. *Int. J. Climatol.*, **26**, 233–249, doi:10.1002/joc.1250.

Sillmann, J., M. Croci-Maspoli, M. Kallache, and R. W. Katz, 2011: Extreme cold winter temperatures in Europe under the influence of North Atlantic atmospheric blocking. *J. Climate*, **24**, 5899–5913, doi:10.1175/2011JCLI4075.1.

Stefanon, M., F. D'Andrea, and P. Drobinski, 2012: Heatwave classification over Europe and the Mediterranean region. *Environ. Res. Lett.*, **7**, 014023, doi:10.1088/1748-9326/7/1/014023.

Tibaldi, S., and F. Molteni, 1990: On the operational predictability of blocking. *Tellus*, **42A**, 343–365, doi:10.1034/j.1600-0870.1990.t01-2-00003.x.

Trigo, R. M., I. F. Trigo, C. C. DaCamara, and T. J. Osborn, 2004: Climate impact of the European winter blocking episodes from the NCEP/NCAR reanalyses. *Climate Dyn.*, **23**, 17–28, doi:10.1007/s00382-004-0410-4.

Whan, K., F. Zwiers, and J. Sillmann, 2016: The influence of atmospheric blocking on extreme winter minimum temperatures in North America. *J. Climate*, **29**, 4361–4381, doi:10.1175/JCLI-D-15-0493.1.

Woollings, T., 2010: Dynamical influences on European climate: An uncertain future. *Philos. Trans. Roy. Soc.*, **368A**, 3733–3756, doi:10.1098/rsta.2010.0040.

Xoplaki, E., J. F. González-Rouco, J. Luterbacher, and H. Wanner, 2003: Mediterranean summer air temperature variability and its connection to the large-scale atmospheric circulation and SSTs. *Climate Dyn.*, **20**, 723–739, doi:10.1007/s00382-003-0304-x.

Zwiers, F. W., X. Zhang, and Y. Feng, 2011: Anthropogenic influence on long return period daily temperature extremes at regional scales. *J. Climate*, **24**, 881–892, doi:10.1175/2010JCLI3908.1.

# List of Acronyms

**AMIP** Atmospheric Model Intercomparison Project

**AR5** Fifth Assessment Report

**CanESM2** second Canadian Earth System Model

**CCCA** Climate Change Centre Austria

**CHAMP** Challenging Minisatellite Payload

**CMIP3** Coupled Model Intercomparison Project phase three

**CMIP5** Coupled Model Intercomparison Project phase five

**CMIP6** Coupled Model Intercomparison Project phase six

**C/NOFS** Communications/Navigation Outage Forecasting System

**FORMOSAT-3/COSMIC** Formosa Satellite mission #3/Constellation Observing System for Meteorology, Ionosphere, and Climate

**FORMOSAT-7/COSMIC-2** Formosa Satellite mission #7/COSMIC 2

**CSD** cold spell day

**DJF** December, January, February

**ECMWF** European Centre for Medium-Range Weather Forecasts

**ENSO** El Niño-Southern Oscillation

**E-OBS** European daily high-resolution gridded dataset

**ERA-40** ECMWF 40-year reanalysis

**ERA-Interim** ECMWF Reanalysis Interim

**FAR** fraction of attributable risk

**FMA** February, March, April

*List of Acronyms*

**GCM** General Circulation Model

**GLONASS** Global Navigation Satellite System (Russia)

**GNSS** Global Navigation Satellite System

**GPH** geopotential height

**GPS** Global Positioning System (USA)

**GRACE** Gravity Recovery and Climate Experiment

**HighResMIP** High Resolution Model Intercomparison Project

**IB** Instantaneous Blocking

**IPCC** Intergovernmental Panel on Climate Change

**JJA** June, July, August

**JMA** Japanese Meteorological Agency

**JRA-25** Japanese 25-year reanalysis (JMA)

**JRA-55** Japanese 55-year reanalysis (JMA)

**LEO** Low Earth Orbit

**MAM** March, April, May

**MERRA** Modern-Era Retrospective analysis for Research and Applications (NASA)

**MERRA-2** second MERRA (NASA)

**MetOp** Meteorological Operational Satellite

**MJJAS** May, June, July, August, September

**NASA** National Aeronautics and Space Administration

**NCAR** National Center for Atmospheric Research

**NCEP** National Centers for Environmental Prediction

**NDJFM** November, December, January, February, March

**NH** Northern Hemisphere

**NWP** numerical weather prediction

**OPSv5.6** occultation processing system version 5.6 (WEGC)

**PDF** Probability Density Function

**PV** potential vorticity

**R-1** NCAR/NCEP reanalysis

**R-2** NCEP–Department of Energy reanalysis

**RCP8.5** Representative Concentration Pathway 8.5

**RO** radio occultation

**SAC-C** Scientific Application Satellite-C

**SE** sampling error

**SH** Southern Hemisphere

**SI** International System of Units

**SON** September, October, November

**UNFCCC** United Nations Framework Convention on Climate Change

**WCRP** World Climate Research Programme

**WEGC** Wegener Center for Climate and Global Change

**WSD** warm spell day

# List of Figures

Part II. Published papers

**Paper I: Exploring atmospheric blocking with
GPS radio occultation observations**

**Paper II: A global perspective on atmospheric blocking using
GPS radio occultation – one decade of observations**

**Paper III: Connecting atmospheric blocking to European
temperature extremes in spring**

# List of Tables

# Bibliography

Adana, F. J. S. de and S. J. Colucci (2005). "Southern Hemisphere Blocking Onsets Associated with Upper-Tropospheric Divergence Anomalies". *J. Atmos. Sci.* 62.5, pp. 1614–1625. DOI: 10.1175/JAS3421.1.

AGRI4CAST (2016). *JRC MARS Bulletin – Crop monitoring in Europe.* URL: https://ec.europa.eu/jrc/sites/default/files/jrc-mars-bulletin-vol24-no5.pdf (visited on 05/31/2016).

Anderson, J. L. (1993). "The Climatology of Blocking in a Numerical Forecast Model". *J. Climate* 6.6, pp. 1041–1056. DOI: 10.1175/1520-0442(1993)006<1041: TCOBIA>2.0.CO;2.

Angerer, B., F. Ladstädter, B. Scherllin-Pirscher, M. Schwärz, A. K. Steiner, U. Foelsche, and G. Kirchengast (2017). "Quality aspects of the WEGC multi-satellite GPS radio occultation record OPSv5.6". *Atmos. Meas. Tech.* 10, pp. 4845–4863. DOI: 10.5194/amt-10-4845-2017.

Anstey, J. A., P. Davini, L. J. Gray, T. J. Woollings, N. Butchart, C. Cagnazzo, B. Christiansen, S. C. Hardiman, S. M. Osprey, and S. Yang (2013). "Multi-model analysis of Northern Hemisphere winter blocking: Model biases and the role of resolution". *J. Geophys. Res.* 118.10, pp. 3956–3971. DOI: 10.1002/jgrd.50231.

Anthes, R. A. (2011). "Exploring Earth's atmosphere with radio occultation: contributions to weather, climate, and space weather". *Atmos. Meas. Tech.* 4, pp. 1077–1103. DOI: 10.5194/amt-4-1077-2011.

Archer, C. L. and K. Caldeira (2008). "Historical trends in the jet streams". *Geophys. Res. Lett.* 35, L08803. DOI: 10.1029/2008GL033614.

Ayarzagüena, B., Y. J. Orsolini, U. Langematz, J. Abalichin, and A. Kubin (2015). "The Relevance of the Location of Blocking Highs for Stratospheric Variability in a Changing Climate". *J. Climate* 28.2, pp. 531–549. DOI: 10.1175/JCLI-D-14-00210.1.

Barnes, E. A. (2013). "Revisiting the evidence linking Arctic amplification to extreme weather in midlatitudes". *Geophys. Res. Lett.* 40. DOI: 10.1002/grl.50880.

*Bibliography*

Barnes, E. A., E. Dunn-Sigouin, G. Masato, and T. Woollings (2014). "Exploring recent trends in Northern Hemisphere blocking". *Geophys. Res. Lett.* 41. DOI: 10.1002/2013GL058745.

Barnes, E. A. and L. M. Polvani (2015). "CMIP5 Projections of Arctic Amplification, of the North American/North Atlantic Circulation, and of Their Relationship". *J. Climate* 28.13, pp. 5254–5271. DOI: 10.1175/JCLI-D-14-00589.1.

Barnes, E. A. and J. A. Screen (2015). "The impact of Arctic warming on the midlatitude jet-stream: Can it? Has it? Will it?" *WIRes. Clim. Change* 6.3, pp. 277–286. DOI: 10.1002/wcc.337.

Barnes, E. A., J. Slingo, and T. Woollings (2012). "A methodology for the comparison of blocking climatologies across indices, models and climate scenarios". *Climate Dyn.* 38.11, pp. 2467–2481. DOI: 10.1007/s00382-011-1243-6.

Barriopedro, D., M. Antón, and J. A. García (2010a). "Atmospheric Blocking Signatures in Total Ozone and Ozone Miniholes". *J. Climate* 23 (14), pp. 3967–3983. DOI: 10.1175/2010JCLI3508.1.

Barriopedro, D. and N. Calvo (2014). "On the Relationship between ENSO, Stratospheric Sudden Warmings, and Blocking". *J. Climate* 27 (12), pp. 4704–4720. DOI: 10.1175/JCLI-D-13-00770.1.

Barriopedro, D., E. M. Fischer, J. Luterbacher, R. M. Trigo, and R. García-Herrera (2011). "The Hot Summer of 2010: Redrawing the Temperature Record Map of Europe". *Science* 332.6026, pp. 220–224. DOI: 10.1126/science.1201224.

Barriopedro, D., R. García-Herrera, and R. Huth (2008). "Solar modulation of Northern Hemisphere winter blocking". *J. Geophys. Res.* 113.D14, D14118. DOI: 10.1029/2008JD009789.

Barriopedro, D., R. García-Herrera, A. R. Lupo, and E. Hernández (2006). "A climatology of northern hemisphere blocking". *J. Climate* 19, pp. 1042–1063. DOI: 10.1175/JCLI3678.1.

Barriopedro, D., R. García-Herrera, and R. M. Trigo (2010b). "Application of blocking diagnosis methods to General Circulation Models. Part I: a novel detection scheme". *Climate Dyn.* 35.7–8, pp. 1373–1391. DOI: 10.1007/s00382-010-0767-5.

Bengtsson, L., K. I. Hodges, and E. Roeckner (2005). "Storm Tracks and Climate Change". *J. Climate* 19.15, pp. 3518–3543. DOI: 10.1175/JCLI3815.1.

Berrisford, P., B. J. Hoskins, and E. Tyrlis (2007). "Blocking and Rossby Wave Breaking on the Dynamical Tropopause in the Southern Hemisphere". *J. Atmos. Sci.* 64.8, pp. 2881–2898. DOI: 10.1175/JAS3984.1.

Bieli, M., S. Pfahl, and H. Wernli (2015). "A Lagrangian investigation of hot and cold temperature extremes in Europe". *Quart. J. Roy. Meteor. Soc.* 141.686, pp. 98–108. DOI: 10.1002/qj.2339.

Biondi, R., A. K. Steiner, G. Kirchengast, and T. Rieckh (2015). "Characterization of thermal structure and conditions for overshooting of tropical and extratropical cyclones with GPS radio occultation". *Atmos. Chem. Phys.* 15.9, pp. 5181–5193. DOI: 10.5194/acp-15-5181-2015.

Black, E., M. Blackburn, G. Harrison, B. Hoskins, and J. Methven (2004). "Factors contributing to the summer 2003 European heatwave". *Weather* 59.8, pp. 217–223. DOI: 10.1256/wea.74.04.

Brunner, L., G. C. Hegerl, and A. K. Steiner (2017). "Connecting atmospheric blocking to European temperature extremes in spring". *J. Climate* 30.2, pp. 585–594. DOI: 10.1175/JCLI-D-16-0518.1.

Brunner, L., N. Schaller, J. Anstey, J. Sillmann, and A. K. Steiner (in press). "Dependence of present and future European temperature extremes on the location of atmospheric blocking". *Geophys. Res. Lett.* DOI: 10.1029/2018GL077837.

Brunner, L. and A. K. Steiner (2017). "A global perspective on atmospheric blocking using GPS radio occultation – one decade of observations". *Atmos. Meas. Tech.* 10, pp. 4727–4745. DOI: 10.5194/amt-10-4727-2017.

Brunner, L., A. K. Steiner, B. Scherllin-Pirscher, and M. W. Jury (2015). "Feasibility of blocking detection in observations from radio occultation". In: *Geophysical Research Abstracts*. Vol. 17. European Geoscience Union General Assembly 2015 (poster), EGU2015–1519.

– (2016). "Exploring atmospheric blocking with GPS radio occultation observations". *Atmos. Chem. Phys.* 16.7, pp. 4593–4604. DOI: 10.5194/acp-16-4593-2016.

Buehler, T., C. C. Raible, and T. F. Stocker (2011). "The relationship of winter season North Atlantic blocking frequencies to extreme cold or dry spells in the ERA-40". *Tellus A* 63.2, pp. 212–222. DOI: 10.1111/j.1600-0870.2010.00492.x.

Cardinali, C. (2009). "Monitoring the observation impact on the short-range forecast". *Quart. J. Roy. Meteor. Soc.* 135.638, pp. 239–250. DOI: 10.1002/qj.366.

*Bibliography*

Carrera, M., R. Higgins, and V. Kousky (2004). "Downstream Weather Impacts Associated with Atmospheric Blocking over the Northeast Pacific". *J. Climate* 17.24, pp. 4823–4839. DOI: 10.1175/JCLI-3237.1.

Cassou, C. and J. Cattiaux (2016). "Disruption of the European climate seasonal clock in a warming world". *Nature Climate Change* 6, pp. 589–594. DOI: 10.1038/nclimate2969.

Cassou, C., L. Terray, and A. S. Phillips (2005). "Tropical Atlantic Influence on European Heat Waves". *J. Climate* 18, pp. 2805–2811. DOI: 10.1175/JCLI3506.1.

Castanheira, J. M. and D. Barriopedro (2010). "Dynamical connection between tropospheric blockings and stratospheric polar vortex". *Geophys. Res. Lett.* 37.13, L13809. DOI: 10.1029/2010GL043819.

Cattiaux, J., R. Vautard, C. Cassou, P. Yiou, V. Masson-Delmotte, and F. Codron (2010). "Winter 2010 in Europe: A cold extreme in a warming climate". *Geophys. Res. Lett.* 37.20, L20704. DOI: 10.1029/2010GL044613.

Catto, J. L., N. Nicholls, C. Jakob, and K. L. Shelton (2014). "Atmospheric fronts in current and future climates". *Geophys. Res. Lett.* 41.21, pp. 7642–7650. DOI: 10.1002/2014GL061943.

Center for Research on Environmental Decisions (2009). *The Psychology of Climate Change Communication: A Guide for Scientists, Journalists, Educators, Political Aides, and the Interested Public.* New York, USA.

Christensen, J. H., K. K. Kumar, E. Aldrian, S.-I. An, I. Cavalcanti, M. de Castro, W. Dong, P. Goswami, A. Hall, J. Kanyanga, A. Kitoh, J. Kossin, N.-C. Lau, J. Renwick, D. Stephenson, S.-P. Xie, and T. Zhou (2013). "Climate Phenomena and their Relevance for Future Regional Climate Change". In: *Climate Change 2013: The Physical Science Basis. Contribution of Working Group I to the Fifth Assessment Report of the Intergovernmental Panel on Climate Change.* Ed. by T. Stocker, D. Qin, G.-K. Plattner, M. Tignor, S. Allen, J. Boschung, A. Nauels, Y. Xia, V. Bex, and P. Midgley. Cambridge, United Kingdom and N: Cambridge University Press, pp. 1217–1308.

Christidis, N., G. S. Jones, and P. A. Stott (2015). "Dramatically increasing chance of extremely hot summers since the 2003 European heatwave". *Nature Climate Change* 5, pp. 46–50. DOI: 10.1038/nclimate2468.

Clark, R. T., S. J. Brown, and J. M. Murphy (2006). "Modeling Northern Hemisphere Summer Heat Extreme Changes and Their Uncertainties Using a Physics

Ensemble of Climate Sensitivity Experiments". *J. Climate* 19.17, pp. 4418–4435. DOI: 10.1175/JCLI3877.1.

Cohen, J., J. A. Screen, J. C. Furtado, M. Barlow, D. Whittleston, D. Coumou, J. Francis, K. Dethloff, D. Entekhabi, J. Overland, and J. Jones (2014). "Recent Arctic amplification and extreme mid-latitude weather". *Nature Geoscience* 7.9, pp. 627–637. DOI: 10.1038/ngeo2234.

Cowan, T., P. van Rensch, A. Purich, and W. Cai (2013). "The Association of Tropical and Extratropical Climate Modes to Atmospheric Blocking across Southeastern Australia". *J. Climate* 26.19, pp. 7555–7569. DOI: 10.1175/JCLI-D-12-00781.1.

Croci-Maspoli, M., C. Schwierz, and H. C. Davies (2007). "A Multifaceted Climatology of Atmospheric Blocking and Its Recent Linear Trend". *J. Climate* 20.4, pp. 633–649. DOI: 10.1175/JCLI4029.1.

Cullen, M. J. P. and K. Ngan (2013). "On the relationship between stratospheric structure and tropospheric blocking patterns". *Phil. Trans. R. Soc. A* 371.1991. DOI: 10.1098/rsta.2012.0180.

D'Andrea, F., S. Tibaldi, M. Blackburn, G. Boer, M. Déqué, M. R. Dix, B. Dugas, L. Ferranti, T. Iwasaki, A. Kitoh, V. Pope, D. Randall, E. Roeckner, D. Strauss, W. Stern, H. Van den Dool, and D. Williamson (1998). "Northern Hemisphere atmospheric blocking as simulated by 15 atmospheric general circulation models in the period 1979–1988". *Climate Dyn.* 14.6, pp. 385–407. DOI: 10.1007/s003820050230.

Davini, P., C. Cagnazzo, and J. A. Anstey (2014a). "A blocking view of the stratosphere-troposphere coupling". *J. Geophys. Res.* 119.19, pp. 11100–11115. DOI: 10.1002/2014JD021703.

Davini, P., C. Cagnazzo, P. G. Fogli, E. Manzini, S. Gualdi, and A. Navarra (2014b). "European blocking and Atlantic jet stream variability in the NCEP/NCAR reanalysis and the CMCC-CMS climate model". *Climate Dyn.* 43.1–2, pp. 71–85. DOI: 10.1007/s00382-013-1873-y.

Davini, P., C. Cagnazzo, S. Gualdi, and A. Navarra (2012). "Bidimensional diagnostics, variability, and trends of Northern Hemisphere blocking". *J. Climate* 25, pp. 6496–6509. DOI: 10.1175/JCLI-D-12-00032.1.

Davini, P. and F. D'Andrea (2016). "Northern Hemisphere Atmospheric Blocking Representation in Global Climate Models: Twenty Years of Improvements?" *J. Climate* 29.24, pp. 8823–8840. DOI: 10.1175/JCLI-D-16-0242.1.

*Bibliography*

Dee, D. P., M. Balmaseda, G. Balsamo, R. Engelen, A. J. Simmons, and J.-N. Thépaut (2014). "Toward a Consistent Reanalysis of the Climate System". *Bull. Amer. Meteor. Soc.* 95.8, pp. 1235–1248. DOI: 10.1175/BAMS-D-13-00043.1.

Dee, D. P., S. M. Uppala, A. J. Simmons, P. Berrisford, P. Poli, S. Kobayashi, U. Andrae, M. A. Balmaseda, G. Balsamo, P. Bauer, P. Bechtold, A. C. M. Beljaars, L. van de Berg, J. Bidlot, N. Bormann, C. Delsol, R. Dragani, M. Fuentes, A. J. Geer, L. Haimberger, S. B. Healy, H. Hersbach, E. V. Hólm, L. Isaksen, P. Kållberg, M. Köhler, M. Matricardi, A. P. McNally, B. M. Monge-Sanz, J.-J. Morcrette, B.-K. Park, C. Peubey, P. de Rosnay, C. Tavolato, J.-N. Thépaut, and F. Vitart (2011). "The ERA-Interim reanalysis: configuration and performance of the data assimilation system". *Quart. J. Roy. Meteor. Soc.* 137.656, pp. 553–597. DOI: 10.1002/qj.828.

Dee, D. P., J. Fasullo, D. Shea, J. Walsh, and National Center for Atmospheric Research Staff (2016). *The Climate Data Guide: Atmospheric Reanalysis: Overview & Comparison Tables.* Accessed November 15th, 2017. URL: https://climatedataguide.ucar.edu/climate-data/atmospheric-reanalysis-overview-comparison-tables.

Della-Marta, P. M., M. R. Haylock, J. Luterbacher, and H. Wanner (2007a). "Doubled length of western European summer heat waves since 1880". *J. Geophys. Res.* 112, D15103. DOI: 10.1029/2007JD008510.

Della-Marta, P. M., J. Luterbacher, H. von Weissenfluh, E. Xoplaki, M. Brunet, and H. Wanner (2007b). "Summer heat waves over western Europe 1880–2003, their relationship to large-scale forcings and predictability". *Climate Dyn.* 29.2, pp. 251–275. DOI: 10.1007/s00382-007-0233-1.

Doblas-Reyes, F. J., M. J. Casado, and M. A. Pastor (2002). "Sensitivity of the Northern Hemisphere blocking frequency to the detection index". *J. Geophys. Res.* 107.D2. DOI: 10.1029/2000JD000290.

Dole, R. M. and N. D. Gordon (1983). "Persistent Anomalies of the Extratropical Northern Hemisphere Wintertime Circulation: Geographical Distribution and Regional Persistence Characteristics". *Mon. Wea. Rev.* 111, pp. 1567–1586. DOI: 10.1175/1520-0493(1983)111<1567:PAOTEN>2.0.CO;2.

Dong, B., R. T. Sutton, T. Woollings, and K. Hodges (2013). "Variability of the North Atlantic summer storm track: mechanisms and impacts on European climate". *Environ. Res. Lett.* 8.3, p. 034037. DOI: 10.1088/1748-9326/8/3/034037.

Dong, L. and S. J. Colucci (2005). "The Role of Deformation and Potential Vorticity in Southern Hemisphere Blocking Onsets". *J. Atmos. Sci.* 62.11, pp. 4043–4056. DOI: 10.1175/JAS3576.1.

Dunn-Sigouin, E. and S.-W. Son (2013). "Northern Hemisphere blocking frequency and duration in the CMIP5 models". *J. Geophys. Res.: Atmos* 118.3, pp. 1179–1188. DOI: 10.1002/jgrd.50143.

Ebita, A., S. Kobayashi, Y. Ota, M. Moriya, R. Kumabe, K. Onogi, Y. Harada, S. Yasui, K. Miyaoka, K. Takahashi, H. Kamahori, C. Kobayashi, H. Endo, M. Soma, Y. Oikawa, and T. Ishimizu (2011). "The Japanese 55-year Reanalysis "JRA-55": An Interim Report". *SOLA* 7, pp. 149–152. DOI: 10.2151/sola.2011-038.

Eccel, E., R. Rea, A. Caffarra, and A. Crisci (2009). "Risk of spring frost to apple production under future climate scenarios: the role of phenological acclimation". *International Journal of Biometeorology* 53.3, pp. 273–286. DOI: 10.1007/s00484-009-0213-8.

Engeln, A. von, J. Teixeira, J. Wickert, and S. A. Buehler (2005). "Using CHAMP radio occultation data to determine the top altitude of the Planetary Boundary Layer". *Geophys. Res. Lett.* 32, L06815. DOI: 10.1029/2004GL022168.

Eyring, V., S. Bony, G. A. Meehl, C. A. Senior, B. Stevens, R. J. Stouffer, and K. E. Taylor (2016). "Overview of the Coupled Model Intercomparison Project Phase 6 (CMIP6) experimental design and organization". *Geosci. Model Dev.* 9.5, pp. 1937–1958. DOI: 10.5194/gmd-9-1937-2016.

Favre, A. and A. Gershunov (2006). "Extra-tropical cyclonic/anticyclonic activity in North-Eastern Pacific and air temperature extremes in Western North America". *Climate Dyn.* 26.6, pp. 617–629. DOI: 10.1007/s00382-005-0101-9.

Feldstein, S. B. and S. Lee (2014). "Intraseasonal and Interdecadal Jet Shifts in the Northern Hemisphere: The Role of Warm Pool Tropical Convection and Sea Ice". *J. Climate* 27.17, pp. 6497–6518. DOI: 10.1175/JCLI-D-14-00057.1.

Fischer, E. M., S. I. Seneviratne, D. Lüthi, and C. Schär (2007a). "Contribution of land-atmosphere coupling to recent European summer heat waves". *Geophys. Res. Lett.* 34.6. DOI: 10.1029/2006GL029068.

Fischer, E. M., S. I. Seneviratne, P. L. Vidale, D. Lüthi, and C. Schär (2007b). "Soil Moisture–Atmosphere Interactions during the 2003 European Summer Heat Wave". *J. Climate* 20.20, pp. 5081–5099. DOI: 10.1175/JCLI4288.1.

*Bibliography*

Fischer, E. M. and R. Knutti (2015). "Anthropogenic contribution to global occurrence of heavy-precipitation and high-temperature extremes". *Nature Climate Change* 5, pp. 560–564. DOI: 10.1038/nclimate2617.

Foelsche, U., B. Scherllin-Pirscher, F. Ladstädter, A. K. Steiner, and G. Kirchengast (2011). "Refractivity and temperature climate records from multiple radio occultation satellites consistent within 0.05 %". *Atmos. Meas. Tech.* 4, pp. 2007–2018. DOI: 10.5194/amt-4-2007-2011.

Francis, J. A. and S. J. Vavrus (2015). "Evidence for a wavier jet stream in response to rapid Arctic warming". *Environ. Res. Lett.* 10.1. DOI: 10.1088/1748-9326/10/1/014005.

Fu, Q. and P. Lin (2011). "Poleward Shift of Subtropical Jets Inferred from Satellite-Observed Lower-Stratospheric Temperatures". *J. Climate* 24.21, pp. 5597–5603. DOI: 10.1175/JCLI-D-11-00027.1.

Fujiwara, M., J. S. Wright, G. L. Manney, L. J. Gray, J. Anstey, T. Birner, S. Davis, E. P. Gerber, V. L. Harvey, M. I. Hegglin, C. R. Homeyer, J. A. Knox, K. Krüger, A. Lambert, C. S. Long, P. Martineau, A. Molod, B. M. Monge-Sanz, M. L. Santee, S. Tegtmeier, S. Chabrillat, D. G. H. Tan, D. R. Jackson, S. Polavarapu, G. P. Compo, R. Dragani, W. Ebisuzaki, Y. Harada, C. Kobayashi, W. McCarty, K. Onogi, S. Pawson, A. Simmons, K. Wargan, J. S. Whitaker, and C.-Z. Zou (2017). "Introduction to the SPARC Reanalysis Intercomparison Project (S-RIP) and overview of the reanalysis systems". *Atmos. Chem. Phys.* 17.2, pp. 1417–1452. DOI: 10.5194/acp-17-1417-2017.

Galarneau Jr., T. J., T. M. Hamill, R. M. Dole, and J. Perlwitz (2012). "A Multiscale Analysis of the Extreme Weather Events over Western Russia and Northern Pakistan during July 2010". *Mon. Wea. Rev.* 140, pp. 1639–1664. DOI: 10.1175/MWR-D-11-00191.1.

García-Herrera, R., J. Diaz, R. M. Trigo, J. Luterbacher, and E. M. Fischer (2010). "A Review of the European Summer Heat Wave of 2003". *Crit. Rev. Env. Sci. Tec.* 40.4. DOI: 10.1080/10643380802238137.

Garriott, E. B. (1904). "Long-range weather forecasts". *Weather Bureau Bulletin* 35.

Gasparrini, A., Y. Guo, M. Hashizume, E. Lavigne, A. Zanobetti, J. Schwartz, A. Tobias, S. Tong, J. Rocklöv, B. Forsberg, M. Leone, M. D. Sario, M. L. Bell, Y.-L. L. Guo, C.-f. Wu, H. Kan, S.-M. Yi, M. de Sousa Zanotti Stagliorio Coelho, P. H. N. Saldiva, Y. Honda, H. Kim, and B. Armstrong (2015). "Mortality risk

attributable to high and low ambient temperature: a multicountry observational study". *Lancet* 386.9991, pp. 369–375. DOI: 10.1016/S0140-6736(14)62114-0.

Gates, W. L. (1992). "AMIP: The Atmospheric Model Intercomparison Project". *Bull. Amer. Meteor. Soc.* 73, pp. 1962–1970. DOI: 10.1175/1520-0477(1992)073<1962:ATAMIP>2.0.CO;2.

Gelaro, R., W. McCarty, M. J. Suárez, R. Todling, A. Molod, L. Takacs, C. Randles, A. Darmenov, M. G. Bosilovich, R. Reichle, K. Wargan, L. Coy, R. Cullather, C. Draper, S. Akella, V. Buchard, A. Conaty, A. da Silva, W. Gu, G.-K. Kim, R. Koster, R. Lucchesi, D. Merkova, J. E. Nielsen, G. Partyka, S. Pawson, W. Putman, M. Rienecker, S. D. Schubert, M. Sienkiewicz, and B. Zhao (2017). "The Modern-Era Retrospective Analysis for Research and Applications, Version 2 (MERRA-2)". *J. Climate* 30.14, pp. 5419–5454. DOI: 10.1175/JCLI-D-16-0758.1.

Gilbert, N. (2010). "Russia counts environmental cost of wildfires". *Nature News.* DOI: 10.1038/news.2010.404.

Gleisner, H., P. Thejll, B. Christiansen, and J. K. Nielsen (2015). "Recent global warming hiatus dominated by low-latitude temperature trends in surface and troposphere data". *Geophys. Res. Lett.* 42, pp. 510–517. DOI: 10.1002/2014GL062596.

Gorbunov, M. E., H.-H. Benzon, A. S. Jensen, M. S. Lohmann, and A. S. Nielsen (2004). "Comparative analysis of radio occultation processing approaches based on Fourier integral operators". *Radio Sci.* 39, RS6004. DOI: 10.1029/2003RS002916.

Gramling, C. (2015). "Arctic impact". *Science* 347.6224, pp. 818–821. DOI: 10.1126/science.347.6224.818.

Grose, M. R., M. J. Pook, P. C. McIntosh, J. S. Risbey, and N. L. Bindoff (2012). "The simulation of cutoff lows in a regional climate model: reliability and future trends". *Climate Dyn.* 39.1, pp. 445–459. DOI: 10.1007/s00382-012-1368-2.

Haarsma, R. J., M. J. Roberts, P. L. Vidale, C. A. Senior, A. Bellucci, Q. Bao, P. Chang, S. Corti, N. S. Fučkar, V. Guemas, J. von Hardenberg, W. Hazeleger, C. Kodama, T. Koenigk, L. R. Leung, J. Lu, J.-J. Luo, J. Mao, M. S. Mizielinski, R. Mizuta, P. Nobre, M. Satoh, E. Scoccimarro, T. Semmler, J. Small, and J.-S. von Storch (2016). "High Resolution Model Intercomparison Project (HighResMIP v1.0) for CMIP6". *Geosci. Model Dev.* 9.11, pp. 4185–4208. DOI: 10.5194/gmd-9-4185-2016.

Hajj, G. A., E. R. Kursinski, L. J. Romans, W. I. Bertiger, and S. S. Leroy (2002). "A technical description of atmospheric sounding by GPS occultation". *J. Atmos. Solar-Terr. Phys.* 64.4, pp. 451–469. DOI: 10.1016/S1364-6826(01)00114-6.

Hall, R., R. Erdélyi, E. Hanna, J. M. Jones, and A. A. Scaife (2015). "Drivers of North Atlantic Polar Front jet stream variability". *Int. J. Climatol.* 35.8, pp. 1697–1720. DOI: 10.1002/joc.4121.

Hansen, J., M. Sato, and R. Ruedy (2012). "Perception of climate change". *PNAS* 109.37, E2415–E2423. DOI: 10.1073/pnas.1205276109.

Hartmann, D. L., A. M. G. K. Tank, M. Rusticucci, L. V. Alexander, S. Brönnimann, Y. Charabi, F. J. Dentener, E. J. Dlugokencky, D. R. Easterling, A. Kaplan, B. J. Soden, P. W. Thorne, M. Wild, and P. M. Zhai (2013). "Observations: Atmosphere and Surface". In: *Climate Change 2013: The Physical Science Basis. Contribution of Working Group I to the Fifth Assessment Report of the Intergovernmental Panel on Climate Change.* Ed. by T. F. Stocker, D. Qin, G.-K. Plattner, M. Tignor, S. K. Allen, J. Boschung, A. Nauels, Y. Xia, V. Bex, and P. M. Midgley. Cambridge, United Kingdom and New York, NY, USA: Cambridge University Press, pp. 195–254.

Haylock, M. R., N. Hofstra, A. M. G. Klein Tank, E. J. Klok, P. D. Jones, and M. New (2008). "A European daily high-resolution gridded data set of surface temperature and precipitation for 1950–2006". *J. Geophys. Res.* 113.D20, D20119. DOI: 10.1029/2008JD010201.

Healy, S. B. and J. N. Thépaut (2006). "Assimilation experiments with CHAMP GPS radio occultation measurements". *Quart. J. Roy. Meteor. Soc.* 132.615, pp. 605–623. DOI: 10.1256/qj.04.182.

Hegerl, G. and F. Zwiers (2011). "Use of models in detection and attribution of climate change". *WIRes. Clim. Change* 2.4, pp. 570–591. DOI: 10.1002/wcc.121.

Ho, S.-P., D. Hunt, A. K. Steiner, A. J. Mannucci, G. Kirchengast, H. Gleisner, S. Heise, A. von Engeln, C. Marquardt, S. Sokolovskiy, W. Schreiner, B. Scherllin-Pirscher, C. Ao, J. Wickert, S. Syndergaard, K. Lauritsen, S. Leroy, E. R. Kursinski, Y.-H. Kuo, U. Foelsche, T. Schmidt, and M. Gorbunov (2012). "Reproducibility of GPS radio occultation data for climate monitoring: Profile-to-profile inter-comparison of CHAMP climate records 2002 to 2008 from six data centers". *J. Geophys. Res.* 117, D18111. DOI: 10.1029/2012JD017665.

Hong, C.-C., H.-H. Hsu, N.-H. Lin, and H. Chiu (2011). "Roles of European blocking and tropical-extratropical interaction in the 2010 Pakistan flooding". *Geophys. Res. Lett.* 38.13. DOI: 10.1029/2011GL047583.

Hoskins, B. J., M. E. McIntyre, and A. W. Robertson (1985). "On the use and significance of isentropic potential vorticity maps". *Quart. J. Roy. Meteor. Soc.* 111.470, pp. 877–946. DOI: 10.1002/qj.49711147002.

Houze Jr., R. A., K. L. Rasmussen, S. Medina, S. R. Brodzik, and U. Romatschke (2011). "Anomalous Atmospheric Events Leading to the Summer 2010 Floods in Pakistan". *Bull. Amer. Meteor. Soc.* 92.3, pp. 291–298. DOI: 10.1175/2010BAMS3173.1.

Hoyer, S. and J. J. Hamman (2017). "xarray: N-D labeled Arrays and Datasets in Python". *J. Open Res. Software* 5. ISSN: 2049-9647. DOI: 10.5334/jors.148.

Hufkens, K., M. A. Friedl, T. F. Keenan, O. Sonnentag, A. Bailey, J. O'Keefe, and A. D. Richardson (2012). "Ecological impacts of a widespread frost event following early spring leaf-out". *Glob. Change Biol.* 18.7, pp. 2365–2377. ISSN: 1365-2486. DOI: 10.1111/j.1365-2486.2012.02712.x.

Hulme, M. (2014). "Attributing weather extremes to 'climate change': A review". *Prog. Phys. Geog.* 38.4, pp. 499–511. DOI: 10.1177/0309133314538644.

IPCC (2012). "Summary for Policymakers". In: *Managing the Risks of Extreme Events and Disasters to Advance Climate Change Adaptation – A Special Report of Working Groups I and II of the Intergovernmental Panel on Climate Change.* Ed. by C. Field, V. Barros, T. Stocker, D. Q. abd D.J. Dokken, K. Ebi, M. Mastrandrea, K. Mach, G.-K. Plattner, S. Allen, M. Tignor, and P. Midgley. Cambridge, UK, and New York, NY, USA: Cambridge University Press, pp. 1–19.

– (2013). *Climate Change 2013: The Physical Science Basis. Contribution of Working Group I to the Fifth Assessment Report of the Intergovernmental Panel on Climate Change.* Ed. by T. F. Stocker, D. Qin, G.-K. Plattner, M. Tignor, S. K. Allen, J. Boschung, A. Nauels, Y. Xia, V. Bex, and P. M. Midgley. Cambridge, United Kingdom and New York, NY, USA: Cambridge University Press. 1535 pp.

Kalnay, E., M. Kanamitsu, R. Kistler, W. Collins, D. Deaven, L. Gandin, M. Iredell, S. Saha, G. White, J. Woollen, Y. Zhu, A. Leetmaa, R. Reynolds, M. Chelliah, W. Ebisuzaki, W. Higgins, J. Janowiak, K. C. Mo, C. Ropelewski, J. Wang, R. Jenne, and D. Joseph (1996). "The NCEP/NCAR 40-Year Reanalysis Project". *Bull. Amer. Meteor. Soc.* 77.3, pp. 437–471. DOI: 10.1175/1520-0477(1996)077<0437: TNYRP>2.0.CO;2.

Kanamitsu, M., W. Ebisuzaki, J. Woollen, S.-K. Yang, J. J. Hnilo, M. Fiorino, and G. L. Potte (2002). "NCEP–DOE AMIP-II Reanalysis (R-2)". *Bull. Amer. Meteor. Soc.* 83.11, pp. 1631–1643. DOI: 10.1175/BAMS-83-11-1631.

Karpechko, A. Y. and E. Manzini (2012). "Stratospheric influence on tropospheric climate change in the Northern Hemisphere". *J. Geophys. Res.: Atmos* 117.D5. DOI: 10.1029/2011JD017036.

Kennedy, D., T. Parker, T. Woollings, B. Harvey, and L. Shaffrey (2016). "The response of high-impact blocking weather systems to climate change". *Geophys. Res. Lett.* 43.13, pp. 7250–7258. DOI: 10.1002/2016GL069725.

Klok, E. J. and A. M. G. Klein Tank (2009). "Updated and extended European dataset of daily climate observations". *Int. J. Climatol.* 29.8, pp. 1182–1191. DOI: 10.1002/joc.1779.

Knutti, R., J. Rogelj, J. Sedláček, and E. M. Fischer (2016). "A scientific critique of the two-degree climate change target". *Nature Geoscience* 9, pp. 13–18. DOI: 10.1038/ngeo2595.

Kobayashi, S., Y. Ota, Y. Harada, A. Ebita, M. Moriya, H. Onoda, K. Onogi, H. Kamahori, C. Kobayashi, H. Endo, K. Miyaoka, and K. Takahashi (2015). "The JRA-55 Reanalysis: General Specifications and Basic Characteristics". *J. Meteor. Soc. Japan* 93.1, pp. 5–48. DOI: 10.2151/jmsj.2015-001.

Kursinski, E. R., G. A. Hajj, W. I. Bertiger, S. S. Leroy, T. K. Meehan, L. J. Romans, J. T. Schofield, D. J. McCleese, W. G. Melbourne, C. L. Thornton, T. P. Yunck, J. R. Eyre, and R. N. Nagatani (1996). "Initial Results of Radio Occultation Observations of Earth's Atmosphere Using the Global Positioning System". *Science* 271.5252, pp. 1107–1110. DOI: 10.1126/science.271.5252.1107.

Kursinski, E. R., G. A. Hajj, J. T. Schofield, R. P. Linfield, and K. R. Hardy (1997). "Observing Earth's atmosphere with radio occultation measurements using the Global Positioning System". *J. Geophys. Res.* 102.D19, pp. 23429–23465. DOI: 10.1029/97JD01569.

Kyselý, J. (2007). "Implications of enhanced persistence of atmospheric circulation for the occurrence and severity of temperature extremes". *Int. J. Climatol.* 27.5, pp. 689–695. DOI: 10.1002/joc.1478.

– (2008). "Influence of the persistence of circulation patterns on warm and cold temperature anomalies in Europe: Analysis over the 20th century". *Global Planet Change* 62.1, pp. 147–163. DOI: 10.1016/j.gloplacha.2008.01.003.

Lau, N.-C. and M. J. Nath (2014). "Model Simulation and Projection of European Heat Waves in Present-Day and Future Climates". *J. Climate* 27.10, pp. 3713–3730. DOI: 10.1175/JCLI-D-13-00284.1.

Lau, W. K. M. and K.-M. Kim (2012). "The 2010 Pakistan Flood and Russian Heat Wave: Teleconnection of Hydrometeorological Extremes". *J. Hydrometeorol.* 13.1, pp. 392–403. DOI: 10.1175/JHM-D-11-016.1.

Lejenäs, H. (1984). "Characteristics of southern hemisphere blocking as determined from a time series of observational data". *Quart. J. Roy. Meteor. Soc.* 110.466, pp. 967–979. DOI: 10.1002/qj.49711046610.

Lejenäs, H. and H. Økland (1983). "Characteristics of northern hemisphere blocking as determined from a long time series of observational data". *Tellus A* 35A.5, pp. 350–362. DOI: 10.1111/j.1600-0870.1983.tb00210.x.

Leroy, S. S., J. A. Dykema, and J. G. Anderson (2006). "Climate benchmarking using GNSS occultation". In: *Atmosphere and Climate: Studies by Occultation Methods.* Ed. by U. Foelsche, G. Kirchengast, and A. K. Steiner. Berlin Heidelberg: Springer, pp. 287–301. DOI: 10.1007/3-540-34121-8_24.

Lhotka, O. and J. Kyselý (2015). "Hot Central-European summer of 2013 in a long-term context". *Int. J. Climatol.* DOI: 10.1002/joc.4277.

Long, C. S., M. Fujiwara, S. Davis, D. M. Mitchell, and C. J. Wright (2017). "Climatology and interannual variability of dynamic variables in multiple reanalyses evaluated by the SPARC Reanalysis Intercomparison Project (S-RIP)". *Atmos. Chem. Phys.* 17.23, pp. 14593–14629. DOI: 10.5194/acp-17-14593-2017.

Lupo, A. R., I. I. Mokhov, M. G. Akperov, A. V. Chernokulsky, and H. Athar (2012). "A Dynamic Analysis of the Role of the Planetary- and Synoptic-Scale in the Summer of 2010 Blocking Episodes over the European Part of Russia". *Advances in Meteorology* 2012. DOI: 10.1155/2012/584257.

Ma, S., A. J. Pitman, R. Lorenz, J. Kala, and J. Srbinovsky (2016). "Earlier green-up and spring warming amplification over Europe". *Geophys. Res. Lett.* 43.5, pp. 2011–2018. DOI: 10.1002/2016GL068062.

Marques, R. d. F. C. and V. B. Rao (1999). "A Diagnosis of a Long-Lasting Blocking Event over the Southeast Pacific Ocean". *Mon. Wea. Rev.* 127.8, pp. 1761–1776. DOI: 10.1175/1520-0493(1999)127<1761:ADOALL>2.0.CO;2.

– (2000). "Interannual variations of blockings in the southern hemisphere and their energetics". *J. Geophys. Res.* 105.D4, pp. 4625–4636. DOI: 10.1029/1999JD901066.

Marshall, A. G., D. Hudson, H. H. Hendon, M. J. Pook, O. Alves, and M. C. Wheeler (2014). "Simulation and prediction of blocking in the Australian region and its influence on intra-seasonal rainfall in POAMA-2". *Climate Dyn.* 42.11, pp. 3271–3288. DOI: 10.1007/s00382-013-1974-7.

Martineau, P., G. Chen, and D. A. Burrows (2017). "Wave events: climatology, trends, and relationship to Northern Hemisphere winter blocking and weather extremes". *J. Climate* 30.15, pp. 5675–5697. DOI: 10.1175/JCLI-D-16-0692.1.

Martius, O., L. M. Polvani, and H. C. Davies (2009). "Blocking precursors to stratospheric sudden warming events". *Geophys. Res. Lett.* 36.14, L14806. DOI: 10.1029/2009GL038776.

Martius, O., H. Sodemann, H. Joos, S. Pfahl, A. Winschall, M. Croci-Maspoli, M. Graf, E. Madonna, B. Mueller, S. Schemm, J. Sedláček, M. Sprenger, and H. Wernli (2013). "The role of upper-level dynamics and surface processes for the Pakistan flood of July 2010". *Quart. J. Roy. Meteor. Soc.* 139.676, pp. 1780–1797. DOI: 10.1002/qj.2082.

Masato, G., B. J. Hoskins, and T. Woollings (2013). "Winter and Summer Northern Hemisphere Blocking in CMIP5 Models". *J. Climate* 26.18, pp. 7044–7059. DOI: 10.1175/JCLI-D-12-00466.1.

Masato, G., T. Woollings, and B. J. Hoskins (2014). "Structure and impact of atmospheric blocking over the Euro-Atlantic region in present-day and future simulations". *Geophys. Res. Lett.* 41.3, pp. 1051–1058. DOI: 10.1002/2013GL058570.

Matsueda, M. (2011). "Predictability of Euro-Russian blocking in summer of 2010". *Geophys. Res. Lett.* 38.6, L06801. DOI: 10.1029/2010GL046557.

Matsueda, M. and H. Endo (2017). "The robustness of future changes in Northern Hemisphere blocking: a large ensemble projection with multiple sea surface temperature patterns". *Geophys. Res. Lett.* 44, pp. 5158–5166. DOI: 10.1002/2017GL073336.

Matsueda, M., H. Endo, and R. Mizuta (2010). "Future change in Southern Hemisphere summertime and wintertime atmospheric blockings simulated using a 20-km-mesh AGCM". *Geophys. Res. Lett.* 37.2. DOI: 10.1029/2009GL041758.

Mattingly, K. S., J. T. McLeod, J. A. Knox, J. M. Shepherd, and T. L. Mote (2015). "A climatological assessment of Greenland blocking conditions associated with the track of Hurricane Sandy and historical North Atlantic hurricanes". *Int. J. Climatol.* 35.5, pp. 746–760. DOI: 10.1002/joc.4018.

McCarty, W., L. Coy, R. Gelaro, A. Huang, D. Merkova, E. B. Smith, M. Sienkiewicz, and K. Wargan (2016). *MERRA-2 Input Observations: Summary and Assessment.* Ed. by R. D. Koster. URL: https://gmao.gsfc.nasa.gov/pubs/docs/McCarty885.pdf.

Medhaug, I., M. B. Stolpe, E. M. Fischer, and R. Knutti (2017). "Reconciling controversies about the 'global warming hiatus'". *Nature* 545, pp. 41–47. DOI: 10.1038/nature22315.

Meehl, G. A., C. Covey, K. E. Taylor, T. Delworth, R. J. Stouffer, M. Latif, B. McAvaney, and J. F. B. Mitchell (2007). "The WCRP CMIP3 Multimodel Dataset: A New Era in Climate Change Research". *Bull. Amer. Meteor. Soc.* 88.9, pp. 1383–1394. DOI: 10.1175/BAMS-88-9-1383.

Meehl, G. A. and C. Tebaldi (2004). "More Intense, More Frequent, and Longer Lasting Heat Waves in the 21st Century". *Science* 305.5686, pp. 994–997. DOI: 10.1126/science.1098704.

Melbourne, W. G., E. S. Davis, C. B. Duncan, G. A. Hajj, K. R. Hardy, E. R. Kursinski, T. K. Meehan, L. E. Young, and T. P. Yunck (1994). *The application of spaceborne GPS to atmospheric limb sounding and global change monitoring.* Tech. rep. Pasadena, California, USA: Jet Propulsion Laboratory, NASA. 147 pp.

Mendes, M. C. D. and I. F. A. Cavalcanti (2014). "The relationship between the Antarctic oscillation and blocking events over the South Pacific and Atlantic Oceans". *Int. J. Climatol.* 34.3, pp. 529–544. DOI: 10.1002/joc.3729.

Mendes, M. C. D., R. M. Trigo, I. F. A. Cavalcanti, and C. C. DaCamara (2008). "Blocking Episodes in the Southern Hemisphere: Impact on the Climate of Adjacent Continental Areas". *Pure Appl. Geophys.* 165.9-10, pp. 1941–1962. DOI: 10.1007/s00024-008-0409-4.

Menzel, A., R. Helm, and C. Zang (2015). "Patterns of late spring frost leaf damage and recovery in a European beech (Fagus sylvatica L.) stand in south-eastern Germany based on repeated digital photographs". *Front. Plant Sci.* 6.110. DOI: 10.3389/fpls.2015.00110.

Menzel, A., T. H. Sparks, N. Estrella, E. Koch, A. Aasa, R. Ahas, K. Alm-Kübler, P. Bissolli, O. Braslavská, A. Briede, F. M. Chmielewski, Z. Crepinsek, Y. Curnel, Å. Dahl, C. Defila, A. Donnelly, Y. Filella, K. Jatczak, F. Måge, A. Mestre, Ø. Nordli, J. Peñuelas, P. Pirinen, V. Remišová, H. Scheifinger, M. Striz, A. Susnik, A. J. H. Van Vliet, F.-E. Wielgolaski, S. Zach, and A. Zust (2006). "European

phenological response to climate change matches the warming pattern". *Glob. Change Biol.* 12.10, pp. 1969–1976. DOI: 10.1111/j.1365-2486.2006.01193.x.

Millar, R. J., J. S. Fuglestvedt, P. Friedlingstein, J. Rogelj, M. J. Grubb, H. D. Matthews, R. B. Skeie, P. M. Forster, D. J. Frame, and M. R. Allen (2017). "Emission budgets and pathways consistent with limiting warming to 1.5°C". *Nature Geoscience* 10, pp. 741–747. DOI: 10.1038/ngeo3031.

Miralles, D. G., A. J. Teuling, C. C. van Heerwaarden, and J. V.-G. de Arellano (2014). "Mega-Heatwave Temperatures due to Combined Soil Desiccation and Atmospheric Heat Accumulation". *Nature Geoscience* 7.5, pp. 345–349. DOI: 10.1038/ngeo2141.

Mitchell, D., P. Davini, B. Harvey, N. Massey, K. Haustein, T. Woollings, R. Jones, F. Otto, B. Guillod, S. Sparrow, D. Wallom, and M. Allen (2017). "Assessing mid-latitude dynamics in extreme event attribution systems". *Climate Dyn.* 48.11, pp. 3889–3901. DOI: 10.1007/s00382-016-3308-z.

Morak, S., G. C. Hegerl, and N. Christidis (2013). "Detectable Changes in the Frequency of Temperature Extremes". *J. Climate* 26.5, pp. 1561–1574. DOI: 10.1175/JCLI-D-11-00678.1.

Nakamura, N. and C. S. Y. Huang (2017). "Local wave activity and the onset of blocking along a potential vorticity front". *J. Atmos. Sci.* 74.7, pp. 2341–2362. DOI: 10.1175/JAS-D-17-0029.1.

National Academies of Sciences, Engineering, and Medicine (2016). *Attribution of Extreme Weather Events in the Context of Climate Change*. Washington DC: The National Academies Press. DOI: 10.17226/21852.

Oliveira, F. N. M., L. M. V. Carvalho, and T. Ambrizzi (2014). "A new climatology for Southern Hemisphere blockings in the winter and the combined effect of ENSO and SAM phases". *Int. J. Climatol.* 34.5, pp. 1676–1692. DOI: 10.1002/joc.3795.

O'Neill, A., W. L. Grose, V. D. Pope, H. Maclean, and R. Swinbank (1994). "Evolution of the Stratosphere during Northern Winter 1991/92 as Diagnosed from U.K. Meteorological Office Analyses". *J. Atmos. Sci.* 51.20, pp. 2800–2817. DOI: 10.1175/1520-0469(1994)051<2800:EOTSDN>2.0.CO;2.

Onogi, K., J. Tsutsui, H. Koide, M. Sakamoto, S. Kobayashi, H. Hatsushika, T. Matsumoto, N. Yamazaki, H. Kamahori, K. Takahashi, S. Kadokura, K. Wada, K. Kato, R. Oyama, T. Ose, N. Mannoji, and R. Taira (2007). "The JRA-25 Reanalysis". *J. Meteor. Soc. Japan* 85.3, pp. 369–432. DOI: 10.2151/jmsj.85.369.

Pall, P., T. Aina, D. A. Stone, P. A. Stott, T. Nozawa, A. G. J. Hilberts, D. Lohmann, and M. R. Allen (2011). "Anthropogenic greenhouse gas contribution to flood risk in England and Wales in autumn 2000". *Nature* 470.7334, pp. 382–385. DOI: 10.1038/nature09762.

Parker, T. J., G. J. Berry, and M. J. Reeder (2014). "The Structure and Evolution of Heat Waves in Southeastern Australia". *J. Climate* 27.15, pp. 5768–5785. DOI: 10.1175/JCLI-D-13-00740.1.

Parker, W. S. (2016). "Reanalyses and Observations: What's the Difference?" *Bull. Amer. Meteor. Soc.* 97.9, pp. 1565–1572. DOI: 10.1175/BAMS-D-14-00226.1.

Parsons, S., J. A. Renwick, and A. J. McDonald (2016). "An Assessment of Future Southern Hemisphere Blocking Using CMIP5 Projections from Four GCMs". *J. Climate* 29.21, pp. 7599–7611. DOI: 10.1175/JCLI-D-15-0754.1.

Peevey, T. R., J. C. Gille, C. R. Homeyer, and G. L. Manney (2014). "The double tropopause and its dynamical relationship to the tropopause inversion layer in storm track regions". *J. Geophys. Res.* 119.17, pp. 10194–10212. DOI: 10.1002/2014JD021808.

Pelly, J. L. and B. J. Hoskins (2003). "A new perspective on blocking". *J. Atmos. Sci.* 60, pp. 743–755. DOI: 10.1175/1520-0469(2003)060<0743:ANPOB>2.0.CO;2.

Perkins, S. E. (2015). "A review on the scientific understanding of heatwaves–Their measurement, driving mechanisms, and changes at the global scale". *Atmos. Res.* 164, pp. 242–267. DOI: 10.1016/j.atmosres.2015.05.014.

Pfahl, S. (2014). "Characterising the relationship between weather extremes in Europe and synoptic circulation features". *Nat. Hazard. Earth Sys.* 14.6, pp. 1461–1475. DOI: 10.5194/nhess-14-1461-2014.

Pfahl, S., C. Schwierz, M. Croci-Maspoli, C. M. Grams, and H. Wernli (2015). "Importance of latent heat release in ascending air streams for atmospheric blocking". *Nature Geoscience* 8, pp. 610–614. DOI: 10.1038/ngeo2487.

Pfahl, S. and H. Wernli (2012). "Quantifying the relevance of atmospheric blocking for co-located temperature extremes in the Northern Hemisphere on (sub-)daily time scales". *Geophys. Res. Lett.* 39.12. DOI: 10.1029/2012GL052261.

Pirscher, B., U. Foelsche, M. Borsche, G. Kirchengast, and Y.-H. Kuo (2010). "Analysis of migrating diurnal tides detected in FORMOSAT-3/COSMIC temperature data". *J. Geophys. Res.* 115, D14108. DOI: 10.1029/2009JD013008.

Poli, P., S. B. Healy, and D. P. Dee (2010). "Assimilation of Global Positioning System radio occultation data in the ECMWF ERA-Interim reanalysis". *Quart. J. Roy. Meteor. Soc.* 136.653, pp. 1972–1990. DOI: 10.1002/qj.722.

Pook, M. J., J. S. Risbey, P. C. McIntosh, C. C. Ummenhofer, A. G. Marshall, and G. A. Meyers (2013). "The Seasonal Cycle of Blocking and Associated Physical Mechanisms in the Australian Region and Relationship with Rainfall". *Mon. Wea. Rev.* 141.12, pp. 4534–4553. DOI: 10.1175/MWR-D-13-00040.1.

Quiroz, R. S. (1986). "The association of stratospheric warmings with tropospheric blocking". *J. Geophys. Res.* 91.D4, pp. 5277–5285. DOI: 10.1029/JD091iD04p05277.

Randel, W. J. and F. Wu (2005). "Kelvin wave variability near the equatorial tropopause observed in GPS radio occultation measurements". *J. Geophys. Res.* 110, D03102. DOI: 10.1029/2004JD005006.

– (2015). "Variability of Zonal Mean Tropical Temperatures Derived from a Decade of GPS Radio Occultation Data". *J. Atmos. Sci.* 72, pp. 1261–1275. DOI: 10.1175/JAS-D-14-0216.1.

Randel, W. J., F. Wu, and W. R. Ríos (2003). "Thermal variability of the tropical tropopause region derived from GPS/MET observations". *J. Geophys. Res.: Atmos* 108.D1, ACL 7-1–ACL 7-12. DOI: 10.1029/2002JD002595.

Renwick, J. A. and M. J. Revell (1999). "Blocking over the South Pacific and Rossby Wave Propagation". *Mon. Wea. Rev.* 127.10, pp. 2233–2247. DOI: 10.1175/1520-0493(1999)127<2233:BOTSPA>2.0.CO;2.

Rex, D. F. (1950a). "Blocking Action in the Middle Troposphere and its Effect upon Regional Climate I: An aerological study of blocking action". *Tellus* 2.3, pp. 196–211. DOI: 10.1111/j.2153-3490.1950.tb00331.x.

– (1950b). "Blocking Action in the Middle Troposphere and its Effect upon Regional Climate II: The climatology of blocking action". *Tellus* 2.4, pp. 275–301. DOI: 10.1111/j.2153-3490.1950.tb00339.x.

– (1951). "The Effect of Atlantic Blocking Action upon European Climate". *Tellus* 3.2, pp. 100–112. DOI: 10.1111/j.2153-3490.1951.tb00784.x.

Rieckh, T., B. Scherllin-Pirscher, F. Ladstädter, and U. Foelsche (2014). "Characteristics of tropopause parameters as observed with GPS radio occultation". *Atmos. Meas. Tech.* 7, pp. 3947–3958. DOI: 10.5194/amt-7-3947-2014.

Rienecker, M. M., M. J. Suarez, R. Gelaro, R. Todling, J. Bacmeister, E. Liu, M. G. Bosilovich, S. D. Schubert, L. Takacs, G.-K. Kim, S. Bloom, J. Chen, D. Collins, A. Conaty, A. da Silva, W. Gu, J. Joiner, R. D. Koster, R. Lucchesi, A. Molod, T. Owens, S. Pawson, P. Pegion, C. R. Redder, R. Reichle, F. R. Robertson, A. G. Ruddick, M. Sienkiewicz, and J. Woollen (2011). "MERRA: NASA's Modern-Era Retrospective Analysis for Research and Applications". *J. Climate* 24, pp. 3624–3648. DOI: 10.1175/JCLI-D-11-00015.1.

Rimbu, N., G. Lohmann, and M. Ionita (2014). "Interannual to multidecadal Euro-Atlantic blocking variability during winter and its relationship with extreme low temperatures in Europe". *J. Geophys. Res.* 119.24, pp. 13621–13636. DOI: 10.1002/2014JD021983.

Rodrigues, R. R. and T. Woollings (2017). "Impact of Atmospheric Blocking on South America in Austral Summer". *J. Climate* 30.5, pp. 1821–1837. DOI: 10.1175/JCLI-D-16-0493.1.

Scaife, A. A., T. Woollings, J. Knight, G. Martin, and T. Hinton (2010). "Atmospheric Blocking and Mean Biases in Climate Models". *J. Climate* 23.23, pp. 6143–6152. DOI: 10.1175/2010JCLI3728.1.

Schär, C., P. L. Vidale, D. Luthi, C. Frei, C. Haberli, M. A. Liniger, and C. Appenzeller (2004). "The role of increasing temperature variability in European summer heatwaves". *Nature* 427, pp. 332–336. DOI: 10.1038/nature02300.

Scherllin-Pirscher, B., C. Deser, S.-P. Ho, C. Chou, W. Randel, and Y.-H. Kuo (2012). "The vertical and spatial structure of ENSO in the upper troposphere and lower stratosphere from GPS radio occultation measurements". *Geophys. Res. Lett.* 39, L20801. DOI: 10.1029/2012GL053071.

Scherllin-Pirscher, B., G. Kirchengast, A. K. Steiner, Y.-H. Kuo, and U. Foelsche (2011a). "Quantifying uncertainty in climatological fields from GPS radio occultation: an empirical-analytical error model". *Atmos. Meas. Tech.* 4, pp. 2019–2034. DOI: 10.5194/amt-4-2019-2011.

Scherllin-Pirscher, B., A. K. Steiner, and G. Kirchengast (2014). "Deriving dynamics from GPS radio occultation: Three-dimensional wind fields for monitoring the climate". *Geophys. Res. Lett.* 41.20, pp. 7367–7374. DOI: 10.1002/2014GL061524.

Scherllin-Pirscher, B., A. K. Steiner, G. Kirchengast, Y.-H. Kuo, and U. Foelsche (2011b). "Empirical analysis and modeling of errors of atmospheric profiles from GPS radio occultation". *Atmos. Meas. Tech.* 4, pp. 1875–1890. DOI: 10.5194/amt-4-1875-2011.

*Bibliography*

Scherllin-Pirscher, B., A. K. Steiner, G. Kirchengast, M. Schwaerz, and S. S. Leroy (2017). "The power of vertical geolocation of atmospheric profiles from GNSS radio occultation". *J. Geophys. Res.: Atmos* 122, pp. 1595–1616. DOI: 10.1002/2016JD025902.

Scherrer, S. C., M. Croci-Maspoli, C. Schwierz, and C. Appenzeller (2006). "Two-dimensional indices of atmospheric blocking and their statistical relationship with winter climate patterns in the Euro-Atlantic region". *Int. J. Climatol.* 26.2, pp. 233–249. DOI: 10.1002/joc.1250.

Schiemann, R., M.-E. Demory, L. C. Shaffrey, S. Jane, P. L. Vidale, M. S. Mizielinski, M. J. Roberts, M. Matsueda, M. F. Wehner, and J. Thomas (2017). "The Resolution Sensitivity of Northern Hemisphere Blocking in Four 25-km Atmospheric Global Circulation Models." *J. Climate* 30.1, pp. 337–358. DOI: 10.1175/JCLI-D-16-0100.1.

Schleussner, C.-F., P. Pfleiderer, and E. M. Fischer (2017). "In the Observational Record Half a Degree Matters". *Nature Climate Change* 7.7, pp. 460–462. DOI: 10.1038/nclimate3320.

Schleussner, C.-F., J. Rogelj, M. Schaeffer, T. Lissner, R. Licker, E. M. Fischer, R. Knutti, A. Levermann, K. Frieler, and W. Hare (2016). "Science and policy characteristics of the Paris Agreement temperature goal". *Nature Climate Change* 6, pp. 827–835. DOI: 10.1038/nclimate3096.

Schmidt, T., S. Heise, J. Wickert, G. Beyerle, and C. Reigber (2005). "GPS radio occultation with CHAMP and SAC-C: global monitoring of thermal tropopause parameters". *Atmos. Chem. Phys.* 5.6, pp. 1473–1488. DOI: 10.5194/acp-5-1473-2005.

Schmidt, T., J. Wickert, G. Beyerle, and S. Heise (2008). "Global tropopause height trends estimated from GPS radio occultation data". *Geophys. Res. Lett.* 35, L11806. DOI: 10.1029/2008GL034012.

Schneidereit, A., S. Schubert, P. Vargin, F. Lunkeit, X. Zhu, D. H. W. Peters, and K. Fraedrich (2012). "Large-Scale Flow and the Long-Lasting Blocking High over Russia: Summer 2010". *Mon. Wea. Rev.* 140.9, pp. 2967–2981. DOI: 10.1175/MWR-D-11-00249.1.

Schreiner, W., C. Rocken, S. Sokolovskiy, S. Syndergaard, and D. Hunt (2007). "Estimates of the precision of GPS radio occultations from the COSMIC/FORMOSAT-3 mission". *Geophys. Res. Lett.* 34, L04808. DOI: 10.1029/2006GL027557.

Schwarz, J. C., G. Kirchengast, and M. Schwaerz (2017). "Integrating uncertainty propagation in GNSS radio occultation retrieval: from bending angle to dry-air atmospheric profiles". *Earth Space Sci.* 4.4, pp. 200–228. DOI: 10.1002/2016EA000234.

Schwärz, M., G. Kirchengast, B. Scherllin-Pirscher, J. Schwarz, F. Ladstädter, and B. Angerer (2016). *Multi-Mission Validation by Satellite Radio Occultation – Extension Project.* Final report for ESA/ESRIN No. 01/2016. University of Graz, Austria: WEGC. 164 pp.

Schwärz, M., B. Scherllin-Pirscher, G. Kirchengast, J. Schwarz, F. Ladstädter, J. Fritzer, and J. Ramsauer (2013). *Multi-Mission Validation by Satellite Radio Occultation.* Final report for ESA/ESRIN No. 01/2013. University of Graz, Austria: WEGC. 187 pp.

Schwierz, C., M. Croci-Maspoli, and H. C. Davies (2004). "Perspicacious indicators of atmospheric blocking". *Geophys. Res. Lett.* 31.6, L06125. DOI: 10.1029/2003GL019341.

Screen, J. A. and I. Simmonds (2013). "Exploring links between Arctic amplification and mid-latitude weather". *Geophys. Res. Lett.* 40.5, pp. 959–964. DOI: 10.1002/grl.50174.

Seneviratne, S. I., D. Lüthi, M. Litschi, and C. Schär (2006). "Land–atmosphere coupling and climate change in Europe". *Nature* 443, pp. 205–209. DOI: 10.1038/nature05095.

Shepherd, T. G. (2014). "Atmospheric circulation as a source of uncertaintyin climate change projections". *Nature Geoscience* 7.10, pp. 703–708. DOI: 10.1038/ngeo2253.

Sillmann, J. and M. Croci-Maspoli (2009). "Present and future atmospheric blocking and its impact on European mean and extreme climate". *Geophys. Res. Lett.* 36.10. DOI: 10.1029/2009GL038259.

Sillmann, J., M. Croci-Maspoli, M. Kallache, and R. W. Katz (2011). "Extreme Cold Winter Temperatures in Europe under the Influence of North Atlantic Atmospheric Blocking". *J. Climate* 24 (22), pp. 5899–5913. DOI: 10.1175/2011JCLI4075.1.

Sillmann, J., T. Thorarinsdottir, N. Keenlyside, N. Schaller, L. V. Alexander, G. Hegerl, S. I. Seneviratne, R. Vautard, X. Zhang, and F. W. Zwiers (2017). "Understanding, modeling and predicting weather and climate extremes: Challenges and opportunities". *Weather and Climate Extremes*. DOI: 10.1016/j.wace.2017.10.003.

Simmons, A. J., P. Berrisford, D. P. Dee, H. Hersbach, S. Hirahara, and J.-N. Thépaut (2017). "A reassessment of temperature variations and trends from global reanalyses and monthly surface climatological datasets". *Quart. J. Roy. Meteor. Soc.* 143.702, pp. 101–119. DOI: 10.1002/qj.2949.

Simmons, A. J., P. Poli, D. P. Dee, P. Berrisford, H. Hersbach, S. Kobayashi, and C. Peubey (2014). "Estimating low-frequency variability and trends in atmospheric temperature using ERA-Interim". *Quart. J. Roy. Meteor. Soc.* 140.679, pp. 329–353. DOI: 10.1002/qj.2317.

Sinclair, M. R. (1996). "A Climatology of Anticyclones and Blocking for the Southern Hemisphere". *Mon. Wea. Rev.* 124.2, pp. 245–264. DOI: 10.1175/1520-0493(1996)124<0245:ACOAAB>2.0.CO;2.

Sitnov, S., I. Mokhov, and A. Lupo (2017). "Ozone, water vapor, and temperature anomalies associated with atmospheric blocking events over Eastern Europe in spring - summer 2010". *Atmos. Environ.* 164.Supplement C, pp. 180–194. DOI: 10.1016/j.atmosenv.2017.06.004.

Small, D., E. Atallah, and J. R. Gyakum (2014). "An Objectively Determined Blocking Index and its Northern Hemisphere Climatology". *J. Climate* 27.8, pp. 2948–2970. DOI: 10.1175/JCLI-D-13-00374.1.

Sousa, P. M., R. M. Trigo, D. Barriopedro, P. M. M. Soares, A. M. Ramos, and M. L. R. Liberato (2017). "Responses of European precipitation distributions and regimes to different blocking locations". *Climate Dyn.* 48.3, pp. 1141–1160. DOI: 10.1007/s00382-016-3132-5.

Stefanon, M., F. D'Andrea, and P. Drobinski (2012). "Heatwave classification over Europe and the Mediterranean region". *Environ. Res. Lett.* 7.1. DOI: 10.1088/1748-9326/7/1/014023.

Steiner, A. K., D. Hunt, S.-P. Ho, G. Kirchengast, A. J. Mannucci, B. Scherllin-Pirscher, H. Gleisner, A. von Engeln, T. Schmidt, C. Ao, S. S. Leroy, E. R. Kursinski, U. Foelsche, M. Gorbunov, S. Heise, Y.-H. Kuo, K. B. Lauritsen, C. Marquardt, C. Rocken, W. Schreiner, S. Sokolovskiy, S. Syndergaard, and J. Wickert (2013). "Quantification of structural uncertainty in climate data records from GPS radio occultation". *Atmos. Chem. Phys.* 13, pp. 1469–1484. DOI: 10.5194/acp-13-1469-2013.

Steiner, A. K., G. Kirchengast, and H. P. Ladreiter (1999). "Inversion, error analysis, and validation of GPS/MET occultation data". *Ann. Geophys.* 17.1, pp. 122–138. DOI: 10.1007/s00585-999-0122-5.

Steiner, A. K., B. C. Lackner, F. Ladstädter, B. Scherllin-Pirscher, U. Foelsche, and G. Kirchengast (2011). "GPS radio occultation for climate monitoring and change detection". *Radio Sci.* 46, RS0D24. DOI: 10.1029/2010RS004614.

Stone, D. A. and M. R. Allen (2005). "The End-to-End Attribution Problem: From Emissions to Impacts". *Clim. Change* 71.3, pp. 303–318. DOI: 10.1007/s10584-005-6778-2.

Stott, P. A., D. A. Stone, and M. R. Allen (2004). "Human contribution to the European heatwave of 2003". *Nature* 432, pp. 610–614. DOI: 10.1038/nature03089.

Sumner, E. J. (1954). "A study of blocking in the Atlantic-European of the northern hemisphere". *Quart. J. Roy. Meteor. Soc.* 80.345, pp. 402–416. DOI: 10.1002/qj.49708034510.

Sun, D.-Z., T. Zhang, Y. Sun, and Y. Yu (2014). "Rectification of El Niño–Southern Oscillation into Climate Anomalies of Decadal and Longer Time Scales: Results from Forced Ocean GCM Experiments". *J. Climate* 27, pp. 2545–2561. DOI: 10.1175/JCLI-D-13-00390.1.

Taguchi, M. (2008). "Is there a statistical connection between stratospheric sudden warming and tropospheric blocking events?" *J. Atmos. Sci.* 65, pp. 1442–1454. DOI: 10.1175/2007JAS2363.1.

Taylor, K. E., R. J. Stouffer, and G. A. Meehl (2012). "An Overview of CMIP5 and the Experiment Design". *Bull. Amer. Meteor. Soc.* 93.4, pp. 485–498. DOI: 10.1175/BAMS-D-11-00094.1.

Tibaldi, S. and F. Molteni (1990). "On the operational predictability of blocking". *Tellus A* 42.3, pp. 343–365. DOI: 10.1034/j.1600-0870.1990.t01-2-00003.x.

Tibaldi, S., E. Tosi, A. Navarra, and L. Pedulli (1994). "Northern and southern hemisphere seasonal variability of blocking frequency and predictability". *Mon. Wea. Rev.* 122, pp. 1971–2003. DOI: 10.1175/1520-0493(1994)122<1971:NASHSV>2.0.CO;2.

Tolkien, J. R. R. (2007). *The Lord of the Rings.* 77-85 Fulham Palace Road, Hammersmith, London: HarperCollinsPublishers.

Torre, A. de la and P. Alexander (2005). "Gravity waves above Andes detected from GPS radio occultation temperature profiles: Mountain forcing?" *Geophys. Res. Lett.* 32, L17815. DOI: 10.1029/2005GL022959.

Trenberth, K. F. and K. C. Mo (1985). "Blocking in the Southern Hemisphere". *Mon. Wea. Rev.* 113.1, pp. 3–21. DOI: 10.1175/1520-0493(1985)113<0003:BITSH>2.0.CO;2.

Trigo, R. M., I. F. Trigo, C. C. DaCamara, and T. J. Osborn (2004). "Climate impact of the European winter blocking episodes from the NCEP/NCAR Reanalyses". *Climate Dyn.* 23.1, pp. 17–28. DOI: 10.1007/s00382-004-0410-4.

Tsuda, T. (2014). "Characteristics of atmospheric gravity waves observed using the MU (Middle and Upper atmosphere) radar and GPS (Global Positioning System) radio occultation". *Proc. Jpn. Acad., Ser. B* 90, pp. 12–27.

Tyrlis, E. and B. J. Hoskins (2008a). "Aspects of a Northern Hemisphere Atmospheric Blocking Climatology". *J. Atmos. Sci.* 65.5, pp. 1638–1652. DOI: 10.1175/2007JAS2337.1.

– (2008b). "The Morphology of Northern Hemisphere Blocking". *J. Atmos. Sci.* 65.5, pp. 1653–1665. DOI: 10.1175/2007JAS2338.1.

United Nations (2015). *Paris Agreement*. URL: http://unfccc.int/files/essential_background/convention/application/pdf/english_paris_agreement.pdf (visited on 10/28/2017).

Unterberger, C., L. Brunner, S. Nabernegg, K. Steininger, A. K. Steiner, E. Stabentheiner, S. Monschein, and H. Truhetz (accepted). "Spring frost risk for regional fruit production under a warmer climate". *PLOS ONE*.

Uppala, S. M. et al. (2005). "The ERA-40 re-analysis". *Quart. J. Roy. Meteor. Soc.* 131.612, pp. 2961–3012. DOI: 10.1256/qj.04.176.

Vial, J. and T. J. Osborn (2012). "Assessment of atmosphere-ocean general circulation model simulations of winter northern hemisphere atmospheric blocking". *Climate Dyn.* 39.1, pp. 95–112. DOI: 10.1007/s00382-011-1177-z.

Vries, H. de, T. Woollings, J. Anstey, R. J. Haarsma, and W. Hazeleger (2013). "Atmospheric blocking and its relation to jet changes in a future climate". *Climate Dynamics* 41.9, pp. 2643–2654. DOI: 10.1007/s00382-013-1699-7.

Wang, C., H. Liu, and S.-K. Lee (2010). "The record-breaking cold temperatures during the winter of 2009/2010 in the Northern Hemisphere". *Atmospheric Science Letters* 11.3, pp. 161–168. DOI: 10.1002/asl.278.

Ware, R., M. Exner, D. Feng, M. Gorbunov, K. Hardy, B. Herman, Y.-H. Kuo, T. Meehan, W. Melbourne, C. Rocken, W. Schreiner, S. Sokolovskiy, F. Solheim, X. Zou, R. Anthes, S. Businger, and K. Trenberth (1996). "GPS sounding of the

atmosphere from low Earth orbit: Preliminary results". *Bull. Amer. Meteor. Soc.* 77.1, pp. 19–40. DOI: 10.1175/1520-0477(1996)077<0019:GSOTAF>2.0.CO;2.

Whan, K., F. Zwiers, and J. Sillmann (2016). "The Influence of Atmospheric Blocking on Extreme Winter Minimum Temperatures in North America." *J. Climate* 29.12, pp. 4361–4381. DOI: 10.1175/JCLI-D-15-0493.1.

White, W. B. and N. E. Clark (1975). "On the Development of Blocking Ridge Activity Over the Central North Pacific". *J. Atmos. Sci.* 32.3, pp. 489–502. DOI: 10.1175/1520-0469(1975)032<0489:OTDOBR>2.0.CO;2.

Wiedenmann, J. M., A. R. Lupo, I. I. Mokhov, and E. A. Tikhonova (2002). "The climatology of blocking anticyclones for the northern and southern hemispheres: block intensity as a diagnostic". *J. Climate* 15, pp. 3459–3473. DOI: 10.1175/1520-0442(2002)015<3459:TCOBAF>2.0.CO;2.

Wise, E. K. (2016). "Five centuries of U.S. West Coast drought: Occurrence, spatial distribution, and associated atmospheric circulation patterns". *Geophys. Res. Lett.* 43.9, pp. 4539–4546. DOI: 10.1002/2016GL068487.

WMO (2017). *WMO Statement on the State of the Global Climate in 2016.* WMO-No. 1189. URL: https://library.wmo.int/opac/index.php?lvl=notice_display&id=19835.

Woollings, T., B. Harvey, and G. Masato (2014). "Arctic warming, atmospheric blocking and cold European winters in CMIP5 models". *Environ. Res. Lett.* 9.1, p. 014002. DOI: 10.1088/1748-9326/9/1/014002.

Woollings, T. (2010). "Dynamical influences on European climate: an uncertain future". *Phil. Trans. R. Soc. A* 368.1924, pp. 3733–3756. DOI: 10.1098/rsta.2010.0040.

Woollings, T., A. Charlton-Perez, S. Ineson, A. G. Marshall, and G. Masato (2010). "Associations between stratospheric variability and tropospheric blocking". *J. Geophys. Res.* 115.D6, D06108. DOI: 10.1029/2009JD012742.

Xoplaki, E., J. F. González-Rouco, J. Luterbacher, and H. Wanner (2003). "Mediterranean summer air temperature variability and its connection to the large-scale atmospheric circulation and SSTs". *Climate Dyn.* 20, pp. 723–739. DOI: 10.1007/s00382-003-0304-x.

Yin, J. H. (2005). "A consistent poleward shift of the storm tracks in simulations of 21st century climate". *Geophys. Res. Lett.* 32.18. DOI: 10.1029/2005GL023684.

Yue, X., W. S. Schreiner, N. Pedatella, R. A. Anthes, A. J. Mannucci, P. R. Straus, and J.-Y. Liu (2014). "Space Weather Observations by GNSS Radio Occultation: From FORMOSAT-3/COSMIC to FORMOSAT-7/COSMIC-2". *Space Weather* 12.11, pp. 616–621. DOI: [10.1002/2014SW001133](https://doi.org/10.1002/2014SW001133).

Zhang, X., G. Hegerl, S. Seneviratne, R. Stewart, F. Zwiers, and L. Alexander (2013). *WCRP Grand Challenge: Understanding and Predicting Weather and Climate Extremes.* Tech. rep. URL: [https://www.wcrp-climate.org/images/documents/grand_challenges/GC_Extremes_v2.pdf](https://www.wcrp-climate.org/images/documents/grand_challenges/GC_Extremes_v2.pdf).

Zwiers, F. W., X. Zhang, and Y. Feng (2011). "Anthropogenic Influence on Long Return Period Daily Temperature Extremes at Regional Scales". *J. Climate* 24.3, pp. 881–892. DOI: [10.1175/2010JCLI3908.1](https://doi.org/10.1175/2010JCLI3908.1).

*Abstract:*

Stationary high-pressure systems at mid-latitudes, termed atmospheric blocking, are frequently connected to extreme weather events such as cold spells and heat waves. Their evolution and impacts in our changing climate have, hence, been extensively investigated in recent decades but several aspects still remain uncertain. This work introduces observations from GPS radio occultation (RO) as a new data set for blocking research. RO is a satellite-based, remote-sensing technique, observing key atmospheric variables such as geopotential height (GPH), temperature, and specific humidity with high accuracy. RO measurements processed at the Wegener Center are used from 2006 to 2016. The feasibility of blocking detection with RO is demonstrated for two blocking events in the Northern Hemisphere. The evolution of both events in summer 2010 and winter 2013 is correctly captured by RO and strong anomalies in atmospheric GPH and temperature are revealed. Observations over the entire RO period are used to systematically detect blocking in both hemispheres. All main blocking regions and the seasonal variability are well represented in the RO data set. The vertical atmospheric structure is particularly well resolved, revealing strong impacts on temperature and specific humidity throughout the entire troposphere and up into the lower stratosphere during blocking. RO is found to be a promising new method, enabling blocking detection and analysis from a single, comprehensive data set available globally at the same high quality. Impacts of blocking on surface extremes in Europe are investigated for a longer period from 1979 to 2014 in the observation-based ERA-Interim and E-OBS records. Statistically significant links between blocking and European temperature extremes are found that change during spring. Blocking impacts in spring are of particular relevance for vegetation and, therefore, need further research, especially in light of continued climate change.

*Zum Inhalt:*

Blockierende Hochdrucklagen in mittleren Breiten (en. *Blocking*) sind ein atmosphärisches Phänomen, das häufig zu Extremereignissen wie Kälte- und Hitzewellen führt. Im Licht des Klimawandels wurde Blocking daher in den letzten Jahrzehnten intensiv erforscht, doch wesentliche Aspekte bleiben weiter unsicher. Diese Arbeit stellt die satellitenbasierte GPS Radiookkultationsmethode (RO) für die Blocking-Forschung vor. RO liefert vertikal hochaufgelöste Messungen wichtiger atmosphärischer Parameter wie Geopotentielle Höhe (GPH), Temperatur und Spezifische Feuchte. Es werden RO Daten von 2006 bis 2016 verwendet, die am Wegener Center prozessiert wurden. In einer Fallstudie, die jeweils ein Blocking in Sommer und Winter untersucht, wird gezeigt, dass RO gut zur Detektion und Untersuchung von Blocking geeignet ist. Die Entwicklung wird korrekt dargestellt und starke Anomalien von atmosphärischer Temperatur und GPH während Blocking werden aufgezeigt. In einer systematischen Untersuchung wird Blocking im gesamten RO Datensatz und global analysiert. Die Blocking-Regionen und saisonale Änderungen werden korrekt abgebildet und es werden Anomalien von Temperatur und Spezifischer Feuchte während Blocking in der gesamten Troposphäre und bis in die untere Stratosphäre nachgewiesen. RO stellt daher einen vielversprechenden, neuen Datensatz für die Blocking-Forschung dar, der die globale Detektion und Analyse von Blocking aus einer einzelnen Quelle mit hoher Qualität erlaubt.

Die Auswirkung von Blocking auf Kälte- und Hitzewellen im europäischen Frühling wird für eine längere Zeitspanne von 1979 bis 2014, basierend auf ERA-Interim und E-OBS Daten, untersucht. Die Ergebnisse zeigen statistisch signifikante Verbindungen zwischen Blocking und Temperaturextremen in Europa. Die Auswirkungen von Blocking-Lagen im Frühling sind von besonderer Wichtigkeit für die Landwirtschaft und gerade im Licht des Klimawandels ist weitere Forschung in diesem Bereich essenziell.